923-03

LISAN PENINSULA POTASH EXPLORATION – DEAD SEA

PHASE I – COMPILATION AND REVIEW OF EXISTING TECHNICAL DATA

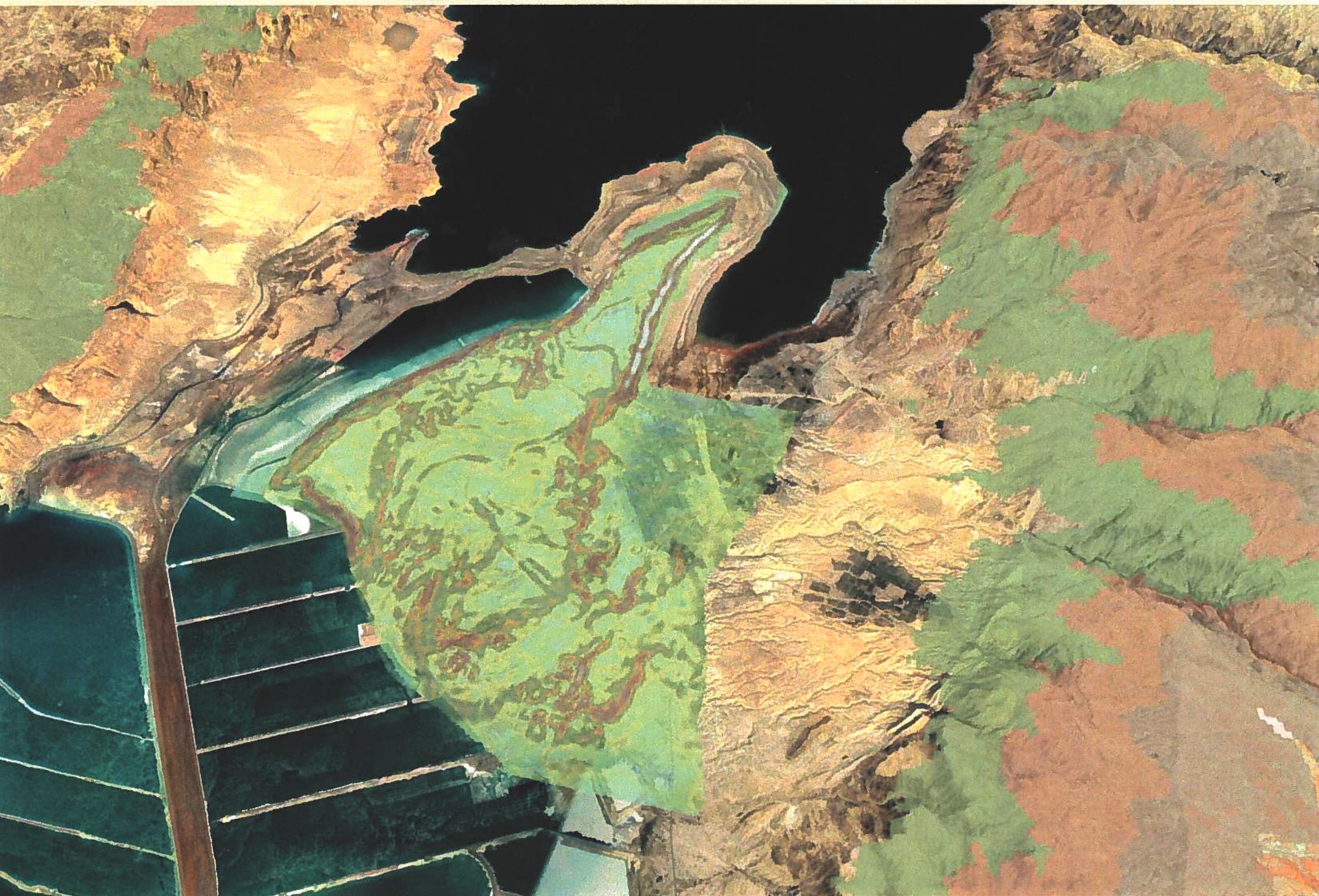

Submitted To:

Ministry of Energy & Mineral Resources
Eng. Amani Al-Azzam
Secretary General
P. O. Box 140027 Amman 11814
JORDAN

Submission Date:

14 November 2019

President of Agapito Associates, Inc.

AGAPITO ASSOCIATES, INC. CORPORATE SEAL COLORADO

Prepared by

AGAPITO ASSOCIATES, INC.
715 Horizon Dr., Ste. 340, Grand Junction, CO 81506
970/242-4220 • FAX 970/245-9234
1536 Cole Blvd., Bldg. 4, Suite 220, Lakewood, CO 80401
303/271-3750 • FAX 303/271-3891
www.agapito.com

MISBAR GEOPHYSICAL SERVICES
مسبار للخدمات الجيوفيزيائية

RPS MAKING COMPLEX EASY

LISAN PENINSULA POTASH EXPLORATION—DEAD SEA

PHASE I—COMPILATION AND REVIEW OF EXISTING TECHNICAL DATA

TABLE OF CONTENTS

Page

1 Executive Summary 1-1
1.1 Property Overview 1-1
1.2 Geology 1-1
1.3 Historical Exploration 1-3
1.4 Existing Technical Data 1-3
1.5 Seismic Reprocessing and Reinterpretation 1-3
1.6 Preliminary Earth Model 1-4
1.7 Interpretation and Conclusions 1-4
1.8 Recommendations 1-5

2 Introduction 2-1
2.1 Overview 2-1
2.2 Terms of Reference 2-2
2.3 Site Visits 2-2
2.4 Due Diligence Process 2-3

3 Property Description and Location 3-1
3.1 Location 3-1
3.2 Access 3-1
3.3 Climate 3-1
3.4 Local Resources and Infrastructure 3-1
3.5 Physiography 3-2
3.6 Mineral Tenure 3-2
3.6.1 APC Operations 3-2
3.6.2 ICL Operations 3-4

4 Geologic Setting and Mineralization 4-1
4.1 Regional Stratigraphy 4-1
4.2 Regional Structure 4-4
4.3 Property Geology 4-5
4.3.1 Stratigraphy 4-5
4.3.2 Structure 4-9
4.3.3 Salt Accumulation 4-9
4.3.4 Mineralization 4-9

5 Historical Exploration 5-1
5.1 Petroleum Drilling and Exploration 5-1
5.2 Potash Drilling 5-1
5.3 Seismic Surveys 5-1

6 Existing Technical Data 6-1
6.1 Drillholes 6-1
6.1.1 Inventory 6-1

6.1.2 Deviation Surveys ... 6-7
6.1.3 Geologic Logs ... 6-7
6.1.4 Geophysical Logs ... 6-9
6.1.5 Stratigraphic Correlations ... 6-11
6.1.6 Assays and Composites ... 6-12
6.1.7 Temperature Data ... 6-12
6.2 Seismic ... 6-13
6.2.1 Two-Dimensional Surveys ... 6-13
6.2.2 Three-Dimensional Surveys ... 6-14
6.2.3 Data Acquisition and Processing ... 6-15
6.3 Data Adequacy for Resource Estimation ... 6-16
6.3.1 Drillholes ... 6-17
6.3.2 Seismic ... 6-20

7 Seismic Reprocessing and Reinterpretation ... 7-1
7.1 Reprocessing ... 7-1
7.1.1 Near-Surface Model ... 7-1
7.1.2 3D Pre-Stack Time Migration ... 7-1
7.1.3 Testing and Parameter Selection ... 7-3
7.1.4 Production Processing ... 7-3
7.2 Interpretation Analysis ... 7-3
7.2.1 General Comments ... 7-3
7.2.2 Salt Reflectivity Interpretive Model ... 7-5
7.2.3 2D and 3D Seismic Horizons ... 7-6
7.2.4 Depth Structure Maps ... 7-8

8 Geology ... 8-1
8.1 Fault Block Structure ... 8-1
8.2 Stratigraphic Picks ... 8-1
8.2.1 Clastic Units ... 8-4
8.2.2 Potash Beds from Assay ... 8-5
8.2.3 Potash Beds from Geophysical Logs ... 8-5
8.3 Potash Bed Composites ... 8-5

9 Preliminary Earth Model ... 9-1
9.1 Methodology ... 9-1
9.2 Model Elements ... 9-2
9.2.1 Surface Terrain ... 9-2
9.2.2 Exploration Drillholes ... 9-3
9.2.3 Stratigraphy ... 9-6
9.2.4 Geologic Structure ... 9-7
9.2.5 Potash Mineralization ... 9-12

10 Interpretation and Conclusions ... 10-1
11 Recommendations ... 11-1
12 References ... 12-1

APPENDIX A—RPS Seismic Reinterpretation Report ... A-1

LIST OF TABLES

Page

Table 3-1. APC Corporate History 3-3
Table 3-2. APC Historical Potash Production....3-4
Table 6-1. Reviewed Well Records....6-2
Table 6-2. Summary of Drillhole Data 6-3
Table 6-1. Available 2D and 3D Seismic Surveys 6-13
Table 6-2. 2D Line Listing....6-14
Table 6-3. Geophysical Values for Evaporite Minerals....6-19
Table 6-4. 3D Acquisition Parameters....6-21
Table 8-1. Stratigraphic Formation Tops....8-3
Table 8-2. Potash Picks from Assays....8-4
Table 8-3. Potash Picks from Elogs and Lithological Logs....8-4
Table 8-4. Potash Bed Composites....8-6
Table 9-1. Model Stratigraphic Units 9-6

LIST OF FIGURES

Figure 1-1. Location Map of Lisan Peninsula 1-2
Figure 4-1. Simplified Geological Map of Jordan....4-2
Figure 4-2. Stratigraphic Column for the Dead Sea Area 4-3
Figure 4-3. General Tectonic Structure of the Dead Sea Basin with Major Faults 4-6
Figure 4-4. Seismic Plan View of the Lisan Peninsula Area showing Interpreted Historical Top and Bottom of the Salt Diapir 4-7
Figure 4-5. Historical Interpretation of Salt Diapirs in the Dead Sea Basin – Line 1 4-8
Figure 4-6. Geology Map of the Eastern Part of the Lisan Peninsula Area 4-8
Figure 4-7. Lisan Peninsula Area of Interest showing the Crest of the Salt Anticline and the Interpreted Border of the Salt Deposits....4-10
Figure 5-1. Lisan Peninsula Area of Interest showing Approximate Location of Historical 2D and 3D Seismic Coverage....5-2
Figure 6-1. Seismic Data Before and After Digitization, Line LIS-93-404....6-13
Figure 6-2. Comparison Between HGS and GSC Old Processing/XL191 6-15
Figure 6-3. Empirical Chart Relating Gamma Ray Deflection to Potassium Content ...6-18
Figure 7-1. Example of a Shot Gather with Bad First Breaks....7-2
Figure 7-2. Snapshot of Lisan 3D Near-Surface Velocity Model 7-2
Figure 7-3. Old Processing versus Misbar PreSTM / XL191 7-3
Figure 7-4. 2D lines Selected for Reprocessing 7-4
Figure 7-5. Processing Workflow....7-5
Figure 7-6. 3D Seismic Interpretation: Full Section and Potash Zone Detail....7-6
Figure 7-7. Salt Reflectivity Interpretive Model 7-7
Figure 7-8. Seismic Interpretation on Two Key 2D Lines: DS-07 and VWJ-13 7-7
Figure 7-9. Northwest–Southeast Arbitrary Line Interpretation through the 3D Volume....7-8
Figure 7-10. Northeast–Southwest Arbitrary Line Interpretation through the 3D Volume....7-8
Figure 7-11. Depth Structure Maps: Top of Salt, Base of Salt, and Cretaceous/ Basement 7-9

Figure 7-12. Depth Structure Maps: Top of Potential Potash, Intra Potential Potash Zone, and Base of Potash Potential 7-10
Figure 7-13. Seismic Depth Structure 3D Views, from the Southwest and the Southeast 7-10
Figure 7-14. Seismic Depth Structure 3D Views, from the Northeast and the Northwest 7-11
Figure 8-1. Historical Interpretation of Salt Diapirs in the Dead Sea Basin – Line 7 8-2
Figure 9-1. Hexagon Mining © MinePlan™ 3D Modeling Software 9-1
Figure 9-2. Block Model Extents 9-2
Figure 9-3. Digital Elevation Model 9-3
Figure 9-4. Model Satellite Image along Jordan Valley 9-4
Figure 9-5. Model Satellite Image across Jordan Valley 9-4
Figure 9-6. Historical Exploration Drillholes in Model 9-5
Figure 9-7. Above-Ground View of Historical Drillholes 9-5
Figure 9-8. Underground View of Historical Drillholes 9-6
Figure 9-9. Drillhole Stratigraphy in Model 9-7
Figure 9-10. Seismic Surfaces in Model 9-8
Figure 9-11. South–North Profile of Seismic Surfaces in Model 9-9
Figure 9-12. Reflectors through Potash Host Interval 9-10
Figure 9-13. Reflectors near P1 and P2 Potash Beds 9-10
Figure 9-14. Top of Salt Surface—Depth Contours 9-11
Figure 9-15. Base of Salt Surface—Depth Contours 9-12
Figure 9-16. P1 Reflector Surface—Depth Contours 9-13
Figure 9-17. Assay Intervals for Drillhole C-4 9-13
Figure 9-18. Drillhole Potash Intercepts Interpreted from Geophysical and Geologic Logs 9-14
Figure 9-19. Drillhole Potash Intercepts Confirmed by Coring and Assay 9-14
Figure 9-20. Drillhole Potash Intercepts with Seismic Reflector Surfaces 9-15
Figure 9-21. Drillholes with Potash Mineralization 9-16
Figure 9-22. Geologic Confidence in Potash Continuity 9-17
Figure 9-23. Geologic Confidence in Potash Continuity for Potash Bed P1 9-17

LIST OF UNITS

°	degree
C	Celsius
cc	cubic centimeter
cm	centimeter
ft	feet or foot
g	gram
g	local acceleration due to gravity
Hz	hertz
km	kilometer
km^2	square kilometer
l	liter
m	meter
M	million
mm	millimeter
ms	millisecond
MSL	mean sea level
MW	megawatt
θN	apparent limestone porosity from a neutron log
ρu	electron density
/	per
%	percent
s	seconds
t	tonnes

LIST OF ACRONYMS AND ABBREVIATIONS

2D	two-dimensional
3D	three-dimensional
AAI	Agapito Associates, Inc.
ANS	Arabian Nubian Shield
APC	Arab Potash Company
API	American Petroleum Institute
BSL	below sea level
BPI	Bit Per Inch
Ca	calcium
$CaCl_2$	calcium chloride
CaO	calcium oxide
©	copyright
$CaSO_4$	anhydrite
$CaSO_4 \cdot 2H_2O$	gypsum
CDP	Common Depth Point
CGG	Compagnie Générale de Géophysique
CIM	Canadian Institute of Mining, Metallurgy and Petroleum
Cl	chloride
CSA	Canadian Securities Administrators
db	decibel

DEM	digital elevation model
DEMUX	demultiplexer
DMO	dip-moveout
DST	drill stem test
DT	sonic log
Elog	electronic log
ENE	east-northeast
Fe_2O_3	iron (III) oxide
GLI	Generalized Linear Inversion
GNT	gamma ray/neutron
GSC	Geophysical Services Center
H_2O	water
HGS	Halliburton Geophysical Services
ICL	Israel Chemical
INOC	Iraq National Oil Company
JBC	Jordan Bromine Company
JGA	Jordanian Geologists Association
K	potassium
K_2O	potassium oxide
KCl	potassium chloride or sylvite
$KCl{\bullet}MgCl_2{\bullet}6H_2O$	carnallite
$KCl{\bullet}NaCl$	sylvinite
KEMAPCO	Arab Fertilizers and Chemicals Industries
MCM	Muwaqqar Chalk Marl
MEIL	Megha Engineering and Infrastructures Ltd.
MEMR	Ministry of Energy and Mineral Resources
Misbar	Misbar Geophysical Services
Mg	magnesium
MgCl	magnesium chloride
MgO	magnesium oxide
MOP	muriate of potash
N	nitrogen
Na	sodium
NAN	north-Arabian-Nubian
NEPCo	National Electric Power Company
NJFC	Nippon Jordan Fertilizer Company
NNW	north-northwest
NNE	north-northeast
NRA	Natural Resources Authority
NYSE	New York Stock Exchange
P	phosphorus
PotashCorp	Potash Corporation of Saskatchewan
PreSTM	pre-stack time migration
Project	Lisan Peninsula Potash Exploration Project
QP	qualified person
ROI	radius of influence
RPS	RPS Group
SDIC	State Development and Investment Corporation
SSE	south-southeast
SSL	Seismograph Service Limited
TASE	Tel Aviv Stock Exchange

™	trademark
TVD	true vertical depth
URC	Umm Rijam Chert-Limestone
USGS	United States Geological Survey
UTM	Universal Transverse Mercator
VP	Vibration Point
WGS	World Geodetic System
WSC	Wadi Shallala Chalk
WSW	west-southwest

1 EXECUTIVE SUMMARY

The Government of Jordan through the Ministry of Energy and Mineral Resources (MEMR) commissioned the Lisan Peninsula Potash Exploration Project (the "Project") to evaluate the future mining potential of prospective potash mineralization contained within the Lisan Peninsula in the Dead Sea. The Project is divided into five phases:

Phase I	Compilation and Review of Existing Technical Data
Phase II	Data Gap Analysis and Exploration Program Development
Phase III	Exploration Program
Phase IV	Evaluation of Exploration Results and Earth Model Development
Phase V	Potash Mineral Resource Estimate

Agapito Associates, Inc. (AAI) was awarded the consultancy services for the Lisan Project by the MEMR on 21 August 2019. The Consultant team comprises AAI, the prime contractor, and subconsultants Misbar Geophysical Services (Misbar) and RPS Group (RPS).

This report represents the completed work product for Phase I—Compilation and Review of Existing Technical Data. Phase I is a due diligence acquisition and review of the existing and historical geologic, seismic, and exploration data relevant to potash mineralization within the Lisan Peninsula.

1.1 Property Overview

On the eastern coast near the south end of the Dead Sea, the Lisan Project is located on the western border of Jordan adjacent to Israel, within the Karak Governorate (Figure 1-1) and west of the town of Al Mazraa. The Peninsula is located approximately 25 km northwest of the city of Al Karak and 80 km southwest of Jordan's capital Amman. The Lisan Project boundary comprises approximately 58.9 square kilometers (km^2) and includes close to 27 km of Dead Sea's coastline.

All of Jordan's Dead Sea mineral production has been produced by Arab Potash Company (APC) since 1956 by pumping its water into solar evaporation ponds, then harvesting and processing the precipitated salts. They are the world's eighth largest potash producer by volume and the only Arab producer. APC has been given the exclusive rights by the Government of Jordan to harvest Dead Sea minerals through 2058. Annual potash production is approximately 2.2 Mt per year with their major customers being China and India.

1.2 Geology

Jordan is north of the Arabian-Nubian Shield (ANS). Precambrian basement crops out in southern Jordan and is overlain by accreted terrains, followed by uplift, erosion, and localized intrusive, volcanic, and volcaniclastic depositions referred to as the Aqaba Complex. The Lower and Middle Cambrian Ram Group was deposited on the peneplane surface; it is predominantly fluvial siliciclastic originating from the basement and includes pulses of marine siliciclastic and carbonates (Powell et al. 2014). The syn-rift Cretaceous to Eocene succession in central and south Jordan is characterised by passive continental margin depositional sequences, which transition upwards from alluvial/paralic to shallow carbonate shelf and pelagic ramp systems (Powell and Moh'd 2011).

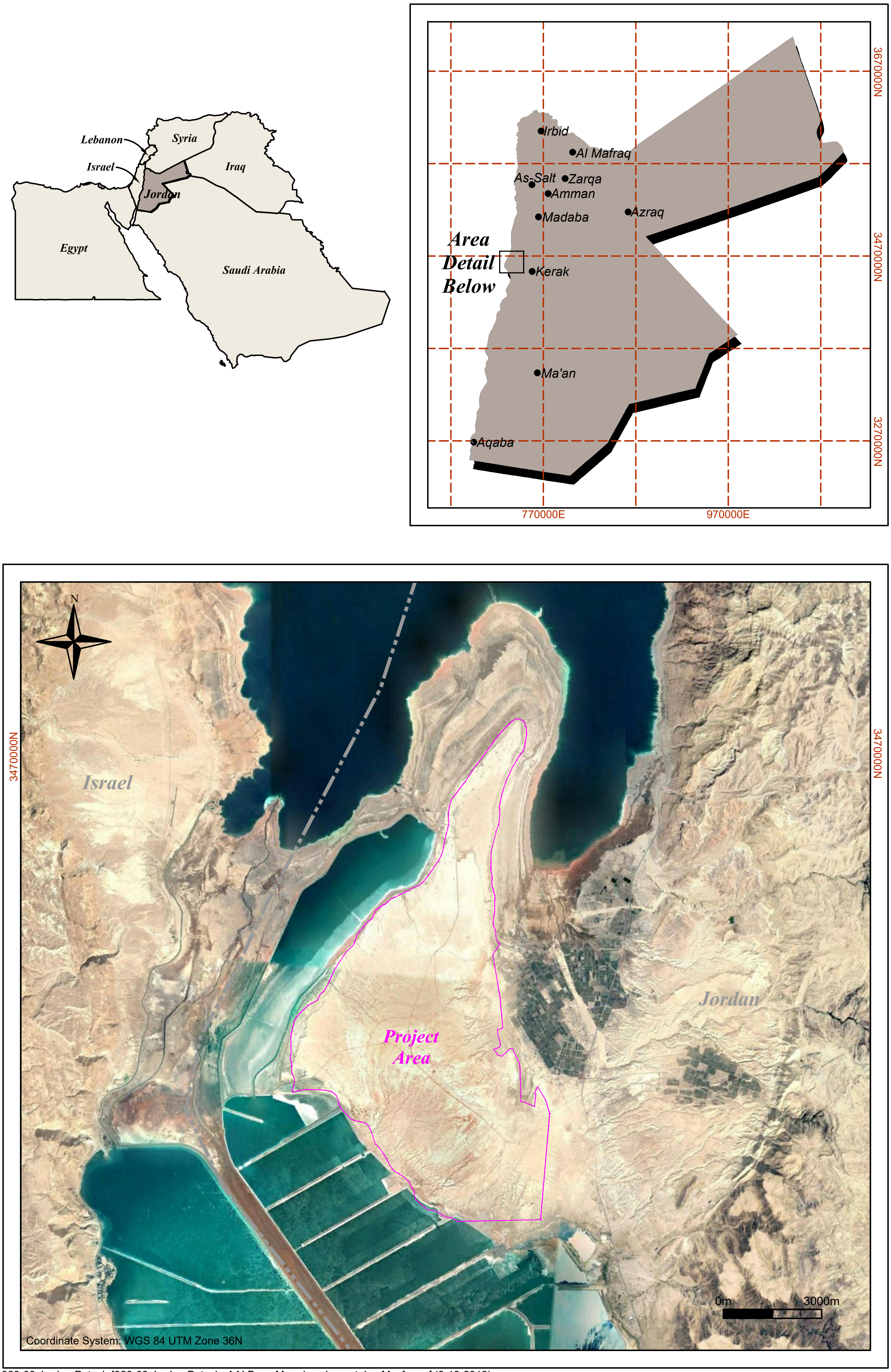

923-03 Jordan Potash [923-03 Jordan Potash_AAI Base Map.dwg; Layout: LocMap]:smvf (9-19-2019)

Figure 1-1. Location Map of Lisan Peninsula

The Dead Sea Basin is a "pull-apart" basin formed between sinistral, left-stepping en-echelon faults. It lies within the Dead Sea Rift, which originated in the Late Oligocene/Early Miocene Epochs. The Lisan Peninsula is situated in the Dead Sea Basin within the Dead Sea area that extends from Lake Tiberias to the Dead Sea in central-west Jordan and is believed to have formed in the Quaternary Period as the result of basin trans-tension and subsidence.

The Lisan Peninsula is a salt diapir within the Dead Sea Basin. It is bound by faulting on the east and west sides. The salt is estimated to be 5 to 7 km thick (Western Geophysical 1994). Two SSE–NNW subparallel sinistral (left-lateral movement strike slip) en-echelon faults are present to the east, which define the Dead Sea Rift basin margin. They are the Ghor-Safi and Wadi-Araba fault zones. To the west, the Lisan Peninsula is bound by the Sedom and Western Border faults. The Sedom fault defines the NNW–SSE flexing that created the Lisan Peninsula and to the south, the Sedom diapirs. Potash mineralization in the Lisan Peninsula is representative of an extreme concentration of hypersaline shallow sea environments. Potassium mineralization is almost exclusively sylvite and carnallite. The depositional environment is a basin isolated from open marine conditions by the rift walls, and faulting and uplift that isolated the Dead Sea area, thereby restricting inflow, which increased density and salinity.

1.3 Historical Exploration

Initial petroleum exploration in the project area was conducted by Phillips and began around the early 1960s. Their initial focus was defining the structure of the salt body within the Lisan Peninsula and determining if there were oil traps on the flanks of the diapir.

Exploration for potash on the Lisan Peninsula stemmed from Phillips initial petroleum work. The Natural Resources Authority (NRA) drilled three exploratory wells in the late-1960s intended for exploration of both potash and petroleum. Drilling exploration slowed until the mid-1980s when an additional four wells were completed for potash exploration.

1.4 Existing Technical Data

MEMR provided AAI with a digital data package of historic exploration works for the Lisan Peninsula and the specific project area of interest. The data encompasses previous drillhole data for oil and gas exploration along with specific potash exploration efforts. Additionally, historical 2D and three-dimensional (3D) seismic data was provided for analysis.

Information for a total of 42 drillholes was received for review, of which, 16 are located within the project boundaries, and five of those 16 penetrate through potash bearing zones.

1.5 Seismic Reprocessing and Reinterpretation

As part of Phase I of the Lisan Potash Exploration Project, the historical 2D and 3D seismic data were reprocessed by Misbar in Amman, Jordan with collaboration from RPS personnel in Calgary, Canada.

The legacy 2D and 3D seismic data are of consistent vintage, poor-to-fair in quality, designed for petroleum exploration, contaminated with out-of-plane noise, and may have sub-optional near-surface corrections. Reprocessing of the legacy 3D data with modern techniques has resulted in an improvement of data quality. Unfortunately, the majority of 2D lines reprocessed did not offer any improvement in areas overlapping the 3D seismic. In general, the overall data quality results in high interpretive risk associated with this dataset.

RPS completed the correlation of geological markers to seismic events from recently reprocessed 2D and 3D seismic data. This step of reprocessing was critical in improving the geophysical data and producing seismic images. Geological guidance from well data was provided by AAI and enabled the identification and mapping of potential potash-bearing zones. Depth structure maps were derived from the seismic data and well-based geology.

The mapped interpreted potash-bearing zones were constrained laterally and in depth. The prospective area in the northern portion of the Project area is well-defined by high confidence seismic interpretation and shows the general structure to rapidly fall off the apex of the Lisan diapir with a northerly dip. The shallower data in the southern Project area does not suggest any steep dips until below the prospective potash zone. This area is potentially more prospective than the northern area but is also considered to have low confidence in the seismic interpretation.

1.6 Preliminary Earth Model

A Preliminary 3D Geological Model of Potash in the Lisan Peninsula was constructed from the historical geological data compiled in Phase I, utilizing Hexagon Mining © MinePlan™ 3D Version 15.40 software (MinePlan) (Hexagon Mining 2019). MinePlan is a state-of-the-art, leading commercial-grade geology and mine planning computer platform developed for the mineral resources industry. The purpose of the model is to provide a preliminary geometric framework and geospatial database for characterizing the Lisan potash deposit that can be used to plan exploration activities in Phase II and, ultimately, estimating the Lisan Peninsula Potash Resource if the Project progresses to Phase V. The model includes the relevant components of the geologic and seismic database, including a surface terrain model in Universal Transverse Mercator (UTM) coordinates, satellite imagery, drillhole collars, downhole surveys, stratigraphic intercepts, potash assays, bed composites, potash intercepts based on geophysical and geologic log interpretation, major faults, and stratigraphic structure derived from seismic interpretation.

The model reveals consistent potash mineralization throughout the southeast quadrant of the Project area. The potential for mineralization elsewhere within the Project boundary is largely indeterminate at this phase due to a lack of drillhole exploration data. The model provides a meaningful tool for designing the details of the exploration program in Phase II.

1.7 Interpretation and Conclusions

Substantial historical exploration data were acquired and evaluated for Phase I. Based on the Phase I evaluation, the authors of this study conclude that potentially-economic potash mineralization exists in a structurally complex environment in the southeastern quadrant of the Lisan Peninsula. Nine of the historical exploration drillholes, including five holes with core and assays, show potash occurring in multiple beds to a depth of at least 1,460 meters (m) with potential continuity over an area as large as 12 km^2 to the southeast inside the Project boundary.

Elsewhere to the west and north, minimal exploration data exist inside or outside the Project boundary. The potash resource is considered “open,” i.e., an exploration target with mineral potential, in these data-poor regions. The open resource footprint represents more than 80 percent (%), or 47 km^2, of the Project area.

Significant faults with major vertical offsets are evident on the western and southeastern margins of the Project boundary based on the reinterpretation of the historical seismic data. Modest faulting is implied elsewhere. The faulting is post-depositional as evidenced by the continuity of key seismic reflectors across fault zones. In some cases, seismic reflectors can be traced over the apex of the Lisan diapir and across much of the Project area, thereby supporting the likelihood that the potash, in bedded form, continues to the south, west, and northeast over some or all of the Project area.

The authors of this study concur with MEMR's opinion that future exploration work has reasonable potential to identify a moderate to substantial potash resource.

1.8 Recommendations

The Phase I investigators recommend that the Project progress to Phase II—Data Gap Analysis and Exploration Program Development based on the Phase I conclusions, principally that the historical data locally confirm the occurrence of potash and reasonable potential exists for discovering a larger resource elsewhere with additional exploration.

The database compiled and corrected in Phase I provides sufficient information for conducting Phase II.

2 INTRODUCTION

The Government of Jordan, through the MEMR, commissioned the Lisan Project to evaluate the future mining potential of prospective potash mineralization contained within the Lisan Peninsula in the Dead Sea. The project is divided into five phases:

Phase I	Compilation and Review of Existing Technical Data
Phase II	Data Gap Analysis and Exploration Program Development
Phase III	Exploration Program
Phase IV	Evaluation of Exploration Results and Earth Model Development
Phase V	Potash Mineral Resource Estimate

AAI was awarded the consultancy services for the Lisan Project by the MEMR on 21 August 2019. The Consultant team comprises AAI, the prime contractor, and subconsultants Misbar and RPS.

2.1 Overview

This report represents the completed work product for Phase I—Compilation and Review of Existing Technical Data. Phase I is a due diligence acquisition and review of the existing and historical geologic, seismic, and exploration data relevant to potash mineralization within the Lisan Peninsula.

In advance of this study, MEMR concluded that the historical database confirms the occurrence of potash within a portion of the Lisan Peninsula and that additional exploration work has the potential to prove even more substantial mineralization. MEMR identified concerns about the quality and completeness of the historical database. Phase I was designed with five objectives to address these concerns:

1. Acquire all relevant data and ensure the completeness of the Lisan data set.
2. Scrutinize the data for accuracy and consistency, and to identify discrepancies.
3. Determine the accuracy of the data and correct historical errors for use with geological modeling.
4. Reprocess and reinterpret historical seismic data using modern techniques.
5. Construct a preliminary, foundational computer earth model from the corrected Phase I data set for use in subsequent phases of the Project.

Phase I work was initiated on 21 August 2019 at the time the consultancy contract was signed in Amman, Jordan. Representatives of AAI, Misbar, and RPS attended the contract signing. A multiday project kickoff meeting was held in Amman during the same week. Key members of the Consultant team visited the Lisan Peninsula as part of the kickoff meeting.

The deadline for acquiring historical technical data was reached on 21 September 2019. Sufficient data were acquired, evaluated, and corrected to meet the objectives of Phase I and facilitate Phase II—Data Gap Analysis and Exploration Program Development in the future.

This report is organized into ten sections with appendices after this introductory section which describe the Project site and geology, historical exploration activities, existing technical data, seismic reprocessing and reinterpretation, preliminary computer modeling, and Phase I interpretation and conclusions.

A computer model, referred to as the Preliminary 3D Geological Model of Potash in the Lisan Peninsula, is a key deliverable of Phase I. The model was constructed based on the historical data compiled in Phase I utilizing Hexagon Mining © MinePlan™ 3D Version 15.40 software (MinePlan) (Hexagon Mining 2019). Features of the model are described in Section 9.

2.2 Terms of Reference

Phase I work is being conducted under the Consultancy Services Agreement for Lisan Peninsula Potash Exploration between the MEMR and AAI, executed on 21 August 2019.

The scope of work is defined by the following documents issued by the MEMR:

- Volume I—Instructions to Tenderers/Conditions of Agreement (issued with the Lisan Peninsula Potash Exploration Project Bid Documents on 3 March 2019)
- Volume II—Terms of Reference (issued with the Lisan Peninsula Potash Exploration Project Bid Documents on 3 March 2019)
- Addendum No.1—Lisan Exploration Clarifications No. 1 (issued 18 March 2019)
- Addendum No. 2—Lisan Exploration Tender (issued 21 March 2019)

The objective of the Project is to provide independent estimates of Mineral Resources and Mineral Reserves which are compatible with Canadian National Instrument (NI) 43-101 reporting standards (Canadian Institute of Mining, Metallurgy and Petroleum [CIM] 2003; Canadian Securities Administrators [CSA] 2016). This requires that the Project advance through Phase V and that any modern exploration activities conform with NI 43-101 reporting standards. The work conducted in Phase I is beyond the scope of NI 43-101 and therefore not subject to NI 43-101 reporting standards. NI 43-101 will be relevant beginning in Phase II where data deficiencies will be identified in terms of NI 43-101 standards and plans for contemporary exploration will be developed. NI 43-101 is directly relevant to all subsequent phases.

Metric units are reported, such as meters, unless otherwise noted. The UTM Zone 36N World Geodetic System (WGS) 1984 geographical coordinate system is used through this study.

2.3 Site Visits

AAI Chief Geologist, Vanessa Santos, made a site visit on Tuesday, 20 August 2019. The trip was organized by the MEMR and Misbar and hosted by APC's Projects and Expansion Manager, Khalid Hijazeen. Members of the MEMR Committee included the Committee Chairman Mohammad Abuqudaira, Geologist Marwan Madanat, and GIS Specialist Hisham Al Zyood. Misbar was represented by General Manager Mohamed Yousef, Geophysical Consultant Abdel Aziz Madi, and Geophysicist Hussein Zawahreh. Roger Edgecombe, Senior Vice President (VP) represented RPS. After visiting the APC offices and meeting with VP Operation Manager and Engineer Mohammad Abu Gheyab, the team took a bus to the Pump Station located on the Lisan Peninsula.

Access to the Lisan Peninsula is restricted and permission to enter the checkpoint must be obtained in advance. APC is building new evaporation ponds on the Lisan Peninsula as well as expanding the causeway on which the pump station is located.

The new ponds and berms are constructed from Lisan Marl material, available from several areas of the Lisan Peninsula. This same material is believed to be suitable for drill pad and road construction, without the need for additional permitting.

Several karst features were observed on the Lisan Peninsula, including sinkholes and terrace collapse. These features will be a factor in planning and executing a drilling program on the Peninsula. The depth and aerial extent of the karst is not known but the literature reveals that between 2000 and 2002, APC lost two salt evaporation ponds to collapse (Closson 2005). It was also discussed that drilling may be restricted in the areas of the new evaporation ponds.

2.4 Due Diligence Process

Official requests for available historical exploration data and relevant reports were made to the MEMR Committee by AAI and Misbar personnel following the 21 August 2019 signing ceremony. Additionally, AAI asked for and received verbal agreement from the Committee Chairman that the time for completing Phase I could be extended up to 1 month to allow for collection of the available Lisan Peninsula data and reports. The data received is summarized in later chapters but includes historical drillhole data, including well reports, geophysical logs, and lithology logs and seismic data, both 2D and 3D. In addition, previous studies of exploration work on the Lisan Peninsula, some specifically for potash, were obtained from MEMR.

The majority of the data used for this report was provided by MEMR. Misbar personnel contacted the Jordanian Geologists Association (JGA) to inquire if they had possession of any relevant data or reports not provided by MEMR. No additional information was provided by the JGA. In addition, similar requests were made to APC to see if relevant data could be obtained, specifically from Engineer Khalid Hijazeen. Engineer Hijazeen sent an APC report (DMT GmbH & Co. KG 2018, APC internal Report) evaluating the nearshore area on the east and west sides of the Lisan Peninsula as part of planning upgrades to the intake pumping stations. This report focuses on areas just outside of the area of interest but could be relevant for determining the top of salt in the offshore area. No additional data or reports were obtained after AAI’s 20 September 2019 cutoff date, so all known available data and historical reports were considered for this Phase I report.

AAI has conducted an extensive internet search for publicly available scientific literature, most of which have been utilized and/or reviewed and are referenced in Section 12, References.

3 PROPERTY DESCRIPTION AND LOCATION

3.1 Location

Located on the eastern coast near the south end of the Dead Sea, the Lisan Peninsula Potash Exploration Project (the "Project") is on the western border of Jordan adjacent to Israel, within the Karak Governorate (Figure 1-1) and west of the town of Al Mazraa. The peninsula is located approximately 25 km northwest of the city of Al Karak and 80 km southwest of Jordan's capital Amman. The Lisan Project boundary comprises approximately 58.9 km^2 and includes close to 27 km of Dead Sea coastline. The Project area is defined as the 1954 waterline, but the entire Peninsula was evaluated as seismic data extended past those boundaries.

3.2 Access

Access to the Project is limited to Jordan's highway system. The intersection of Jordan Valley Highway 65 and Karak Highway 50 is located just east of the Project site. The Jordan Valley Highway 65 runs north and south along Jordan's western border with Israel, while the Karak Highway 50 runs east through the city of Al Karak, approximately 30 km away. The Karak Highway intersects the King's Highway 35 in Al Karak. The King's Highway is another north and south travelway that runs adjacent to the capital of Amman. Jordan's rail transport has approximately 510 km of narrow-gauge rail but is used only for passenger transport and tourism (RAILMED 2019).

APC currently trucks their product south along the Jordan Valley Highway to warehouses in Ghor Al Safi (20 km south) or the port city of Aqaba (200 km south) (APC 2019a).

3.3 Climate

A Mediterranean (dry summer) climate characterizes the Project area, with hot, dry summers and mild wetter winters with an average annual temperature of 26.1 degrees Celsius (°C). The lowest temperatures typically occur in January with an average nightly low of approximately 12.7°C. The highest temperatures typically occur in August with an average high around 39.7°C. The wet season is typically December through March and accounts for approximately 78% of the area's average annual precipitation (approximately 42 mm). Climate data was provided by Wikipedia (2019).

3.4 Local Resources and Infrastructure

Electric power in the region is provided by the National Electric Power Company's (NEPCo) grid. The majority of NEPCo's (2019) power grid is made up of fuel oil, natural gas, and diesel power plants in generation facilities across the country. The area's climate makes water a valuable resource for both industry and personal use. The local industrial operations rely on boreholes to provide water to the operations. Due to the industrial nature of the region, there are existing pipelines that supply natural gas to APC's potash and bromine plants. Natural gas is currently being supplied by Tamar Petroleum Ltd (MarketScreener 2018).

The Karak Governorate has a population of approximately 317,000 people, which provides the industrial area with a pool of skilled professional, technical, and tradespersons. Mutah University is one of the largest universities in Jordan and is located in Mu'tah, 26 km southeast of the Project site. The Governorate's local resources are dominated by tourism, agriculture, and industry. The agricultural sector consists of tomatoes, bananas, wheat, barley, livestock (mainly sheep and goats), and chicken farming (COTECNO ABT ALCHEMIA CDG MGA 2005).

3.5 Physiography

The Dead Sea currently sits at an elevation of 430.5 m below mean sea level (MSL), making it the lowest land elevation on Earth. Its water level drops more than 1 m per year due to water being diverted or extracted from the Jordan River, which feeds the Dead Sea at its northern end. Jordan and Israel utilize the water for public use and irrigation. In the 1970s, the Dead Sea's water elevation level dropped below an underwater ridge that divides the shallower South Basin with the deeper Northern Basin. Water remains in the South Basin, even though it is located 35 m above the current Dead Sea surface elevation due to the industrial pumping of Dead Sea water into solar evaporation ponds for potash production for both countries; however, if not for the pumping of sea water to the evaporative ponds, the South Basin would be dry.

The Lisan Peninsula is located between the north and south basins and its surface elevation is approximately 320–400 m below median sea level (Jordanian Geologists Association 2014). Few species can survive the harsh desert conditions and are sparsely found in the region. Examples of local flora include the thorny keel, desert mugwort, and zygophyllum bush.

According to the United States Geological Survey (USGS) "Seismic Risk of Jordan" (Kovach 1987), the Project is located in an area with seismic intensity of VIII. Seismic intensity VIII on the Modified Mercalli Intensity Scale describes the shaking as severe, with the potential for considerable damage or partial collapse to ordinary surface (non-specially designed) structures (USGS 2019).

3.6 Mineral Tenure

Subsurface mineral tenure on the Lisan Peninsula is controlled exclusively by the Government of Jordan. APC infrastructure is located on the Lisan Peninsula, including a pump station and evaporation ponds, but APC does not hold the subsurface mineral tenure.

3.6.1 APC Operations

Founded in 1956 and headquartered in Amman, APC produces potash from the Dead Sea's water using solar evaporation ponds. APC is the worlds' eighth largest potash producer by volume and the only Arab producer. The majority shareholder is China's State Development and Investment Corporation (SDIC), who purchased Potash Corporation of Saskatchewan's (PotashCorp) 28% stake as a stipulation for its merger with Agrium to form Nutrien. The second largest shareholder of the company is the Jordanian Government who owns 27%. Highlights of APC's history are sourced from APC's 2018 Annual Report and are listed in Table 3-1. APC employs 1,700 people.

Annual production for APC's Dead Sea operation has averaged 2.2-Mt KCl over the last 5 years, while 2018 production was 2.4-Mt KCl. Major APC customers are China and India, which purchased 48% and 15%, respectively, of APC's 2018 production (APC 2019b). China is the top consumer of the world's potash production. Historical production from the last 5 years is found in Table 3-2 (APC 2019b).

Table 3-1. APC Corporate History (after APC 2019b)

Year	History
1956	The Arab Potash Company was established on 7th July as a pan-Arab public shareholding company to extract potash from Dead Sea minerals.
1958	The Government of the Hashemite Kingdom of Jordan granted APC exclusive rights to extract manufacture and market minerals from the Dead Sea until 2058.
1976	The project began with tests and experiments to determine the parameters of various technologies and ideas.
1979	Construction work started on the project and was completed in 1982. A major engineering challenge was to build the dykes on the unstable sea bed. Sixteen million cubic meters of earth material were displaced in the process of building about (117) kilometers of seepage proof dykes eight meters wide at the top. More dykes were added later.
1983	APC began production at an initial total capacity of 1.2 million metric tons of KCl product per year. Production capacity was later optimized to reach 1.4 million tons KCl per year at the end of the eighties.
1988	APC posted its first profit and began plans to diversify production by studying bromine and downstream products.
1994	Construction of a second plant of a 0.4 million ton KCl per year capacity at a cost of US $120 million brought up total production capacity to 1.8 million tons KCl per year.
1997 -99	Joint Venture Agreements and construction of bromine and derivatives plants and potassium nitrate, magnesia and salt were concluded. APC invested about US $ 500 million in the downstream. It signed JV agreements with Albemarle of The United States to establish the Jordan Bromine Company (JBC) and with Kemira of Finland to establish KEMAPCO in Aqaba.
2003	PotashCorp (Potash Corporation of Saskatchewan) bought 28% of APC shares from the Government of Jordan and became a strategic partner. Sales surpassed 2 million tons KCl for the first time.
2004	Construction began on the second Cold Crystallization Plant with an investment of USD 450 million aiming to bring capacity to 2.35 million tons KCl per year. APC opened its first overseas sales office in Kuala Lumpur, Malaysia
2007	APC became the 100% owner of KEMAPCO after buying Kemira of Finland's shares in the Company. KEMAPCO produces 120K tons per year of the high value nutrient (potassium nitrate)
2008	Mining royalties rose from JD 15 to JD 125 per ton KCl, with a ceiling of 25% of net profits. This makes APC's royalties the highest of all potash producers in the world. APC consolidated annual sales approached 0.8 billion dollars. Profits soared to 500 million dollars. APC production surpassed the 2-million-ton KCl mark for the first time in its history.
2009	Rent for concessionary land rose from JD 200,000 per annum to JD 1,500,000 per annum. APC began shipping in bulk containers.
2010	The new Cold Crystallization Plant was inaugurated by HM the King and APC reached an official potash production capacity of 2.35 million tons KCl per year. As part of the expansion, the Aqaba warehouse became the largest Potash Export terminal in the world.
2013	APC and Sinofert of China sign a 600,000 ton per year MoU, witnessed by His Majesty King Abdullah II and President Xi Jinping of the People's Republic of China.
2014	• APC opens a second sales office in New Delhi, India. • APC container shipments reach a record. • APC sales reach a record at 2.244 Mt KCl.
2015	For the first time, APC completed 5,000,000 working hours without lost time injuries, which are defined as injuries that the injured person to take time off for treatment.
2018	Because of the merger between PotashCorp and Agrium to form Nutrien, PotashCorp's majority stake in APC was sold to China's State Development and Investment Corp (SDIC).

Table 3-2. APC Historical Potash Production

Year	Production (Mt KCl)
2014	2.09
2015	2.36
2016	2.00
2017	2.32
2018	2.44

APC owns all, or portions of, several downstream and complementary industries related to Dead Sea minerals as follows:

- Arab Fertilizers and Chemicals Industries (KEMAPCO), 100% ownership—Produces potassium nitrate fertilizer, dicalcium phosphate, animal feed, and nitric acid
- Numeira Mixed Salts and Mud Company, 100% ownership—Dead Sea Cosmetics producer
- Jordan Bromine Company (JBC), Joint Venture with Albemarle Holdings—Produces bromine and bromine derivatives
- Nippon Jordan Fertilizer Company (NJFC), 20% ownership—Produces NPK (nitrogen [N], phosphorus [P], and potassium [K]) and ammonium phosphate fertilizers for Japan

3.6.2 ICL Operations

Potash is produced by ICL on the western side of the Dead Sea via a solar evaporation process similar to APC's Dead Sea operations. ICL was founded in 1968 and is headquartered in Tel Aviv. ICL was granted exclusive rights to Dead Sea mineral extraction by the Government of Israel thought 2030. ICL is a publicly traded company on the New York Stock Exchange (NYSE) and the Tel Aviv Stock Exchange (TASE), and focuses on three markets: agriculture, food, and engineered materials.

ICL is a global company that has operations in Israel, Europe, North and South America, and China. Currently, ICL produces bromine, potash, magnesium, and phosphate rock. In 2018, ICL produced approximately 4.9-Mt KCl from Israel and Spain combined; 3.8-Mt KCl were produced from the Dead Sea.

4 GEOLOGIC SETTING AND MINERALIZATION

A literature search for the geology, structure, and stratigraphic history of the Dead Sea Area in Jordan reveals an extensive bibliography, with evolving theories from the middle of the last century to present day. Those authors depended on extensive fieldwork and bio-stratigraphic studies, a brief summary of which is presented herein. A complete bibliography of reviewed literature is provided in Section 12, References.

Jordan is north of the ANS. Precambrian basement crops out in southern Jordan and is overlain by accreted terrains, followed by uplift, erosion, and localized intrusive, volcanic, and volcaniclastic depositions (Aqaba Complex) (Figure 4-1). The subsequent Ram Group, of the Lower and Middle Cambrian Period, was deposited on the peneplane surface; it is predominantly fluvial siliciclastic originating from the basement and includes pulses of marine siliciclastic and carbonates (Powell et al. 2014). It is worth noting the Ram Group is an important regional aquifer. The syn-rift Cretaceous to Eocene succession in central and south Jordan is characterised by passive continental margin depositional sequences, which transition upwards from alluvial/paralic to shallow carbonate shelf and pelagic ramp systems (Powell and Moh'd 2011).

The Dead Sea Basin is a "pull-apart" basin formed between sinistral, left-stepping en-echelon faults. It lies within the Dead Sea Rift, which originated in the Late Oligocene/Early Miocene Epochs. The Lisan Peninsula is situated in the Dead Sea Basin within the Dead Sea area that extends from Lake Tiberias to the Dead Sea in central-west Jordan and is believed to have formed in the Quaternary Period as the result of basin trans-tension and subsidence. Connection to the Mediterranean Sea allowed for evaporite deposition, which was severed in the Pliocene Epoch by continued uplift in the Rift. The Dead Sea was not connected to the Gulf of Aqaba to the south due to uplift separating the areas (Al-Zoubi and ten Brink 2001).

The modern Dead Sea formed as Lake Lisan shrank due to evaporation leaving broad beach terraces (Bandel et al. 2016). The area is dominated by karst due to drawdown and groundwater dissolution along the evaporite facies. The currently defined Project exploration area under consideration and the Lisan Peninsula shoreline in 1954 are shown in Figure 1-1.

Potash mineralization in the Lisan Peninsula is representative of an extreme concentration of hypersaline shallow sea environments. Potassium mineralization is almost exclusively sylvite and carnallite. The depositional environment is a basin isolated from open marine conditions by the rift walls, and faulting and uplift that isolated the Dead Sea area, thereby restricting inflow, which increased density and salinity.

4.1 Regional Stratigraphy

The stratigraphic interpretation of Jordan has evolved from early oil and gas exploration, field work, age dating, and biostratigraphic analysis. The published literature documents in detail, the age, description, and depositional history of the region; a summary of that work represents current theory as to age and placement (Figure 4-2) (MEMR NRA 1987 and 1988; MEMR Geology Directorate 2018).

The regional stratigraphy is divided into pre- and syn-wrench sediments (Porosity Ltd 2009). Pre-Wrench is from the Cambrian to Early Cretaceous Periods to the Miocene Epoch and are dominated by asymmetrical basin fill from a series of erosional events and shallow

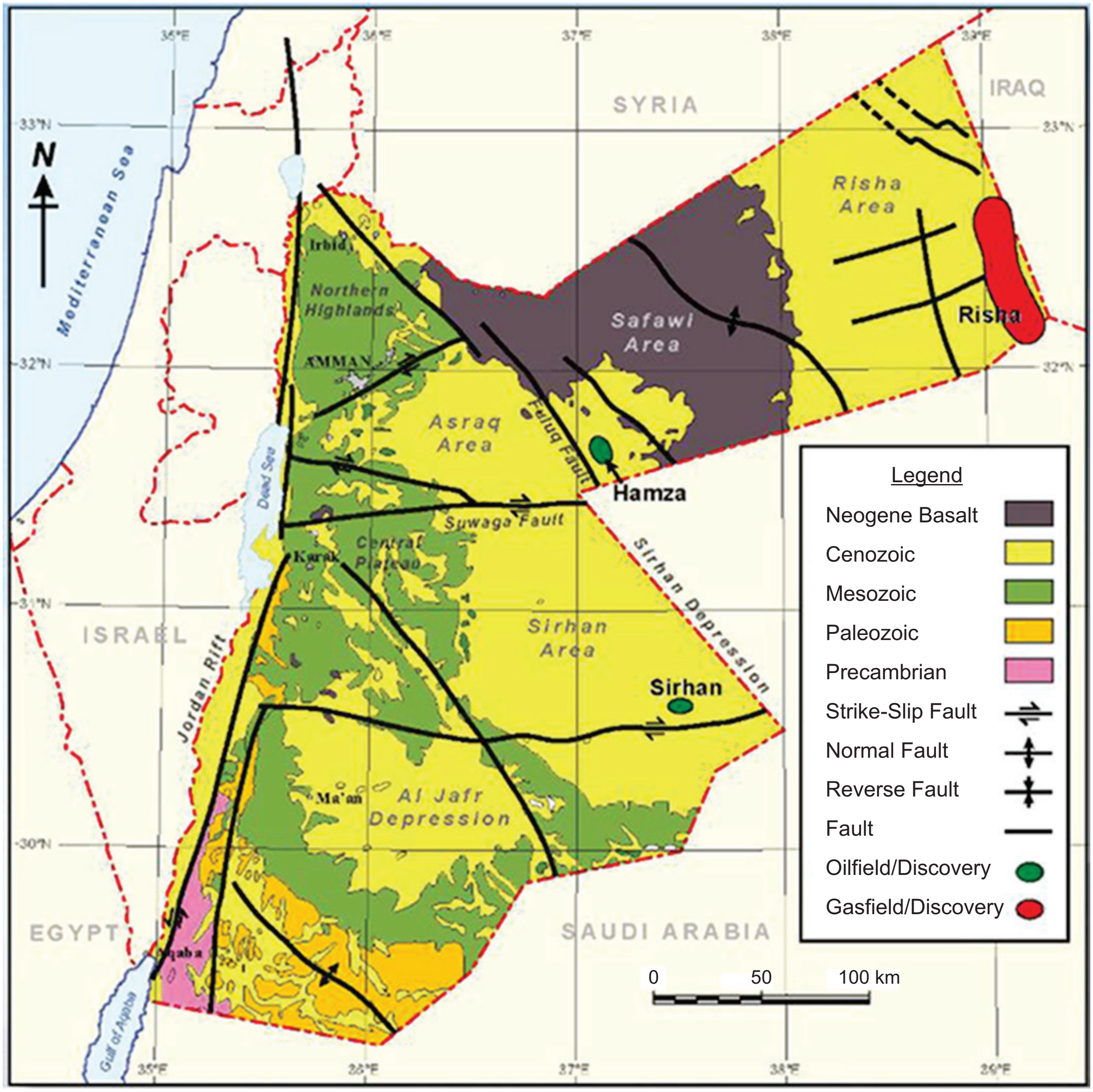

Figure 4-1. Simplified Geological Map of Jordan (after NRA 2006, in Naylor et al. 2013)

Sea environments. The Cambrian derives from the Pre-Cambrian granitoid basement deposited on a peneplane surface, with the clastics showing increased maturity over time. The Early Cambrian (Salib Formation) is made up of pebbly sandstones and conglomerates from high-energy fluvial deposits with minor marine influences. By the mid-Cambrian (Burj Formation and Umm Ishrin Sandstone), a north-flowing high-velocity fluvial system was followed by a marine sequence triggered by a sea level rise. Late Cambrian to Ordovician deposits are not found in the general area (Powell et al. 2014).

The overlying and unconformable Permian to Triassic sediments are characterized by transitioning alluvial to marginal marine and marine that are characterized by red-bed alluvial lithofacies deposited in a humid-tropical climate by low-sinuosity rivers, and overlain by

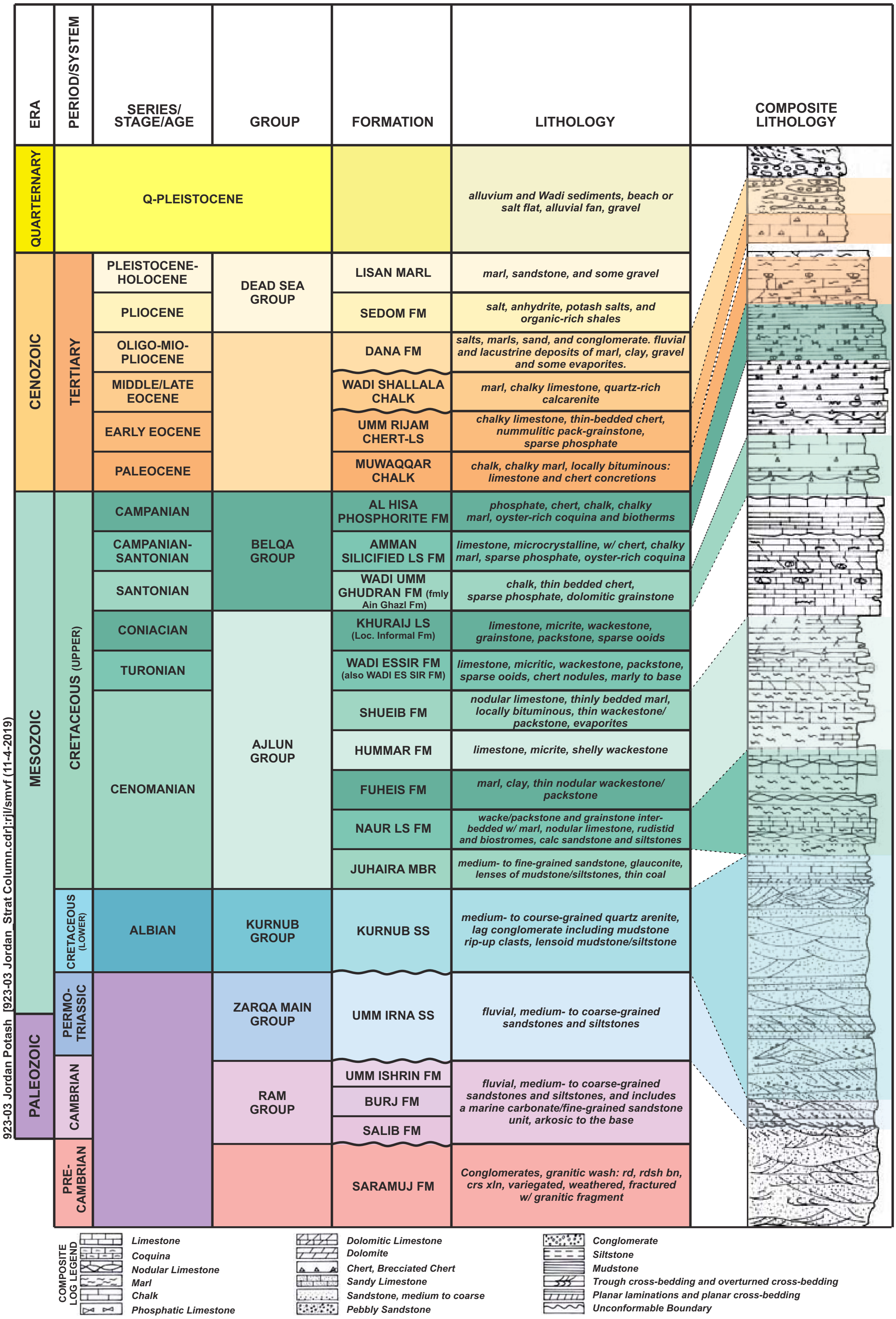

Figure 4-2. Stratigraphic Column for the Dead Sea Area (after MEMR NRA 1987 and 1988; MEMR Geology Directorate 2018; Closson 2011; Powell et al. 2016)

shallow marine siliciclastics with thin carbonates and ripple cross-laminated siltstones and sandstones with desiccation cracks marking the initial Triassic marine transgression in the region. In the Dead Sea area, this is the Umm Irna Sandstone (Powell et al. 2016).

The mid- to Late Cretaceous Period to Tertiary Miocene Epoch to present day syn-rift deposits consists of three major sedimentary groups: Kurnub, Ajlun, and Belqa. The Cretaceous Kurnub Sandstone Group is fluvial quartz arenite, and unconformably overlies the Permo-Triassic boundary. Shallow marine influences with higher sedimentation rates in the Dead Sea area are attributed to the continued subsidence to the Neo-Tethys Basin and transgression from the north and west.

The Ajlun Group (Late-Albian/Cenomanian to Mid-Coniacian) consists of shallow marine carbonates with marine fluvial siliciclastics at the base in the south and east and minor fluvial siliciclastics and peritidal evaporites resulting from transgression.

The Late Cretaceous–Eocene Belqa Group consists mainly of chalk, chalky marl, chert, and phosphorite sands deposited in a pelagic or hemi-pelagic ramp setting (Read 1985; Burchette and Wright 1992). The phosphate consists of pellets, fish teeth, and bone fragments. This is a largely transgressive sequence with localized sabkha evaporites and nearshore fluvial siliciclastics to deeper shelf mudstones and limestones. The base is a regional disconformity.

Flooding during the early Tertiary Period resulted in the deposition of the Muwaqqar Chalk Marl (MCM) (Paleocene) as dark, chalky marl with basal phosphatic grains and some limestones. Bitumen may be present and oil shales are well developed. For most of the Eocene Epoch, the area remained below the sea surface in a similar environment, noted by paleontological changes from ammonites in the MCM to burrow structures and other bioturbation in the Early Eocene aged Umm Rijam Chert-Limestone (URC) (also the Taqya Formation in the north), consisting of darker chalky marl. The Wadi Shallala Chalk (WSC) (Middle/Late Eocene) represents a transition to lighter colored and white chalk with basal oyster beds and flinty concretions (Bandel and Salameh 2013).

Along the Dead Sea margin, the Dana Conglomerate (Oligocene–Neogene) overlies the Ajlun Group. Within the Dead Sea Basin, continued syn-sedimentary extensional rifting results in facies changes from conglomerate to marl and sand and salt from fluvial to lacustrine to deeper water.

The Sedom Formation (also called Amora or Gomorra) (Wyllie 1931; Zak 1967) consists of rock salt with lamina of silt and gypsum. The Sedom Formation is the potash-hosting formation in the Project area. In the Dead Sea Basin, it may be shallow in depth within the Lisan Peninsula and crops out in Mount Sedom on the western side of the Dead Sea, in a smaller salt dome. The Sedom lagoon developed into the Lisan Lake after being cut off from the Mediterranean Sea. The late Pleistocene Lisan Marl is thinly laminated marl with gypsum, cross-bedded calcarenite sand, and oolites deposited in the saline lake. Facies change to gravel in the regression deposits at the lake edges.

4.2 Regional Structure

The African Plate formed at the collision of the Gondwana supercontinent and Eurasia. By the late Eocene, the Tethys Sea regressed to form the modern Mediterranean Sea, and the area now representing Jordan became terrestrial. The Late Oligocene transgression flooded northern Jordan, and the developing Jordanian Rift collected largely clastic sediments shed from the surrounding highlands from the east. Within the Rift, hypersaline brines were deposited and subsequently covered by additional terrestrial deposits (Bandel and Salameh 2013).

The Dead Sea Basin is a "pull-apart" basin formed between sinistral, left-stepping en-echelon faults. It lies within the Dead Sea Rift which originated in the Late Oligocene/Early Miocene. The northern part of the Basin holds the Dead Sea, a hypersaline lake ranging from a depth of 720-m below sea level (bsl) to 410-m bsl. To the east is the Wadi-Araba Fault, defining the boundary between the Precambrian Basement to the east and Basin fill to the east. To the west are the Western Border Fault and parallel Sedom Fault, shown in Figure 4-3.

Historical interpretations of the salt from geophysical studies (Figure 4-4) have mapped structure on the top and bottom of salt showing a north-northeast (NNE) to south-southwest (SSW) axis of deformation that includes the Lisan Peninsula and the much smaller Sedom Diapir. Newly reprocessed seismic data confirms this structural trend of the axis of the Diapir on the Peninsula. In the historical seismic interpretation, sediments are shown to have subsided away from the edges of both diapirs (Lisan and Sedom) to form salt-withdrawal basins or rim synclines (a reflection event that emphasizes the subsidence of the rim syncline marked by "RS") (Figure 4-5).

4.3 Property Geology

The Lisan Peninsula is a salt diapir within the Dead Sea Basin. It is bound by faulting on the east and west as shown in Figure 4-3. The salt is estimated to be 5 to 7 km thick (Western Geophysical 1994). Two SSE–NNW subparallel sinistral (left-lateral movement strike slip) en-echelon faults are present to the east, which define the Dead Sea Rift basin margin. They are the Ghor-Safi and Wadi-Araba fault zones. To the west, the Lisan Peninsula is bound by the Sedom and Western Border faults. The Sedom fault defines the NNW–SSE flexing that created the Lisan Peninsula and to the south the Sedom diapirs. The east-northeast (ENE) to west-southwest (WSW) En Gedi fault to the north and the subparallel Boqeq fault to the south of the Lisan Peninsula are mapped and inferred from seismic studies (Al-Zoubi ten Brink 2001).

The diapir is roughly 13 km × 10 km, with an estimated maximum depth of 7.2 km. The axis of the diapir is proximate to the historical Lisan-1 and NRA-3 drillholes (Section 5). The top of the diapir is near the surface and may be represented by the dissolution of salt and the formation of a salt crust of gypsum, anhydrite, and remnant clastic units.

4.3.1 Stratigraphy

The formation of interest in the Lisan Peninsula is the Sedom Salt, host to the potassium salts. The Pliocene Sedom Formation, formed by evaporation and deposition, in a hypersaline lake in the extensional basin. Sediments are halite interbedded with gypsum, marly chalk, dolomite, and shale. The Peninsula consists of the diapiric Pliocene Sedom Formation evaporites and the overlying Pleistocene Lisan Formation (Lisan Marl) composed of continental lacustrine and fluvial sediments with some marine influence (Bandel et al. 2016). The Lisan Formation covers most of the Lisan Peninsula. Potash was precipitated before the salt deformation.

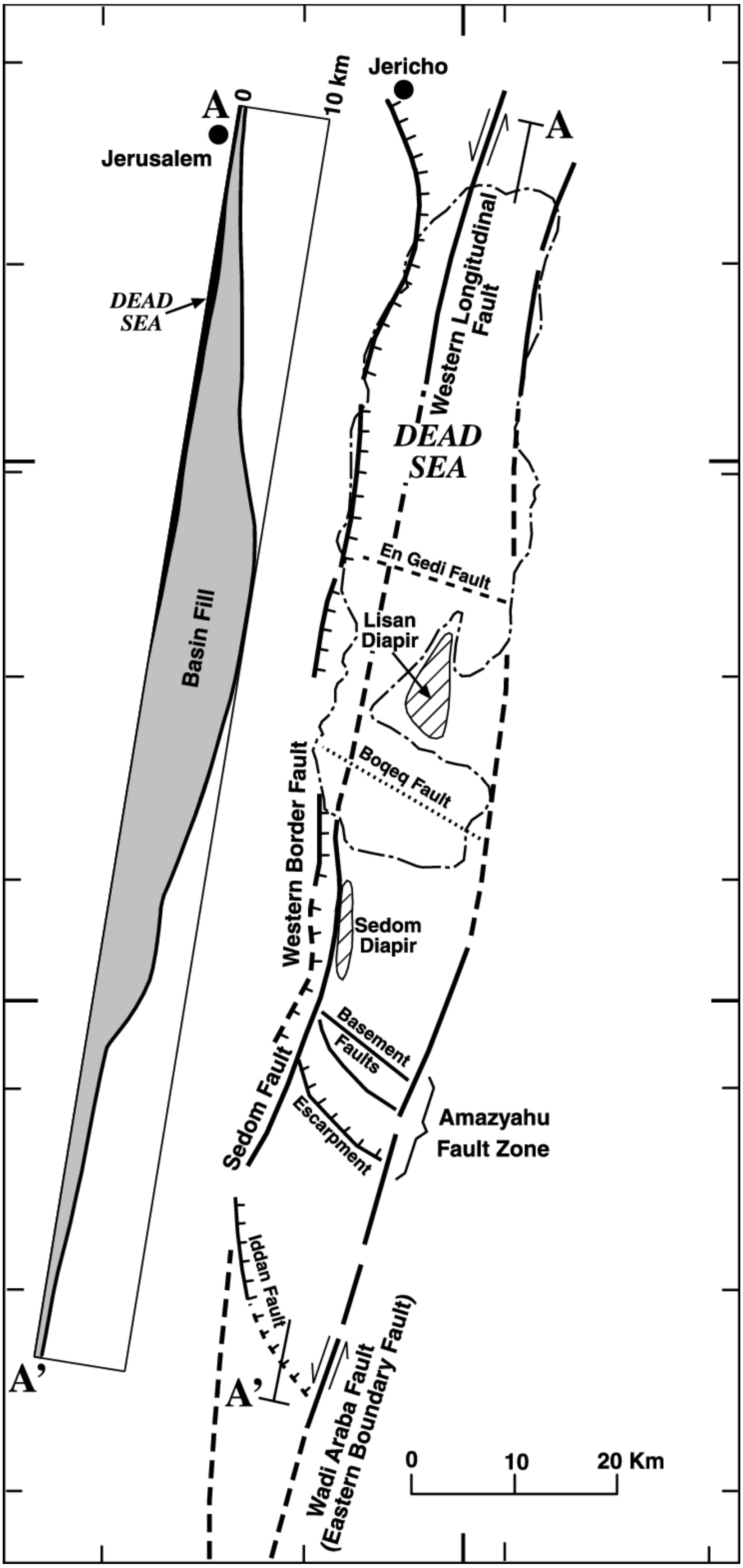

Figure 4-3. General Tectonic Structure of the Dead Sea Basin with Major Faults (Al-Zoubi and ten Brink 2001)

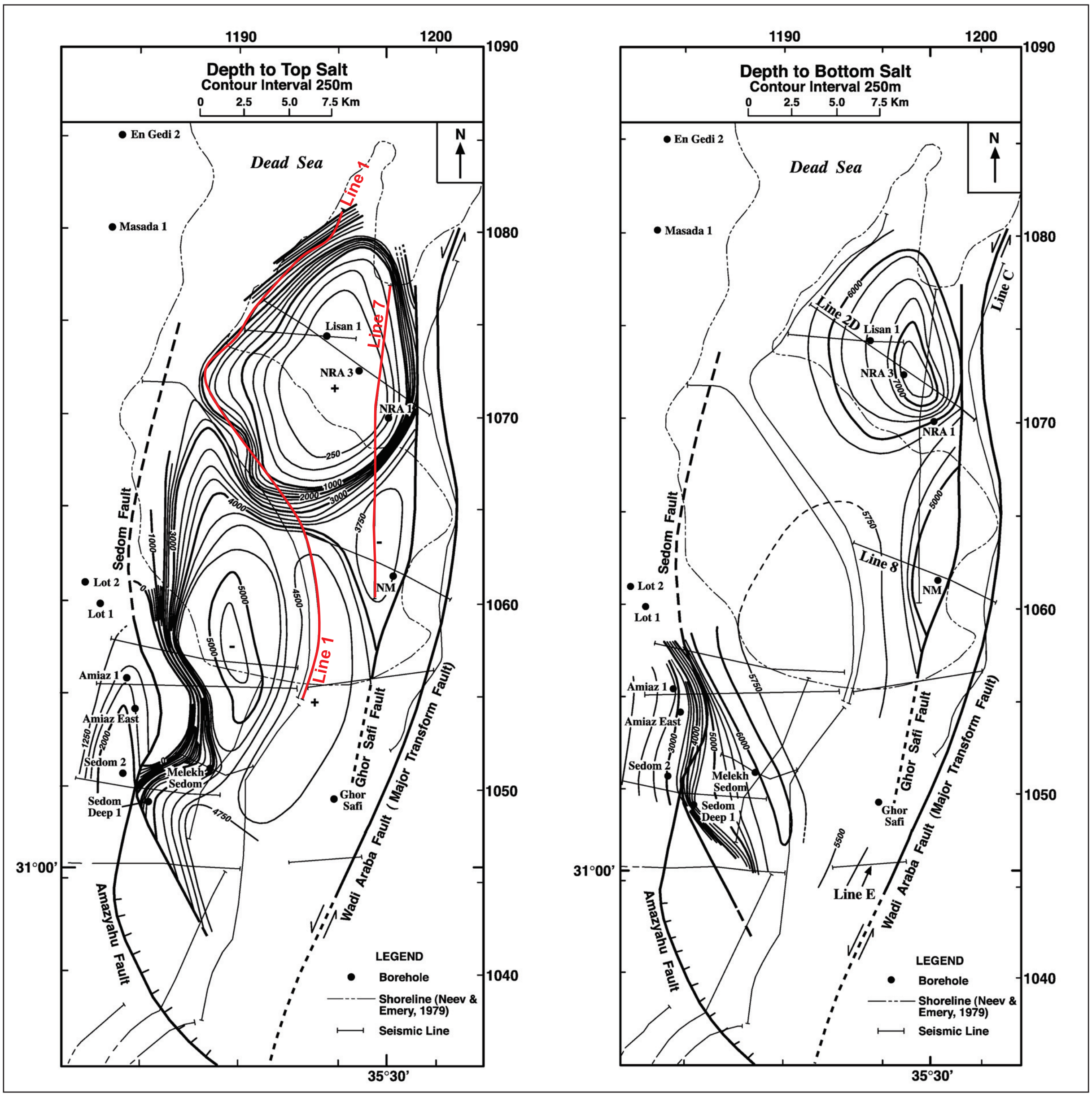

923-03 Jordan[923-03 Fig 8-1 Seismic Plan View.cdr]rjl(10-9-2019)

Figure 4-4. Seismic Plan View of the Lisan Peninsula Area showing Interpreted Historical Top and Bottom of the Salt Diapir (after Western Geophysical 1994)

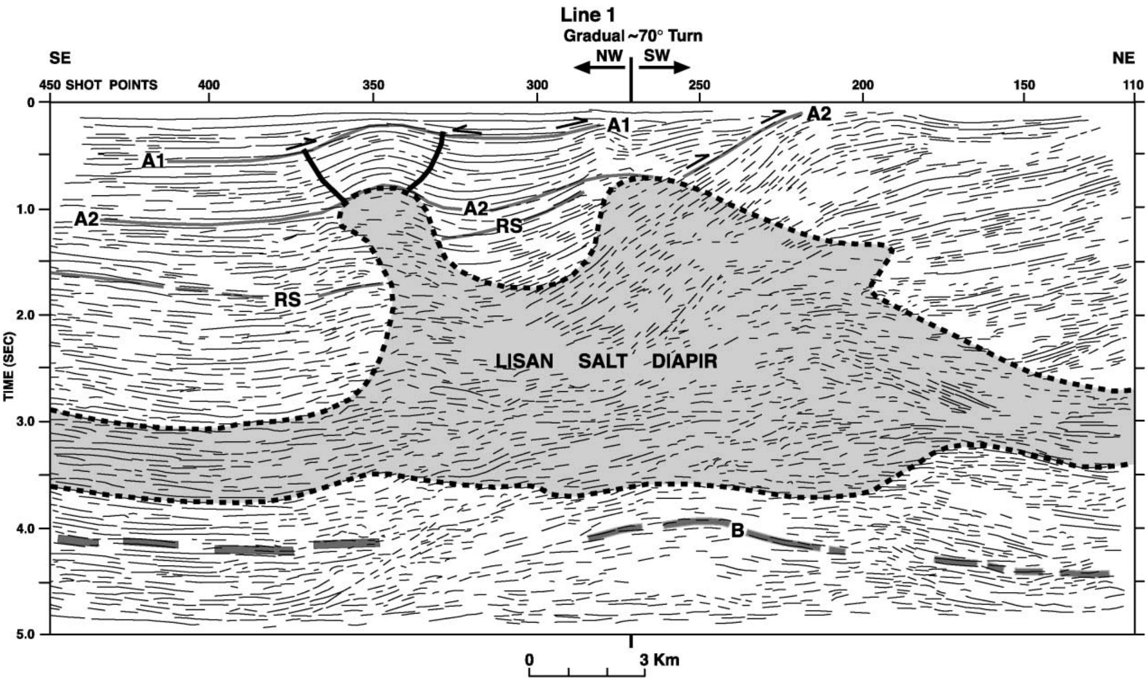

Figure 4-5. Historical Interpretation of Salt Diapirs in the Dead Sea Basin – Line 1 (Al-Zoubi and ten Brink 2001)

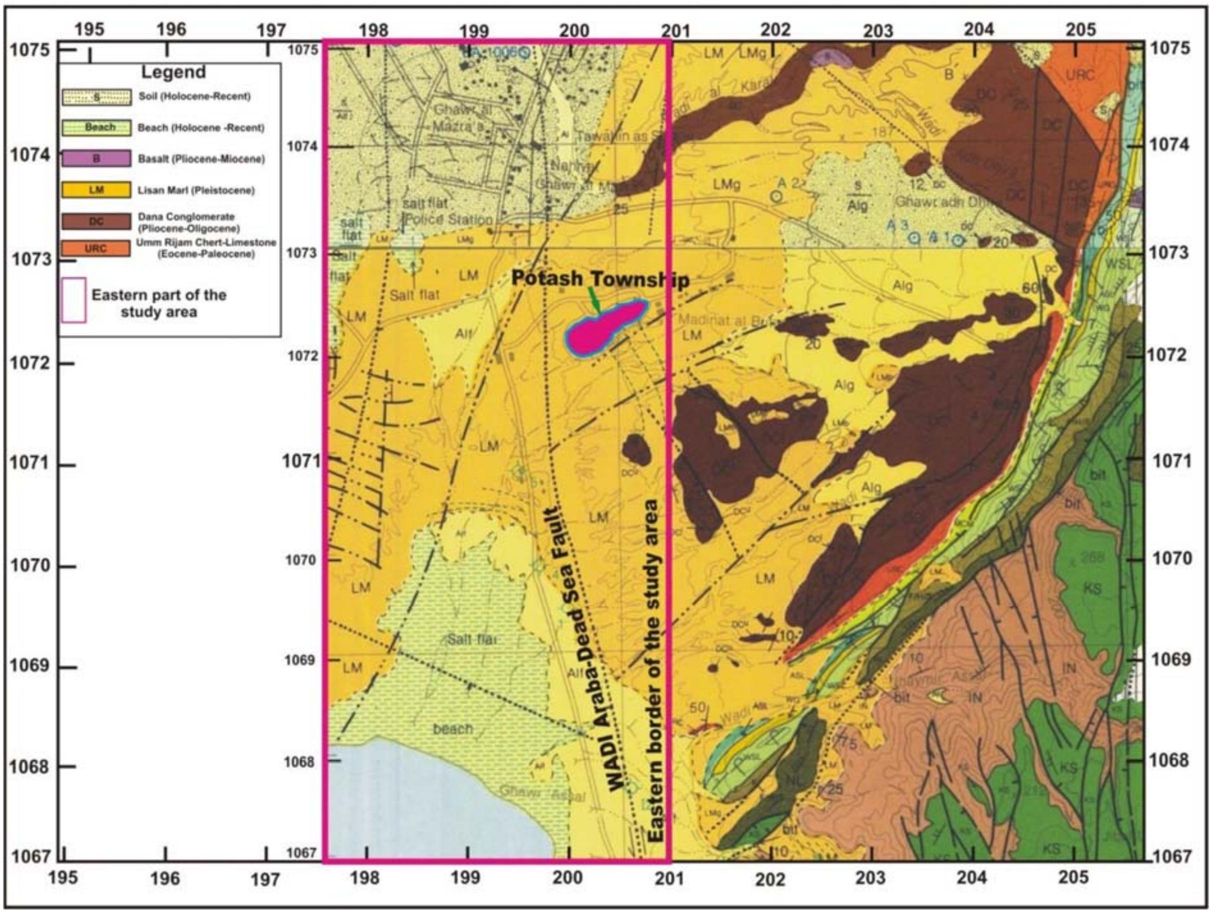

Figure 4-6. Geology Map of the Eastern Part of the Lisan Peninsula Area (MEMR Geology Directorate 2015)

The Oligocene-Miocene Dana Formation has salt beds as well as coarser clastic sediments, including conglomerates. The Formation lies on the flanks of the structure and represents early salt accumulation within the Dead Sea Rift.

4.3.2 Structure

The Wadi-Araba (Dead Sea) fault is N–S and NNW–SSE trending, very close to the southern part of the Dead Sea with vertical displacement of about 2,000 m towards the west. On the Lisan Peninsula, the fault is masked by up to 30 m of Lisan Marls draped over most of the Peninsula but marks the eastern bound of the salt deposition against older Cambrian siliciclastics and the Precambrian basement (Figure 4-7, MEMR Geology Directorate 2015).

The Lisan Peninsula has relief of no more than 50 m and large parts have karst-generated sinkholes developing due to drawdown of the Dead Sea. The axis of the salt diapir is to the southwest.

RPS completed the correlation of geological markers to seismic events from recently reprocessed 2D and 3D seismic data. This step of reprocessing was critical in improving the geophysical data and producing seismic images. Geological guidance from well data was provided by AAI and enabled the identification and mapping potential of potash-bearing zones. Depth structure maps were derived from the seismic data and well-based geology.

The new seismic interpretation may show onlapping zones as Sedom salt, which suggests continued salt deposition as the diapir developed (Section 7). This is significant as the salt beds appear relatively flattened on the flanks and crest of the anticline. While confidence in the potash picks within the salts is not certain and will need to be field checked with drilling, it is noteworthy that persistent reflectors are seen at relatively shallow intervals. Discontinuity of the depth surfaces may be due to faulting. To the south, all structures are high, whereas to the north of the apex, the structures all dip rapidly to the north.

The mapped interpreted potash-bearing zones were constrained laterally and in depth. The prospective area in the northern portion of the Project area is well-defined by high confidence seismic interpretation and shows the general structure to rapidly fall off the apex of the Lisan diapir with a northerly dip. The shallower data in the southern Project area does not suggest any steep dips until below the prospective potash zone. This area is potentially more prospective than the northern area but is also considered to have low confidence in the seismic interpretation.

4.3.3 Salt Accumulation

The average dimensions of the Lisan diapir, according to interpretation of the salt dome in seismic profiles, are about 13 km by about 10 km with an average thickness of 6 km, perhaps as deep as 7 km. These dimensions give a salt volume of 780 cubic kilometers (km^3) (Al-Zoubi and ten Brink 2001).

4.3.4 Mineralization

Potash is used to describe any number of potassium salts. The minerals of interest here are sylvite (KCl) and carnallite, a potassium magnesium chloride ($KCl \bullet MgCl_2 \bullet 6H_2O$) used to produce Muriate of Potash (MOP) and magnesium chloride (MgCl). MgCl may be present as a separate mineral (bischofite) in some beds as indicated by examination of

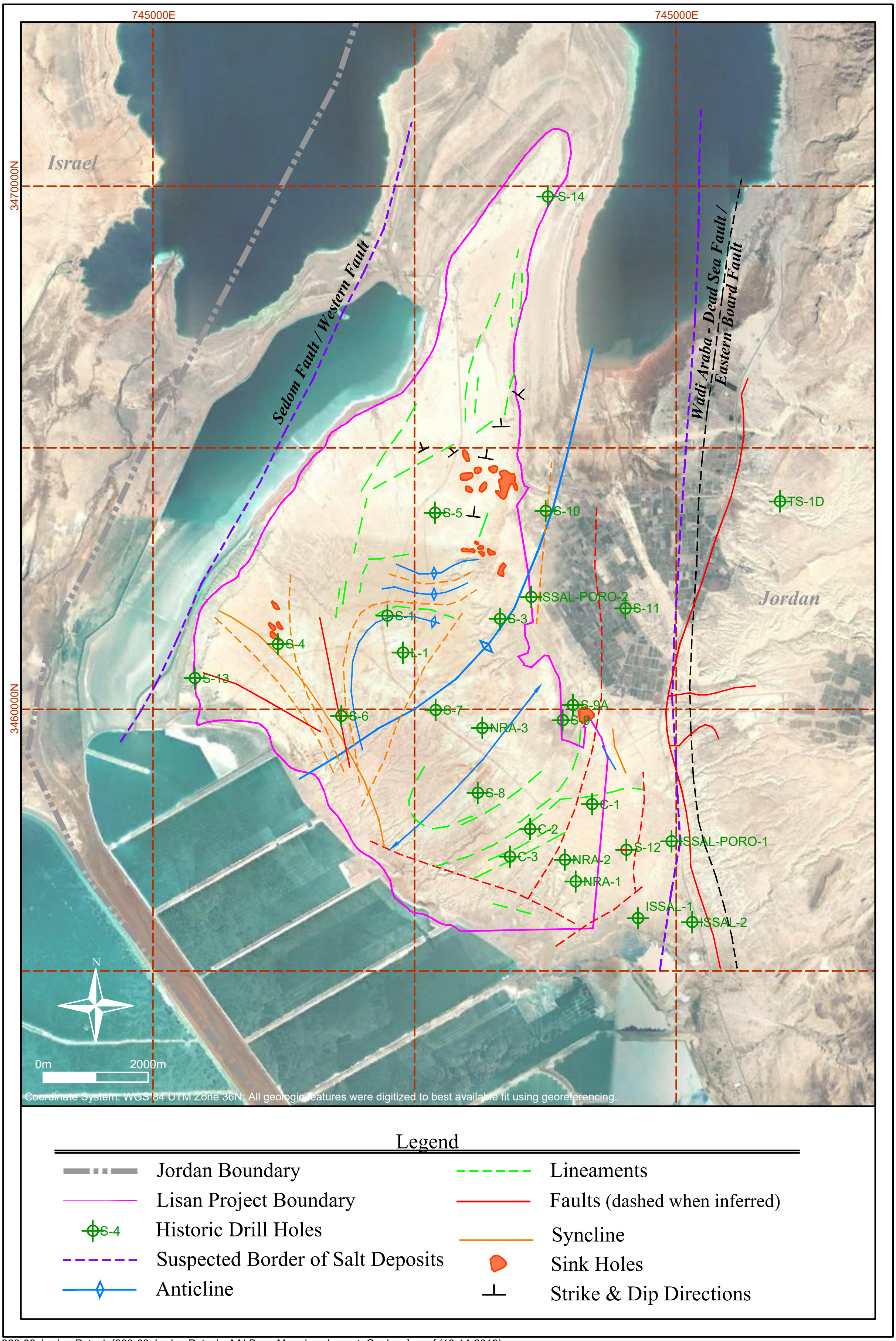

923-03 Jordan Potash [923-03 Jordan Potash_AAI Base Map.dwg; Layout: Geology]:smvf (10-14-2019)

Figure 4-7. Lisan Peninsula Area of Interest showing the Crest of the Salt Anticline and the Interpreted Border of the Salt Deposits

historical assay work and the geophysical logs. Sylvite is nominally 63 percent (%) potassium oxide (K_2O), while carnallite is 17% K_2O. Sylvinite (KCl•NaCl) is the rock form of the minerals sylvite and halite as usually found in nature. The dominant economic potash currently in production is sylvite.

KCl is the most common potassium source used in agriculture with over 90% of global production used for plant nutrition. Potash is known as MOP with a typical analysis of 0-0-60 (expressed as N-P-K: nitrogen-phosphorous-potassium) with a chemical formula of KCl. Its nutrient composition is approximately 50–52% potassium (K), 60–63% K_2O, and 45–47% chloride (Cl) (International Plant Nutrition Institute 2019).

The potash mineralization in the Lisan Peninsula is representative of an extreme concentration of hypersaline shallow sea environments. Potassium mineralization is almost exclusively sylvite and carnallite. The depositional environment is a basin isolated from open marine conditions by the rift walls, and faulting and uplift that isolated the Dead Sea area, thereby restricting inflow, increasing density, and increasing salinity. Drawdown is simple evaporation in an isolated basin resulting in brine concentration and precipitation. This is the classic "bulls-eye" model (Garrett 1996). In the case of the Dead Sea, continued extensional faulting, both isolated the basin and allowed for the continual precipitation of salts. The dominant potash mineralization is carnallite with some sylvinite. Further faulting in the narrow trough resulted in continued shedding of clastics into the basin.

A basin cut off from open marine conditions will experience drawdown by evaporation in an arid to semi-arid environment. In the absence of sediment influx, precipitation will proceed from limestone to dolomite to gypsum and anhydrite to halite. Depending on the composition and influences of the brine at that time, the remaining potassium, magnesium, sulfates, and chlorides will progress from potassium and magnesium sulfates to sylvite and then carnallite. Each cycle, in theory, represents a complete regressive and transgressive event. The ideal cycle in the vertical orientation would be a mirror of this, with the peak of evaporation represented by halite and potash sandwiched in the center of a cycle. In the Dead Sea Basin, siliciclastic units may represent a flood event on the basin edge at the base of a cycle, or a sediment influx, which breaks at the top of the evaporation cycle. These cycles are silty carbonates, anhydrites (with later partial alteration to gypsum), halite and black shale, suggesting the influence of a reflux basin. Due to the narrow nature of the Dead Sea Rift, coarser sediments of sand and conglomerates flooded into the Rift, stopping evaporite formation and potash precipitation. The vertical component, as represented by electronic logs (Elogs) and core, is a broader area of accommodation within the Basin that may be influenced by location in the medial or distal part of the Basin and/or proximity to structure and/or sediment source. In this context, the evaporites will have contemporaneous formations of anhydrite and carbonates towards the basin edge.

The formation of carnallite and sylvite are proposed as being primary and secondary, respectively. Brine chemistry will influence the precipitation of potash, i.e. availability of potassium, magnesium, sulfates, and chlorides (Williams-Stroud 1994).

It is known that calcium enrichment will trigger precipitation of sylvite, by way of sulfate depletion to gypsum ($CaSO_4 \cdot 2H_2O$) and anhydrite ($CaSO_4$). Dolomitization will result in calcium enrichment in the Dead Sea Basin by reducing the availability of magnesium for the formation of carnallite. Alternatively, exposure and erosion of dolomite and introduction into the Basin could cause magnesium enrichment resulting in carnallite precipitation. It has also been proposed that the clastic units may act as a magnesium sink in the clay structures, also resulting in calcium enrichment (Williams-Stroud 1994).

In the simplest and most direct methodology, exploration would try to identify areas of likely sylvinite and carnallite formation in the Dead Sea Basin where the salts are thickest. This method excludes the post-depositional action of the salts, which can be exceedingly mobile and are influenced by later structure and sediment loading as seen in the Lisan Peninsula. The current placement of the potash minerals within the diapir reflects that salt mobilization. The Sedom Formation has pushed into and defined the Peninsula, and the potash salt beds may be discontinuous and at high angle, broken up by the salt tectonism.

The presence and concentration of potash in the southeast part of the Lisan Peninsula and in the shallower parts of the Sedom salt is likely the result of the bias in distribution and depth of the drillholes. No deep holes exist in the western and northern part of the Peninsula so are inconclusive as to the presence of potash in those areas. Furthermore, both sylvite and carnallite are extremely soluble, especially in the case of the latter, and drilling conditions may not have been optimal to detect potash. If the drilling mud is not supersaturated with respect to potash, the mineral will partially or completely dissolve away skewing the presence, grade, and thickness information.

Bromine is a secondary mineral of economic importance to APC. Historical core assays do not quantify this information. Concentrations of 4.56 grams per liter (g/l) are reported in the Dead Sea (MEMR Geology Directorate 2015).

5 HISTORICAL EXPLORATION

Exploration on the Lisan Peninsula commenced with targeting oil and gas in the early 1960s with Phillips Petroleum Co. (Phillips) drilling a series of wells into the top of the salt diapir to further define the structure. Their initial exploration was based on decreased gravity anomalies previously mapped through a gravimetrical survey over the area.

5.1 Petroleum Drilling and Exploration

Initial petroleum exploration in the Lisan Project area was conducted by Phillips and began around the early 1960s. Their initial test wells were focused on defining the structure of the salt body within the Lisan Peninsula to determine if there were oil traps on the flanks of the diapir. Subsequent oil and gas exploration in the area recommenced in the mid-1980s and has continued with sporadic wildcat wells through the mid-2000s. Most of the exploration efforts have been focused to the flanks, primarily to the east of the salt dome, and are not within the specific Project boundaries. The Dead Sea Basin oil and gas exploration area is currently listed in an open status through MEMR with an area of 10,841 km^2 and a total of 20 wells completed for oil and gas exploration (Hashemite Kingdom of Jordan 2019). The exploration work did not result in any commercial discoveries. It is thought that the "traps' are insufficiently mature in the region to allow for economic accumulation (Western Geophysical 1994).

In addition to the oil and gas drilling, efforts were also made in the 1980s using gravity and magnetic surveys to further define the tectonic structure and target areas for seismic surveying.

5.2 Potash Drilling

Exploration for potash on the Lisan Peninsula stemmed from Phillips initial search for petroleum targets. Following Phillips exploration campaign, the NRA drilled three wells in the late-1960s intended for combined potash and petroleum exploration (NRA-1, NRA-2, and NRA-3). During the drilling of these three wells, core samples were obtained approximately every 50 m (NRA 1968).

In the mid-1980s, the NRA recommenced potash exploration in the Lisan Peninsula with four wells, C-1 through C-4, with the prospect of further defining the potash occurrences observed in the 1960s-era NRA drillholes. All four drillholes were cored and laboratory analysis for potash was conducted on selected sample intervals. No cores were made available to AAI for review. Sylvinite, carnallite and bischofite mineralization are interpreted where detailed assay results are found in the historical data. Detailed results, which are summarized later in Sections 8, include both assayed results and interpreted geophysical potash picks.

5.3 Seismic Surveys

According to the Petroleum Exploration contract areas in Jordan, the Lisan Peninsula is a part of the Dead Sea contract area. All acquired seismic data in the Project area were done for oil and gas exploration between 1982 and 1993 by four different seismic contractors.

The available historical seismic data inside the Project area consists of a total of 26 2D seismic lines and one 3D seismic survey (Figure 5-1). Not all lines were of sufficient quality to reprocess (Section 6.2).

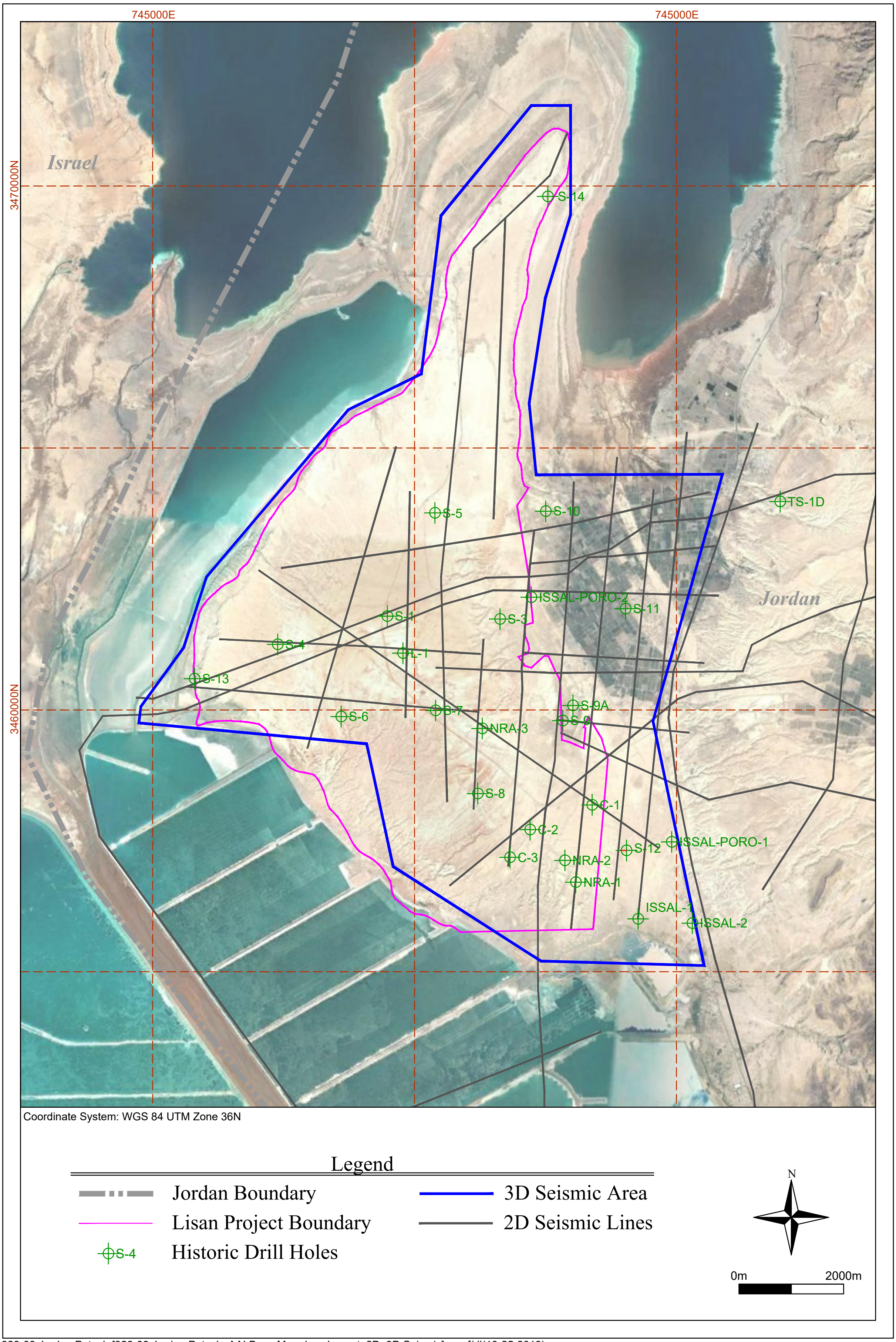

923-03 Jordan Potash [923-03 Jordan Potash_AAI Base Map.dwg; Layout: 2D_3D Seismic]:smvf/rjl(10-25-2019)

Figure 5-1. Lisan Peninsula Area of Interest showing Approximate Location of Historical 2D and 3D Seismic Coverage

6 EXISTING TECHNICAL DATA

The MEMR provided AAI with a digital data package of historical exploration works for the Lisan Peninsula and specific Project area of interest. The data encompasses previous drillhole data for oil and gas exploration along with specific potash exploration efforts. Additionally, historical 2D and 3D seismic data was provided for analysis. This section outlines an inventory and assessment of quality and adequacy of the historical data received. This section is a catalog of the data received and reviewed. Table 6-1 presents a listing of the drillholes and reviewed well records.

6.1 Drillholes

6.1.1 Inventory

Information for a total of 42 drillholes was received for review, of which 16 are located within the Project boundaries, with 5 of those 16 penetrating through potash-bearing zones. A detailed listing of the available information for each drillhole is outlined below and further summarized in Table 6-2:

1. AH-02
   a. Geophysical logs (LIS [Structured Query Logic output file], PDF [Portable Document Format], and JPEG [Joint Photographic Experts Group] formats)
   b. Core sample report (PDF)
   c. Completion and testing report (PDF)
   d. Final drilling report (PDF)
   e. Crude oil geochemistry (PDF)
2. ASH-01
   a. Geophysical logs (PDF)
   b. Drilling report (PDF)
   c. Geological report (PDF)
   d. Final well report (PDF)
   e. Formation evaluation log (PDF)
3. BH-2
   a. Composite lithology log (JPEG)
4. BH-4
   a. Composite lithology log (JPEG)
5. C-1
   a. Composited potassium chloride (KCl) assay data and lithologic strip log provided in MEMR Geology Directorate (2015) report (PDF)
   b. Geological report containing drilling operations, lithology log, chemical analysis, and x-ray and spectrographic analyses
6. C-2
   a. Composited potassium chloride (KCl) assay data and lithologic strip log provided in MEMR Geology Directorate (2015) report (PDF)
   b. Geophysical logs (LIS, PDF, and JPEG)
7. C-3
   a. Lithologic strip log provided in MEMR Geology Directorate (2015) report (PDF)

Table 6-1. Reviewed Well Records

				Coordinates (UTM Zone 36N WGS84)			
Drillhole Identifier	**Operator**	**Year**	**Purpose**	**Easting (m)**	**Northing (m)**	**Elevation (GL-m)**	**Depth (m)**
AH-02	NRA	1993	O&G	743598.8	3480181.0	-380.0	1471.0
ASH-01	Transglobal	2005	O&G	742778.7	3475638.0	-375.0	1390.0
BH-2	NRA	1993	Water	Coordinate information not verified			
BH-4	NRA	1992	Water	Coordinate information not verified			
C-1‡	**NRA**	**1987**	**Potash**	**738393.6**	**3458187.0**	**-341.0**	600.2
C-2‡	**NRA**	**1987**	**Potash**	**737207.3**	**3457713.0**	**-354.0**	1400.0
C-3‡	NRA	1988	Potash	736822.0	3457185.0	-360.0	500.0
C-4	**NRA**	**1989**	**Potash**	**737699.5**	**3455629.0**	**-385.0**	506.0
GS-01	Amoco	1972	O&G	735377.4	3435907.0	-335.0	600.0
GTZ-2D	NRA	1986	Geothermal	Coordinate information not verified			1314.0
GTZ-3D	NRA	1986	Geothermal	Redacted in well report document			1100.0
HD-01	NRA	1994	O&G	743892.4	3481539.0	-387.3	575.0
ISAAL-01	Transglobal	2001	O&G	739270.0	3456010.0	-395.0	3315.0
ISAAL-01 ST	Transglobal	2001	O&G	739270.0	3456010.0	-395.0	3315.0
ISAAL-02	Transglobal	2004	O&G	740305.0	3455930.0	-397.0	2870.0
ISAAL-PORO-1	Porosity Ltd	2008	O&G	739910.0	3457479.0	-361.0	2703.4
ISAAL-PORO-2	**Porosity Ltd**	**2009**	**O&G**	**737230.0**	**3462150.0**	**-373.0**	**4195.5**
JV-01	Phillips	1959	O&G	746147.8	3524054.0	-335.0	600.0
JV-02	NRA	1991	O&G	743210.8	3526189.0	-335.0	600.0
LISAN-01‡	NRA	1960	O&G	734777.2	3461084.0	-310.0	3672.0
NM-01	**NRA**	**1994**	**O&G**	**739076.1**	**3448075.0**	**-394.0**	2900.0
S-1‡	Phillips	1960	Exploration	734479.0	3461791.0	-310.0	306.4
S-3‡	Phillips	1960	Exploration	736631.1	3461734.0	-365.7	306.4
S-4‡	Phillips	1960	Exploration	732388.9	3461249.0	-342.8	306.0
S-5‡	Phillips	1960	Exploration	735390.1	3463760.0	-338.2	305.0
S-6‡	Phillips	1960	Exploration	733599.6	3459873.0	-346.9	109.5
S-7‡	Phillips	1960	Exploration	735404.6	3459989.0	-339.7	130.2
S-8‡	Phillips	1960	Exploration	736208.8	3458403.0	-327.0	307.0
S-9	Phillips	1960	Exploration	737831.9	3459795.0	-365.5	90.2
S-9A	Phillips	1960	Exploration	738027.7	3460085.0	-366.4	150.3
S-10	Phillips	1960	Exploration	737507.3	3463792.0	-388.3	316.1
S-11	Phillips	1960	Exploration	739028.3	3461932.0	-363.3	247.5
S-12	Phillips	1960	Exploration	739049.5	3457315.0	-373.4	193.2
S-13‡	Phillips	1960	Exploration	730801.2	3460597.0	-373.0	316.0
S-14‡	Phillips	1960	Exploration	737545.2	3469803.0	-358.0	133.0
TS-1D	NRA	1987	O&G	741982.1	3463976.0	-300.0	632.5
TS-21	NRA	1987	O&G	Not provided in well report			62.0
WGB-01	Amoco	1989	O&G	726016.7	3404056.0	-335.0	600.0
WM-01	Transglobal	1999	O&G	743979.9	3480263.0	-306.0	627.0
WM-02	Transglobal	2005	O&G	742778.7	3475638.0	-375.0	1390.0
NRA-1‡	**NRA**	**1967**	**Potash**	**738082.1**	**3456710.0**	**-362.0**	1346.0
NRA-2‡	**NRA**	**1967**	**Potash**	**737873.7**	**3457126.0**	**-360.0**	1014.0
NRA-3‡	**NRA**	**1968**	**Potash**	**736292.7**	**3459646.0**	**-337.0**	1345.0

Bold typeface: Drillhole containing potash intervals
‡ Drillhole within project boundary

Table 6-2. Summary of Drillhole Data

Drillhole Identifier	Composite and Master Logs (Mud Logs)	Lithologic Logs	Geophysical Logs: GR	NPHI	DT	RHOB	CALI	PE	Temperature Data	Well Logs (LAS & LIS Format)	Well Reports, Drilling & Completion	Well Reports, Final Geological Reports	Geological & Geochemistry Reports	Deviation Survey	Assay Data*
AH-02	x	x	x	x	x	x	x	x	x	x	x	x	x	x	
ASH-01	x	x	x	x		x	x	x	x	x	x	x	x	x	
BH-2		x	x		x										
BH-4		x	x		x										
C-1ǂ		x	x												x
C-2ǂ		x	x	x	x	x	x	x	x	x					x
C-3ǂ		x													
C-4		x	x									x			x
GS-01											x				
GTZ-2D		x							x		x				
GTZ-3D									x						
HD-01	x	x	x	x		x	x	x	x	x	x	x	x	x	
ISAAL-01		x	x	x		x	x	x	x	x	x	x	x	x	
ISAAL-01 ST	x	x							x			x			
ISAAL-02	x	x	x	x		x		x	x		x	x	x	x	
ISAAL-PORO-1	x	x	x	x	x	x	x	x	x	x	x	x	x	x	
ISAAL-PORO-2	x	x	x	x	x	x	x	x	x	x		x	x	x	
JV-01	x	x	x	x			x				x	x		x	
JV-02		x													
LISAN-01ǂ			x	x			x			x					
NM-01	x	x	x	x	x	x	x		x	x	x	x	x	x	
S-1ǂ															
S-3ǂ															
S-4ǂ															
S-5ǂ															
S-6ǂ															
S-7ǂ															
S-8ǂ															
S-9															
S-9A															
S-10															
S-11															
S-12															
S-13ǂ															
S-14ǂ															
TS-1D		x	x	x		x	x	x	x	x			x		
TS-21															
WGB-01	x	x	x	x	x	x	x	x	x		x	x	x	x	
WM-01	x	x	x		x		x		x	x		x			
WM-02			x	x	x	x	x	x	x		x	x		x	
NRA-1ǂ	x	x	x												x
NRA-2ǂ		x	x												x
NRA-3ǂ		x	x												

O&G = oil and gas; GR = gamma ray; NPHI = neutron; DT = sonic log; RHOB = density; CALI =Caliper; PE = photo electric ǂ Drillhole within Project boundary

8. C-4
    a. Composited KCl assay data and lithologic strip log provided in MEMR Geology Directorate (2015) report (PDF)
    b. Geological report containing drilling operations, lithology log, chemical analysis, and x-ray and spectrographic analyses (PDF)
9. GS-01
    a. Drilling and completion report (PDF)
10. GTZ-2D
    a. Well report including stratigraphy and lithology (PDF)
11. GTZ-3D
    a. Well report including stratigraphy and lithology (PDF)
12. HD-01
    a. Geophysical logs (LIS, PDF, and JPEG)
    b. Core sample report (PDF)
    c. Drill stem test (DST) report (PDF)
    d. Final geological report (PDF)
    e. Well log evaluation report (PDF)
13. ISAAL-01 and ISAAL-01-ST (Sidetrack)
    a. Geophysical logs (LIS and PDF)
    b. Final well report (PDF)
    c. Composite mudlog (PDF)
    d. Final geological report (PDF)
    e. Biostratigraphy study (PDF)
14. ISAAL-02
    a. Geophysical logs (PDF and TIFF [Tagged Image File Format])
    b. Formation evaluation report (PDF)
    c. Geologic prognosis report (PDF)
    d. Composite mudlog (PDF)
    e. Biostratigraphy report (PDF)
    f. Final geological report (PDF)
    g. Final well report (PDF) (TransGlobal Petroleum Jordan 2005)
    h. Final drilling report (PDF)
15. ISAAL-PORO-01
    a. Geophysical logs (LAS [LASer])
    b. Composite mudlog (PDF)
    c. Final well report (PDF)
    d. DST report (PDF)
    e. Petrophysical evaluation report (PDF)
    f. Petrographic study (PDF)
    g. X-ray diffraction analysis (PDF)
    h. Bio-stratigraphic comparison (PDF)
    i. Stratigraphic correlation (PDF)
    j. Structural correlation (PDF)
    k. X-ray fluorescence analysis (PDF)
    l. Biostratigraphy study (PDF)
    m. Biostratigraphic report (PDF)
    n. Daily drilling reports (PDF)

16. ISAAL-PORO-02
    a. Geophysical logs (LAS)
    b. Biostratigraphy study (PDF)
    c. Composite mudlog (PDF)
    d. Final well report (PDF)
    e. X-ray diffraction report (PDF)
17. JV-01
    a. Geophysical logs (PDF and TIFF)
    b. Daily drilling reports (PDF)
    c. Completion and testing report (PDF)
18. JV-02
    a. Composite mudlog (PDF)
    b. Final drilling report (PDF)
19. Lisan-01
    a. Geophysical logs (PDF and JPEG)
    b. Lithology strip log (PDF)
20. NM-01
    a. Geophysical logs (LIS, PDF, and JPEG)
    b. Vertical seismic profile and report (PDF and SGY [Society of Exploration Geophysicists])
    c. Final drilling report (PDF)
    d. Well log evaluation (PDF)
    e. Composite mudlog (PDF)
21. S-1
    a. Depth to salt from MEMR Geology Directorate (2015) report (PDF)
22. S-3
    a. Depth to salt from MEMR Geology Directorate (2015) report (PDF)
23. S-4
    a. Depth to salt from MEMR Geology Directorate (2015) report (PDF)
24. S-5
    a. Depth to salt from MEMR Geology Directorate (2015) report (PDF)
25. S-6
    a. Depth to salt from MEMR Geology Directorate (2015) report (PDF)
26. S-7
    a. Depth to salt from MEMR Geology Directorate (2015) report (PDF)
27. S-8
    a. Depth to salt from MEMR Geology Directorate (2015) report (PDF)
28. S-9
    a. Depth to salt from MEMR Geology Directorate (2015) report (PDF)
29. S-9A
    a. Depth to salt from MEMR Geology Directorate (2015) report (PDF)
30. S-10
    a. Depth to salt from MEMR Geology Directorate (2015) report (PDF)

31. S-11
    a. Depth to salt from MEMR Geology Directorate (2015) report (PDF)
32. S-12
    a. Depth to salt from MEMR Geology Directorate (2015) report (PDF)
33. S-13
    a. Depth to salt from MEMR Geology Directorate (2015) report (PDF)
34. S-14
    a. Depth to salt from MEMR Geology Directorate (2015) report (PDF)
35. NRA-1
    a. Composite mud log (PDF)
    b. Composited KCl assay data and lithologic strip log provided in MEMR Geology Directorate (2015) report (PDF)
    c. Single page gamma ray log (PDF) in the NRA (1987) report on exploration for potash in the Lisan Peninsula
36. NRA-2
    a. Composited KCl assay data and lithologic strip log provided in MEMR Geology Directorate (2015) report (PDF)
    b. Single page gamma ray log (PDF) in the NRA (1987) report on exploration for potash in the Lisan Peninsula
37. NRA-3
    a. Lithologic strip log provided in MEMR Geology Directorate (2015) report (PDF)
    b. Single page gamma ray log (PDF) in the NRA (1987) report on exploration for potash in the Lisan Peninsula
38. TS-1D
    a. Geophysical logs (LISLIS, PDF, and JPEG)
    b. Composite mud log (PDF)
    c. Biostratigraphy report (PDF)
    d. Microfloral analysis report (PDF)
39. TS-21
    a. Palynological report (PDF)
40. WGB-01
    a. Geophysical logs (PDF)
    b. Composite mud log (PDF)
    c. Final drilling operations report (PDF)
    d. Final well report (PDF)
41. WM-01
    a. Geophysical logs (LIS and PDF)
    b. Composite mud log (PDF)
    c. Final drilling report (PDF)
    d. Final geological report (PDF)
42. WM-02
    a. Geophysical logs (PDF)
    b. Drilling operations report (PDF)
    c. Final geological report (PDF)
    d. Composite mud log (PDF)

6.1.2 Deviation Surveys

Deviation surveys are present for 11 of the drillholes in the data provided: AH-02, ASH-01, ISAAL-01, ISAAL-02, ISAAL-PORO-01, ISAAL-PORO-02, HD-01, JV-01, NM-01, WGB-01, and WM-01. From the surveys provided, the majority were provided as tables of single- or multi-shot survey data within the drilling reports. These surveys provide only orientation and not direction. ASH-01, ISAAL-01, ISAAL-PORO-01, and ISAAL-PORO-2 provided deviation surveys with both inclination and direction. Deviation survey data is not available for any of the drillholes located within the Project boundary.

6.1.3 Geologic Logs

A varying degree of geologic logs and geologic information are provided for the drillholes. Some information is compiled into specific geologic well reports, while other information pertaining to lithology is presented as graphical lithology logs or mud logs. The available geologic log information for each drillhole is discussed below:

1. AH-02
   a. Composite well log with basic lithologic information presented alongside the gamma ray and sonic geophysical curves
   b. Core sample report along with thin section petrography of a sandstone interval for oil and gas analysis
   c. Final lithologic log briefly describing the major rock formations present along with depicting the cored intervals and casing depths
2. ASH-01
   a. Composite mud log showing detailed lithology and descriptions, formation tops, drilling parameters, and total gas monitoring
   b. Final geological report documenting all details of the drillhole geology and oil and gas shows
3. BH-2
   a. Composite lithological log briefly describing major lithology changes, highlighting formation tops, cored intervals, and casing depths plotted next to the gamma ray log
4. BH-4
   a. Composite lithological log briefly describing major lithology changes, highlighting formation tops, cored intervals, and casing depths plotted next to the gamma ray log
5. C-1
   a. Brief lithologic strip log showing basic lithology provided as a figure in the 2015 MEMR Geology Directorate report
   b. Geologic well report summarizing the drilling and coring, along with lithologic descriptions and potash assay results
6. C-2
   a. Brief lithologic strip log showing basic lithology provided as a figure in the 2015 MEMR Geology Directorate report

7. C-3
    a. Brief lithologic strip log showing basic lithology provided as a figure in the 2015 MEMR Geology Directorate report
8. C-4
    a. Brief lithologic strip log showing basic lithology provided as a figure in the 2015 MEMR Geology Directorate report
    b. Geologic well report summarizing the drilling, coring, along with lithologic descriptions and potash assay results
9. GS-01
    a. Brief description of the rock types encountered along with a description of one core recovered is contained in a drilling and completion report
10. GTZ-2D
    a. Lithology descriptions and formation tops in final well report
11. GTZ-3D
    a. Lithology descriptions and formation tops in final well report
12. HD-01
    a. Composite lithology log with brief rock descriptions and formation tops plotted next to geophysical traces
    b. Core description and thin section analysis for sidewall cores
    c. Final geologic report containing cuttings and core descriptions
13. ISAAL-01 and ISAAL-ST
    a. Composite mud log showing detailed lithology and descriptions, formation tops, drilling parameters, and total gas monitoring
    b. Final geologic report with stratigraphy and lithology descriptions
    c. Final well report with lithology descriptions and formation evaluation
14. ISAAL-02
    a. Composite mud log showing detailed lithology and descriptions, formation tops, drilling parameters, and total gas monitoring
    b. Geological prognosis report summarizing stratigraphy and lithology, drillhole conditions, and oil and gas formation evaluation
    c. Composite log plotting lithology and stratigraphy next to geophysical traces and casing details
    d. Final geologic report with stratigraphy, lithology, and correlation and structural comparison to ISAAL-01
15. ISAAL-PORO-01
    a. Composite mud log showing detailed lithology and descriptions, formation tops, drilling parameters, and total gas monitoring
    b. Petrophysical and formation evaluation for oil and gas
    c. Composite mud log showing detailed lithology and descriptions, formation tops, and drilling parameters plotted with the geophysical traces
16. ISAAL-PORO-02
    a. Lithology percentage log with respect to depth
    b. Composite mud log showing detailed lithology and descriptions, formation tops, drilling parameters, and total gas monitoring
    c. Composite mud log showing detailed lithology and descriptions, formation tops, and drilling parameters plotted with the geophysical traces

   d. Final well report with formation tops and lithology descriptions, including description of one core sample taken

17. JV-01
    a. Geologic report with lithology descriptions
18. JV-01
    a. Composite lithology log with formation tops and brief lithological descriptions
19. Lisan-01
    a. No specific geologic logs available
20. NM-01
    a. Composite log with brief lithology descriptions plotted with geophysical traces
    b. Well log evaluation report with detailed lithology and descriptions, including. crossplots and interpretation for evaporite mineral sequences
21. S-1 through S-14
    a. No specific geologic logs available
22. NRA-1
    a. Composite strip log with graphical lithology plotted next to K_2O
23. NRA-2
    a. Composite strip log with graphical lithology plotted next to the gamma ray curve
24. NRA-3
    a. Composite strip log with graphical lithology plotted next to the gamma ray curve
25. TS-1D
    a. Composite lithology log with formation tops and brief lithological descriptions plotted next to geophysical traces
26. TS-21
    a. Brief lithology descriptions for samples used for palynological testing
27. WGB-01
    a. Composite mud log showing detailed lithology and descriptions, formation tops, and drilling parameters plotted with the geophysical traces
    b. Field lithology logs within the final well report
28. WM-01
    a. Composite mud log showing detailed lithology and descriptions, formation tops, drilling parameters, and total gas monitoring
    b. Stratigraphic formation tops and detailed lithological descriptions within the final geological report
29. WM-02
    a. Composite mud log showing detailed lithology and descriptions, formation tops, drilling parameters, and total gas monitoring

6.1.4 Geophysical Logs

The available geophysical logs for the drillholes in the provided data are outlined below along with the format(s) they were provided in. Only the main geophysical logging runs and tools are summarized without specifying the specific logged depths or intervals for each drillhole.

1. AH-02
   a. Gamma ray, spectral gamma ray, caliper, density and density porosity, neutron and neutron porosity, sonic, photo electric, dip meter, casing collar locator, deviation, hole volume, resistivity and formation micro resistivity, and perforation (LIS, PDF, and JPEG)
2. ASH-01
   a. Gamma ray, density and density porosity, neutron and neutron porosity, photo electric, sonic, resistivity, casing collar locator (PDF)
3. BH-2
   a. Gamma ray (JPEG)
4. BH-4
   a. Gamma ray (JPEG)
5. C-1
   a. Gamma ray provided as one-page figure in 2015 MEMR Geology Directorate report (PDF)
6. C-2
   a. Gamma ray, caliper, sonic, photo electric, neutron porosity, density and density porosity, and spectral gamma ray (LIS, PDF, and JPEG)
7. C-3
   a. No geophysical data available
8. C-4
   a. Gamma ray log provided as a single page figure within the well completion report (PDF)
9. GS-01
   a. No geophysical data available
10. GTZ-2D
    a. Porosity and resistivity logs as excerpts within well completion report (PDF)
11. GTZ-3D
    a. Porosity and resistivity logs as excerpts within well completion report (PDF)
12. HD-01
    a. Gamma ray, density and density porosity, neutron and neutron porosity, photo electric, sonic, resistivity and formation micro resistivity, deviation, and borehole volume, (LIS, PDF, and JPEG)
13. ISAAL-01 and ISAAL-01-ST (Sidetrack)
    a. Gamma ray, neutron and neutron porosity, density, photo electric, caliper, and dip meter (LIS and PDF)
14. ISAAL-02
    a. Gamma ray, neutron and neutron porosity, density, photo electric, caliper, and resistivity (PDF)
15. ISAAL-PORO-01
    a. Gamma ray, spectral gamma ray, neutron and neutron porosity, density, photo electric, caliper, sonic, cement bond, casing collar locator, deviation, and resistivity formation micro resistivity (LIS and PDF)

16. ISAAL-PORO-02
    a. Gamma ray, spectral gamma ray, neutron and neutron porosity, density, photo electric, caliper, sonic, cement bond, casing collar locator, deviation, and resistivity and formation micro resistivity (LIS and PDF)
17. JV-01
    a. Gamma ray, neutron, caliper, resistivity, spontaneous potential (PDF and TIFF)
18. JV-02
    a. No geophysical data available
19. Lisan-01
    a. Gamma ray, neutron, caliper, resistivity, and spontaneous potential (PDF and JPEG)
20. NM-01
    a. Gamma ray, spectral gamma ray, neutron and neutron porosity, density, photo electric, caliper, sonic, dip meter, resistivity, casing collar locator and perforations, and vertical seismic profile (LIS, PDF, JPEG, SGY)
21. S-1 through S-14
    a. No geophysical data available
22. NRA-1
    a. Gamma ray log as single page figure in 1987 potash exploration program report (PDF)
23. NRA-2
    a. Gamma ray log as single page figure in 1987 potash exploration program report (PDF)
24. NRA-3
    a. Gamma ray log as single page figure in 1987 potash exploration program report (PDF)
25. TS-1D
    a. Gamma ray, caliper, neutron, density, photo electric, resistivity (LIS, PDF, and JPEG)
26. TS-21
    a. No geophysical data available
27. WGB-01
    a. Gamma ray, caliper, neutron, sonic, density, photo electric, spontaneous potential, and resistivity (PDF)
28. WM-01
    a. Gamma ray, spectral gamma ray, caliper, neutron, sonic, density, photo electric, , spontaneous potential, resistivity, variable density, and dip meter (LIS and PDF)
29. WM-02
    a. Gamma ray, caliper, neutron, sonic, density, photo electric, and resistivity (PDF)

6.1.5 Stratigraphic Correlations

Stratigraphic and structural correlations were presented in the dataset obtained for the ISAAL-01, ISAAL-02, and ISAAL-PORO-01 drillholes. The correlation performed here broadly links the major formation tops between the three drillholes and presents a through-fault generating offset between ISAAL-01 and ISAAL-02. Three section correlations are given for the stratigraphic units with the datum placed at different formation tops.

Additional cross sections exist within the 2015 MEMR Geology Directorate report showing the top of the salt and Lisan Marl Formation in sections across the Lisan Peninsula. Different potash beds or seams are listed here but are not correlated to one another in the graphical sections.

6.1.6 Assays and Composites

Historical laboratory chemical analysis data for potash determination conducted by the NRA for drillholes C-1 and C-4 was included in the provided dataset. The primary analysis was for calcium (Ca), magnesium (Mg), sodium (Na), potassium (K), and chloride (Cl) to be used for determining KCl. Sampling intervals for C-1 were approximately 5 m and sampling intervals for C-4 ranged from 1 to 3 m. Additionally, x-ray diffraction was performed on select samples to verify mineralogy.

Composite assay results are provided in the 2015 MEMR Geology Directorate report for drillholes NRA-1, NRA-2, C-1, C-2, and C-4. A total of 17 composited KCl intervals are listed with two in each drillhole, aside from C-4, which contains nine total composite intervals.

6.1.7 Temperature Data

Temperature data for the drillholes listed below was provided in table format for specific downhole points. The majority of the data was extracted from information within a drillhole or well report or recorded during geophysical logging marking the bottom-hole temperature (BHT). Temperature ranges are from 38°C at the shallowest depth reading of 394 m to a maximum of 96.1°C in ISAAL-01 at 2,940 m depth. The deepest reading was at 89.0°C at 4,195 m depth. Within the Sedom Salt, the highest temperature is recorded in ISAAL-PORO-2 at 89°C. These readings are helpful in the evaluation for solution mining as higher temperatures are generally favorable for increased solubility of potash. The temperatures are very high relative to other locations and should prove to be very favorable for solution mining.

- AH-02
- ASH-01
- HD-01
- ISAAL-01
- ISAAL -02
- ISAAL PORO-01
- ISAAL PORO-02
- NM-01
- WGB-01
- TS-1D
- WM-01
- WM-02
- C-2

Temperature data is also present in an extended form with full temperature profiles from geophysical logs over the depth profile for the drillholes below:

- ASH-01
- GTZ-2D
- GTZ-3D

6.2 Seismic

The historical Lisan Peninsula is covered by four seismic surveys; three 2D surveys and one 3D survey, listed in Table 6-1, that were completed for oil and gas exploration purposes in different years with different field geometrical configurations.

Table 6-1. Available 2D and 3D Seismic Surveys

Acquisition Contractor	Year	Type of Survey		Number of Channels	Fold	Sweep
		3D Survey	2D Lines			
CGG	1982		9	48	24	8-50 Hz/10 s
INOC	1985		12	96	24	8-60 Hz/10 s
Western Geophysical	1988		4	240	120	8-96 Hz/10 s
SSL	1993	1	1	242 (2D) 480 (3D)	60 30	8-72 Hz/10 s

Note: All surveys were done using Vibroseis
CGG = Compagnie Générale de Géophysique; INOC = Iraq National Oil Company;
SSL = Seismograph Service Limited; Hz = hertz; s = seconds

6.2.1 Two-Dimensional Surveys

Twenty-six 2D seismic lines with a total length of approximately 277 km cross the Lisan area (see Table 6-2). Those lines belong to four different vintages; lines prefixed DS were shot in 1982 by CGG and in 1985 by the INOC, while VWJ lines were shot in 1988 by Western Geophysical (see Figure 6-1). One extra Line (LIS-93-404) was shot during the same period of the 3D survey. It intersected the northern part of the 3D survey area. Some of the seismic data was provided in SEG-Y format; however, a portion of the data was only available as hard copies. All the hard-copy seismic sections (24 scanned PDFs) were digitized and transformed into standard SEG-Y[1] format, trace headers of the resulting SEG-Y files were updated with the coordinates of Common Depth Point (CDP) (WGS1984 – UTM Zone 36N), and the resulting files were loaded into the interpretation workstation.

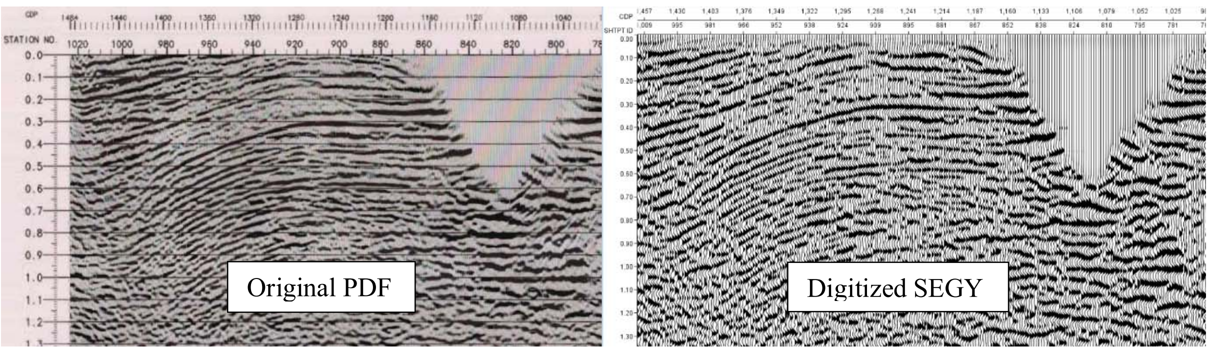

Figure 6-1. Seismic Data Before and After Digitization, Line LIS-93-404

[1] SEG-Y is one of several standard file formats developed by the Society of Exploration Geophysicists for storing geophysical data.

Table 6-2. 2D Line Listing

Vintage	Line Name	Reprocessed by Misbar	Digitized by Misbar	Length (km)	Comment
CGG (1982)	DS-01			11.2	Hard copy not available
	DS-02	✓	✓	10.5	
	DS-03		✓	13.3	
	DS-04		✓	12.8	
	DS-05		✓	31.6	
	DS-06		✓	5.9	
	DS-07	✓	✓	19.5	
	DS-16N	✓	✓	28.5	
	DS-17	✓	✓	9.6	
INOC (1986)	DS-76			2.6	Hard copy not available
	DS-76A	✓	✓	6.5	
	DS-77		✓	3.5	
	DS-77A	✓	✓	5.3	
	DS-78		✓	3.7	
	DS-79		✓	4.3	
	DS-80		✓	5.8	
	DS-80A	✓	✓	3.5	
	DS-81	✓	✓	6.8	
	DS-82		✓	9.0	
	DS-83		✓	7.8	
	DS-84	✓	✓	9.3	
Western Geophysical (1988)	VWJ-13	✓	✓	16.4	
	VWJ-14		✓	11.4	
	VWJ-15		✓	6.9	
	VWJ-16		✓	9.1	
SSL (1993)	LIS-93-404		✓	23.0	

6.2.2 Three-Dimensional Surveys

The most inclusive seismic survey in the area is the Lisan 3D survey. The Lisan 3D survey was shot during February–May 1993 and covers around 100 km^2 that comprises most of the known Lisan Peninsula area. SSL, Party 199/786, conducted two parts of the 3D Vibroseis seismic survey on behalf of the NRA.

Two different data recording geometries were used. In the north, 480 trace shots were recorded on 4 receiver lines (120 traces each) with the receiver lines laid north–south, 300 m apart. In the south, 480 trace shots were recorded on 6 receiver lines (80 traces each) with the receiver lines laid east–west, 200 m apart. The source lines were perpendicular to the receiver lines and were 200 m apart. Both receiver and source intervals were 50 m (Table 6-3).

The seismic data was processed twice before: in 1993 by Halliburton Geophysical Services (HGS) and in 2001 by Geophysical Services Center (GSC). Four 3D volumes were collected (GSC/HGS final and migrated stacks in SEG-Y format). HGS files appeared to be corrupted due to issues in their SEG-Y format, and those corrupt files were rectified and written into standard SEGY format (revision 1.0). Figure 6-2 shows a comparison between the HGS and GSC processing.

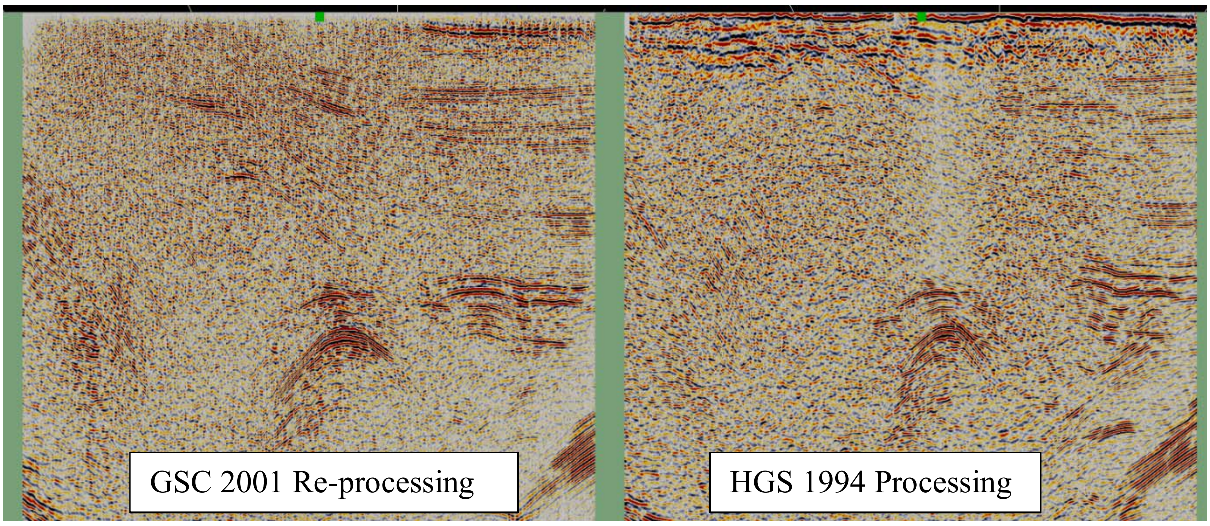

Figure 6-2. Comparison Between HGS (1993) and GSC (2001) Old Processing/XL191

6.2.3 Data Acquisition and Processing

6.2.3.1 General Comments

Rather than discuss, in detail, the legacy data acquisition and processing, RPS has provided general comments on how these items affect the current interpretation of the data. Details on the legacy data acquisition and processing can be found within the archives of the MEMR for those wishing to investigate further.

6.2.3.2 Seismic Data Acquisition

Lisan legacy 2D seismic data were acquired with deep petroleum exploration parameters consistent for 1980s level technology. Notwithstanding the generally poor- to fair-quality of the data, an important artefact in the presence of salt domes is 1) side-swipe noise for seismic profiles off any axis of symmetry and 2) salt-flank reflections. These are critical to understand as conventional 2D processing is inadequate to mitigate their presence.

In 1993, approximately 100 km^2 of 3D seismic was acquired in two separate surveys and merged together to form a single volume for interpretation (SSL 1993). Again, parameters are consistent for deep petroleum exploration. Ideally, the data would have been acquired as a single survey, but seismic technology available at the time was not adequate. The advantages of a well-designed and acquired 3D seismic survey in the Lisan area should have reduced the effect of side-swipe and salt-flank reflections with the appropriate processing. However, the acquisition on two parts limited the azimuth of the surveys and likely negated the potential benefits of the 3D data.

Typically, the 2D data will have higher resolution in both time and spatial frequency compared to 3D data. However, what 3D data loses in resolution it gains in spatial coherency and correct positioning of reflections not in line with seismic sources. Thus, there is a trade-off between coherency and resolution, and this requires the use of both 2D and 3D data for optimal interpretation.

A shortcoming that afflicts both 2D and 3D seismic data is the near-surface solution. This correction accounts for elevation and velocity variations in the near-surface which can drastically affect the imaging of deeper data. In many cases, a separate refraction survey is conducted to better constrain the near-surface solution, but this was not done at Lisan.

In summary, the legacy 2D and 3D seismic data are of consistent vintage, poor-to-fair in quality, designed for petroleum exploration, contaminated with out-of-plane noise, and may have sub-optional near-surface corrections. The advancement in processing technology offers the opportunity to re-examine these data through a new lens and to modify the processing parameters for shallow potash targets.

6.2.3.3 Seismic Data Time Processing

As part of Phase I of the Lisan Potash Exploration Project, the historical 2D and 3D seismic data were reprocessed by Misbar in Amman, Jordan with collaboration from RPS personnel in Calgary, Canada.

In Section 6.2.3.2, the near-surface solution was identified as a critical limiting factor for producing a clear subsurface image. Previous processing used a generalized linear inversion refraction statics method to solve for velocity variations in the near-surface. In contrast, Misbar applied a modern tomographic ray-tracing approach to refraction statics. The Misbar approach can provide superior results in the case where velocity variation departs from a layer-cake model. The Lisan Peninsula has topographical variations such as wadis and karsted surfaces which are not well-represented as simple horizontally stratified layers. Therefore, an uplift in imaging is expected using tomographic refraction statics.

In addition to the use of a more modern static solution, another area for leveraging the modern processing algorithms is through the use of PreSTM which would not have been available to data processors when the historical seismic data was originally processed. Processing using PreSTM of fit-for-purpose data should theoretically account for side-swipe and salt-flank reflections, as discussed in the previous section. The original post-stack migration could not account for these and resulted in images containing conflicting dips, making interpretation difficult. A second round of reprocessing used dip-moveout (DMO) plus post-stack migration, a predecessor to PreSTM. Neither of these approaches yielded an adequate image but did provide a starting point for evaluating whether PreSTM is a useful approach.

6.3 Data Adequacy for Resource Estimation

For use in potash resource estimation, drillholes and related drillhole data require verification by a Qualified Person (QP) who is certified and knowledgeable in assessing the related data. In resource reporting, typically historical data is not considered adequate for use in the resource estimation unless the QP can physically vet and verify it. Therefore, the assays and geophysical picks are not reliable for use with Mineral Resource estimation under NI 43-101 standards. However, the composites, as calculated, are applied to the Preliminary 3D Geological computer model because they provide a useful confirmation of potash targets that can be used for guiding future exploration drilling.

6.3.1 Drillholes

The drillholes and corresponding drillhole information provided are considered historical data for the purposes of determining a modern resource estimate. However, much of the data reviewed is useful in estimating a potential resource and defining an exploration target. Verification and re-analysis of any available historical drill core would be required to consider the historical data applicable to include in a modern resource estimation. The historical core and detailed associated data are not available other than what has been summarized in reports.

6.3.1.1 Depth

The depth or length of the drillholes throughout the Lisan Project area provide reasonable certainty that most observed potash occurrences are within 2,000 m of depth from surface. Within the Project bounds specifically, analyzation of the data provided shows all potash occurrences within 1,500 m of the ground surface. With respect to mineral resource estimation, a maximum depth of 1,500 m complies with current industry guidelines for solution mining to meet the requirement for establishing a reasonable prospect for eventual economic extraction of the quantified resource. The data analyzed is considered historical and not applicable to include in a modern resource estimate; however, the historical data indicates the potash occurrences over the Project area are within a suitable depth for solution mining techniques.

6.3.1.2 Location and Density

Necessary drillhole spacing for resource estimation varies greatly based on location, deposit type, and mineralogy. For industrial minerals in bedded deposits, a radius of influence (ROI) is assigned around each drillhole, with different radii corresponding to different resource classifications for the observed thickness and grade occurrences measured in the drillhole to extend laterally a certain distance. The radii used for each resource classification are dependent on the level of confidence in the geologic continuity between each drillhole combined with an assessment of the deposit type and comparison with radii used in similar scenarios. The influence, spacing, and density of the drillholes over an exploration area is then important for creating an overlapping footprint of radii for correlation of mineral grades and thicknesses.

The current historical drillholes were not designed and spaced with the intention of targeting and creating a potash resource estimate. The 1960s-era NRA drillholes and the 1980s “C” drillholes indicate the presence of potash intervals, but do not have enough corroborative data for defining specific geologic drillhole correlation throughout the extent of the area.

6.3.1.3 Deviation Surveys

Directional or deviation surveys are performed to acquire continuous measurements of the downhole dip angle and corresponding azimuth of the drillhole. These measurements are then applied during resource estimation in conjunction with the strike and dip of the mineral target to convert from an apparent dip and thickness to a true thickness. This is significant in steeply dipping deposits or highly deviated wells as the apparent and true thicknesses can vary substantially.

Some of the historical oil and gas wells near the Project area contain deviation data; however, without a dip meter log or core samples, a correction from apparent thickness to true thickness cannot be calculated. Calculation of the true vertical depth (TVD) from the deviation survey data can be made and was performed where the data was available.

6.3.1.4 Geophysical Logs

A geophysical logging suite is utilized for analysis of the borehole and the geophysical responses of the characteristic lithology. Additionally, if core samples are taken, the logs are necessary for correcting the drilled depth to the actual depth to account for drill pipe stretching and for use in selecting samples for laboratory analysis.

Downhole gamma ray logs in combination with sonic, neutron, density, and caliper logs may be used to identify the presence of potash. Naturally occurring radioactivity in the form of the ^{40}K isotope derived from the potassium in the potash beds, gives a characteristic signature that is used to estimate grade. Schlumberger chiefly advanced the correlation between gamma ray response and potassium content, beginning in the 1960s with the interpretation of Elogs in the Prairie Evaporite Formation in Saskatchewan. E. R. Crain, a Schlumberger geophysicist, furthered this work and related log response to apparent K_2O content, the customary unit of the potash industry. The established methodology developed by Schlumberger calculates K_2O%, combining gamma ray American Petroleum Institute (API) units and correcting to hole diameter (from caliper logs) and mud weight (Figure 6-3). In combination with the other logs, mineralogy may be determined. Experience has shown good agreement between the estimation when compared with assay, but cannot be considered certifiable in a resource assessment.

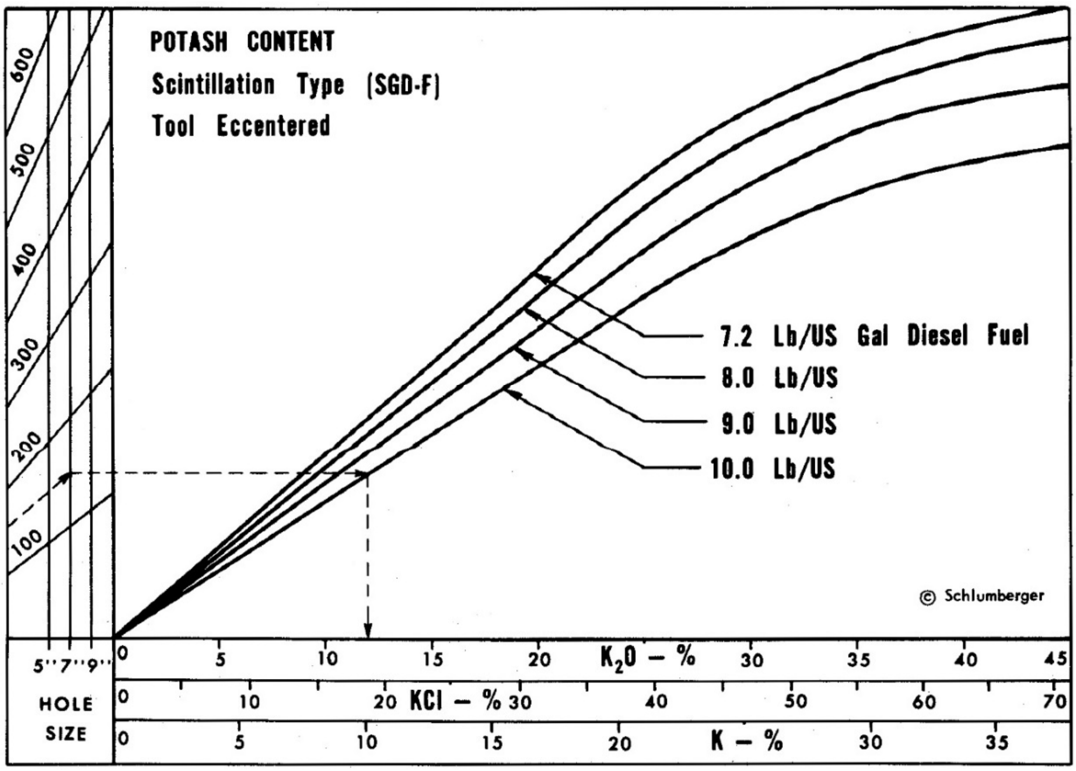

Figure 6-3. Empirical Chart Relating Gamma Ray Deflection to Potassium Content (after Schlumberger 1991; best available image)

Elogs may be influenced by any number of factors, including rock type influences, initial calibration, logging speed, temperature, borehole fluid type, and mud weight.

Caliper logging provides an indication of wash-out, which may indicate the presence of very soluble minerals, i.e. sylvinite or carnallite. A gamma reading in a washed out zone may be attenuated due to the increased hole diameter. A more complex combined mineralogy may give responses resulting in misinterpretation.

Borehole Compensated Sonic is in current use and helps to eliminate effects of hole size change. The formation density log measures electron density, which is closely related to true bulk density and is expressed in modern wells as ρu, density units in grams per cubic centimeter (g/cc). It is influenced by rock matrix density, porosity, and pore fluid density. They are most effectively performed in an uncased hole; however, modern tooling is capable of compensating for cased hole applications.

Neutron logs are generally used in the oil industry to define and determine zones of porosity by responding to the amount of formation hydrogen present. It is expressed as "effective porosity," the porosity that contains fluids. Neutron logs may be used with more than one type of porosity log (%) for greater accuracy in determining lithology. Historical logs are in API units (counts per second) and are calibrated to limestone or sandstone in a "clean" environment with oil- or water-filled pores (Schlumberger 1968).

Typical readings of log responses for evaporite minerals are shown in Table 6-3.

Table 6-3. Geophysical Values for Evaporite Minerals (after Schlumberger 1991)

Mineral	Composition	Specific Gravity (g/cc)	Log Density (g/cc)	Sonic (msec/ft)	Neutron (θN)	GNT (θN)	Gamma (API)	K_20 (%)
Anhydrite	$CaSO_4$	2.96	3.0	50	0	0	0	0
Carnallite	$KCl•MgCl_2•6H_2O$	1.61	1.6	78	65	65	200	17
Gypsum	$CaSO_4•2H_2O$	2.32	2.4	52	49		0	0
Halite	NaCl	2.17	2.0	67	0		0	0
Kainite	$MgSO_4•KCl•3H_2O$	2.13	1.1		45		225	18.9
Langbeinite	$K_2SO_4•2MgO_4$	2.83	2.8	52	0		275	22.6
Polyhalite	$K2SO_4•MgSO_4•2CaSO_4•2H_2O$	2.78	2.8	57.5	15		180	15.5
Sylvite	KCl	1.98	1.9	74	0		500	63
Calcite	$CaCO_3$	2.71	2.7	47.5	0		0	0
Dolomite	$CaMg(CaO_3)_2$	2.87	2.9	43.5	4		0	0
Limestone		2.54	2.5	62	10		5–10	0
Dolomite		2.68	2.7	58	13.5		10–20	0
Shale			2.2–2.8	70–150	25–60		80–140	0

msec/ft = millisecond per foot; θN = apparent limestone porosity from a neutron log; GNT = gamma ray/neutron

6.3.1.1 Stratigraphic Correlations

Stratigraphic correlations and assessments are important for understanding the interpretation of the regional and local geology. An evaluation of the stratigraphy is discussed in Section 4, Geologic Setting and Mineralization. The correlations given or derived from the historical data can be used as guides for aiding in the analysis of modern data that would be contributable toward a resource assessment.

6.3.1.1 Assays and Composites

The current assay and composite data from the historical core holes in the NRA and "C" series is documented in a summary report and in a couple of instances, tables of interval data were included within an overall well report. The information cannot be independently verified or validated with the physical core specimens or detailed laboratory procedures and certificates; therefore, the analytical data alone is not sufficient for inclusion in a modern resource assessment.

6.3.2 Seismic

Although the seismic acquisition techniques and parameters used were suitable for the technologies available in 1980s and 90s, the surveys were not shot for the purpose of potash exploration, which meant that the designs were optimized to image the deep targets. Moreover, an effort was made to increase the seismic energy and enhance the signal through the use of heavy source and receiver arrays.

In general, the seismic data quality varies from poor to good; the difference in quality can be attributed mainly to the recording parameters. For 2D data, better quality can be clearly seen on "VWJ-" lines where shorter trace intervals and longer offsets were used with a higher fold of 120 (Western Geophysical 1988, VWJ vintage). The INOC survey clearly has the poorest data quality due to the use of an irregular geometry (off-end shooting) and a low fold of 24. Two 2D lines are missing part of the field data and another four lines are missing the field and supporting documents.

The 3D survey was shot over the entire Lisan Peninsula following as closely as possible to the Peninsula shoreline. This meant that the outline of the 3D grid is highly irregular. The data quality in the north part is generally better than the south part; this can be attributed to geologic factors as well as to the acquisition parameters used. A total of 347 records were found to have geometry errors. See Table 6-4 for the 3D acquisition parameters.

Table 6-4. 3D Acquisition Parameters

General Parameters	South 3D	North 3D
Acquisition Contractor	SSL	SSL
Original Client	NRA	NRA
Date Acquired	February–May 1993	February–May 1993
Area (km^2)	80	14
No. of Active Stations	480	480
No. of Active Lines	6 × 80	4 × 120
Receiver Line Interval (m)	300	200
Receiver Interval (m)	50	50
Geophone Type	SM4 – 10 Hz	SM4 – 10 Hz
Geophone Array	12 × 3-arm windmill	12 × 3-arm windmill
Source Line Spacing (m)	200	200
Source Interval (m)	50	50
Nominal Fold	30	30
Source Parameters		
Source Type	Vibroseis	Vibroseis
Vibrator Type	Y2700	Y2700
Number of Vibrators	4	4
Sweep Frequency (Hz)	8-72	8-72
Sweep Type	Linear	Linear
Sweep Length (s)	11	11
No. of Sweeps per VP	4	4
Tapers	Cosine 300 ms	Cosine 300 ms
Instrumentation		
Recorder	SERCEL SN368+LXU	SERCEL SN368+LXU
Filters	Lo-Cut (OUT) HI-Cut (125 Hz, 63 db/octave)	Lo-Cut (OUT) HI-Cut (125 Hz, 63 db/octave)
Data Format	SEG-D, DEMUX, 6,250 BPI	SEG-D, DEMUX, 6,250 BPI
Sample Rate (ms)	2	2

SEG-D is a specialized format intended for field recording of seismic data.

DEMUX (demultiplexer) is a device that takes a single input line and routed it to one of several digital output lines.

ms = millisecond; db = decibel; VP = Vibration Point; BPI = Bit Per Inch

7 SEISMIC REPROCESSING AND REINTERPRETATION

7.1 Reprocessing

The Dead Sea Lisan Peninsula is considered to be one of the most challenging areas in Jordan for seismic imaging. The presence of thick surface layers of marl and clay impeded with salt/gypsum as well as an active karst system cause inhomogeneities in the surface which distorts the seismic signal; an accurate near-surface model is needed in order to correct for this distortion. Three-dimensional tomographic static solutions have an advantage compared to conventional 3D statics solutions such as Generalized Linear Inversion (GLI) and delay time. Tomographic solutions can solve issues of abrupt changes in the near-surface seismic velocities, both vertically and laterally.

Another challenge for seismic imaging in the Lisan Peninsula is the presence of a salt dome. The strong contrast in acoustic impedance at the sediment-evaporate interface does not allow seismic signals to penetrate well below the salt, so the seismic image is usually poor (dim spots). Also, the salt dome shape is causing complex ray path (P-S mode conversions, reflected refractions, etc.), which makes the imaging of seismic data a real challenge. Three-dimensional pre-stack time migration (PreSTM) has an obvious advantage over the old techniques of post-stack time migration and can improve the imaging of seismic data significantly.

The emphasis of the seismic data re-processing was to properly image and enhance the continuity of shallow seismic reflectors, so special attention was given to refraction statics solution and velocity analysis.

7.1.1 Near-Surface Model (Refraction Statics)

To develop the near-surface model, first break picking was carried out on shot gathers over all the available offsets. The quality of the first breaks were very good in general, with the exception of the southeast part of the Lisan Peninsula (Figure 7-1).

A near-surface velocity model was derived using tomographic inversion of the first break data (Figure 7-2). First an initial velocity model was roughly estimated using available information about the area; the model was then updated iteratively with first break data until it converged. After convergence, the average root mean square (RMS) error between the actual and modeled first breaks is less than 7 ms, which is considered a very good result for tomographic refraction statics. The maximum depth of the final velocity model was set to –650 m, refraction statics were computed from a fixed datum of –400 m, and the replacement velocity was 3,000 m/s.

7.1.2 3D Pre-Stack Time Migration

Three-dimensional Kirchhoff PreSTM was used to image the seismic data. Data is sorted into common offset cubes, then a 3D migration operator (diffraction summation) is formed based on seismic RMS velocities. The data is then processed and output into CDP gathers. The output gathers were analyzed for residual move-out (RMO) and a final PreSTM velocity model was created. Figure 7-3 shows a comparison of the old processing with the PreSTM velocity model.

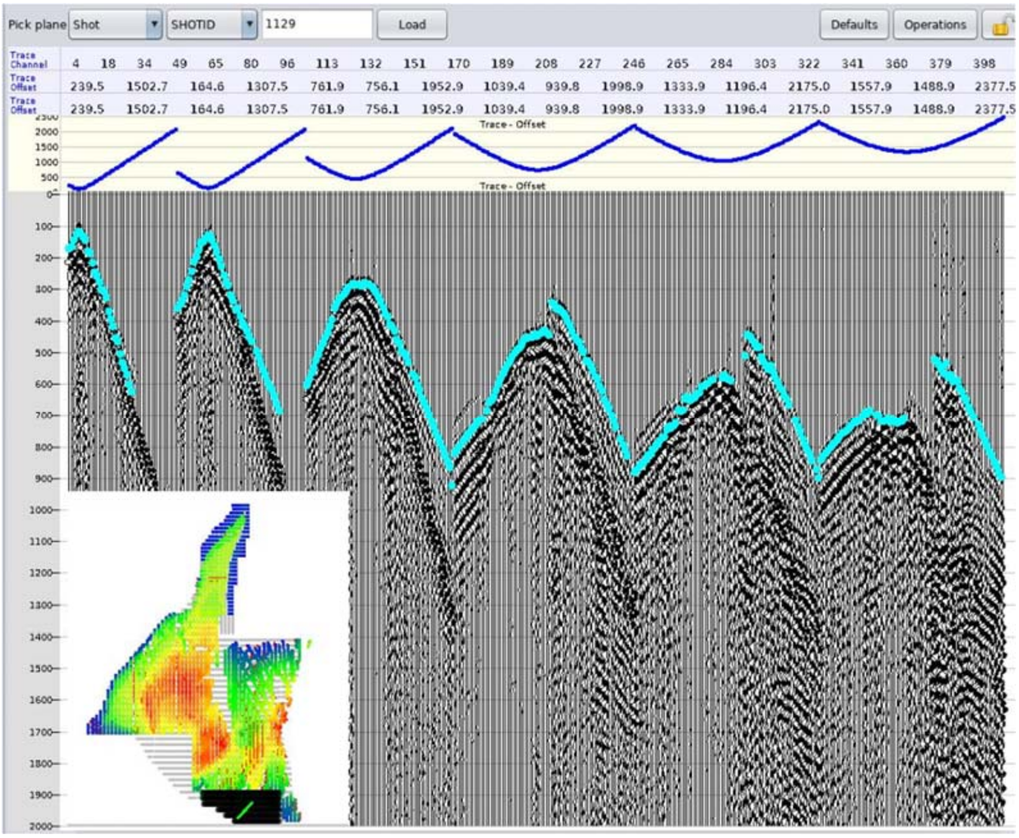

Figure 7-1. Example of a Shot Gather with Bad First Breaks

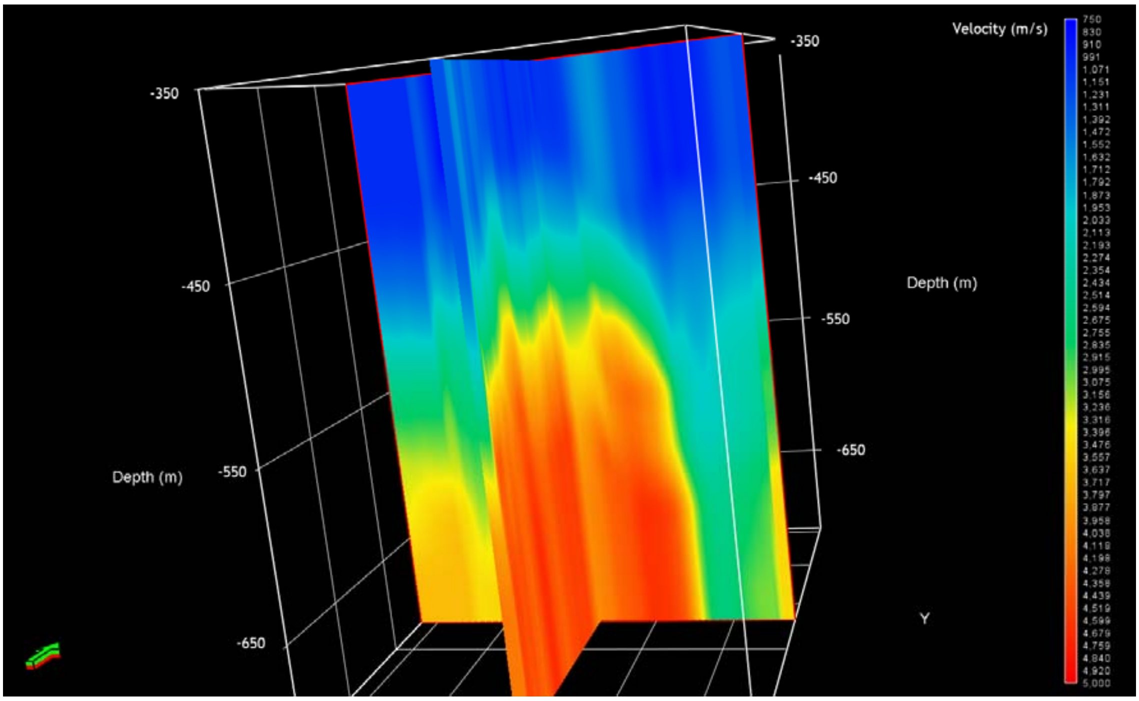

Figure 7-2. Snapshot of Lisan 3D Near-Surface Velocity Model

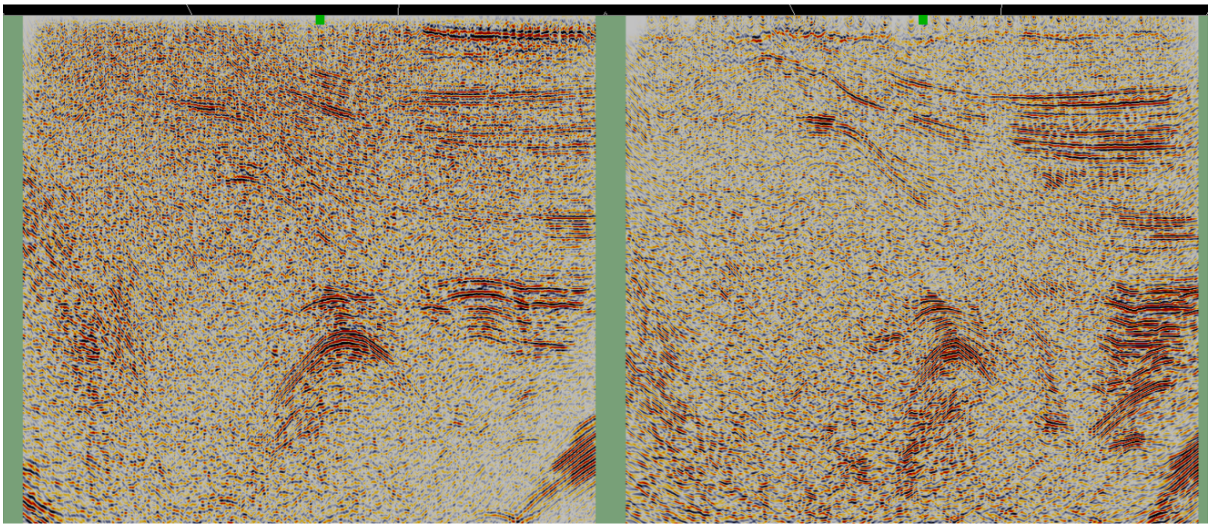

Figure 7-3. Old Processing (GSC) versus Misbar PreSTM / XL191

7.1.3 Testing and Parameter Selection

Several processes were tested to select the optimum parameters; this included amplitude scaling, noise attenuation, deconvolution and pre-stack time migration. Identical parameters were used for processing the 2D and 3D seismic data where possible.

7.1.4 Production Processing

The complete 3D volume (approximately 100 km^2) and ten seismic lines with a total length of 116 km were reprocessed (Figure 7-4). It was specifically important to reprocess the 2D lines that cross the 3D volume where the 3D data is poor or low fold and also to reprocess the lines closest to the wells and drillholes.

A standard seismic processing workflow was used to process the 2D and 3D data, as shown in Figure 7-5. Parameters developed in the testing phase were used for production processing.

7.2 Interpretation Analysis

7.2.1 General Comments

Following the acquisition and processing of the original 3D seismic survey, Western Atlas (1993) provided a thorough interpretation for petroleum, prospectively on the Lisan Peninsula. However, the Western Atlas (1993) work did not consider any shallow reflections which were correlated to potash-bearing strata.

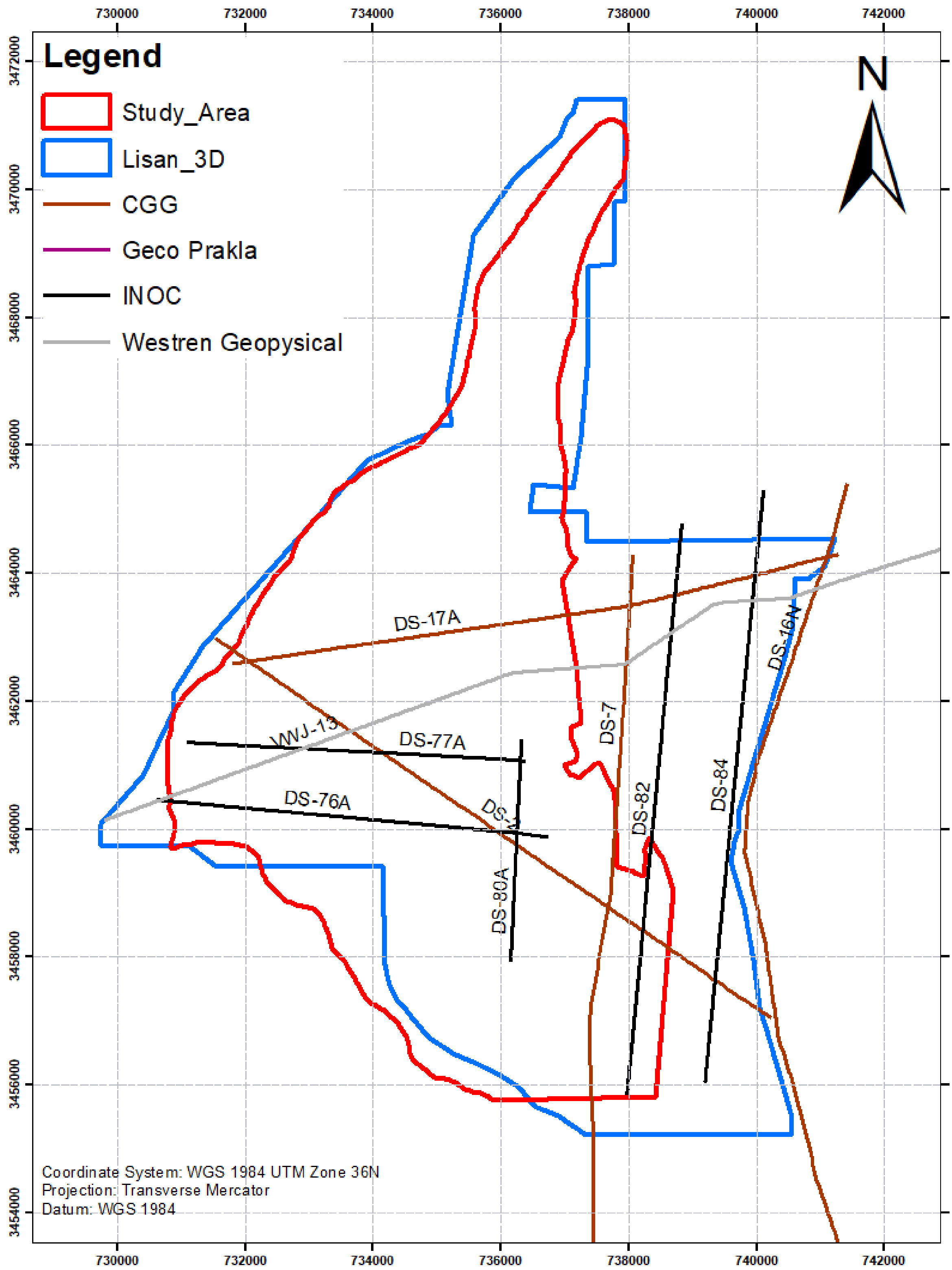

Figure 7-4. 2D lines Selected for Reprocessing

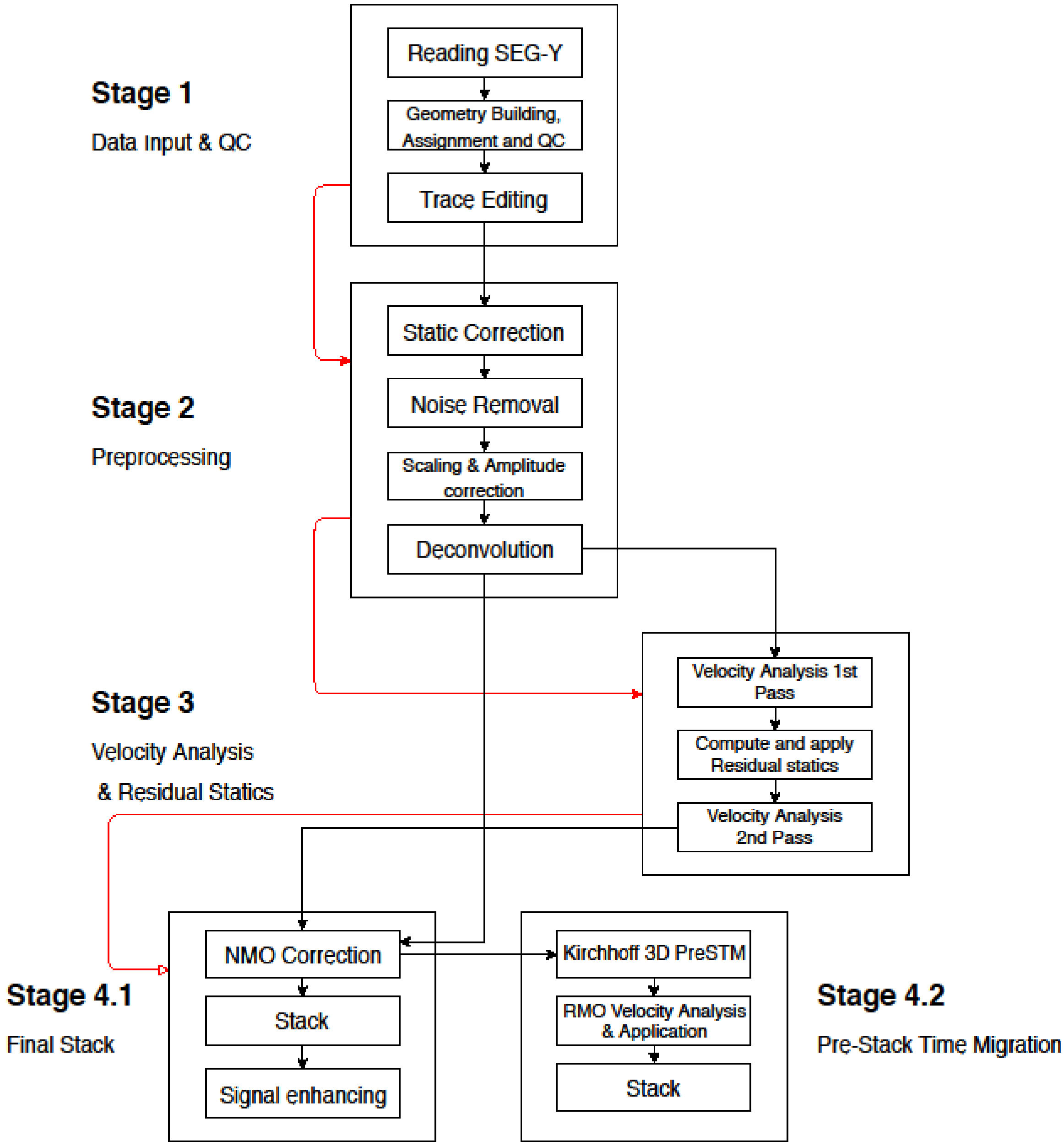

Figure 7-5. Processing Workflow

7.2.2 Salt Reflectivity Interpretive Model

The simple geologic model provided in Figure 8-1 represents the salt as one massive layer. However, the seismic data along a general representative north-to-south profile (Figure 7-6) approximate to the eastern side of the Lisan Peninsula, suggests that there are zones of varying reflectivity below the salt top encountered by the shallow wells. There appear to be four reflectivity packages below the Top of Salt:

- High reflectivity potash-bearing zone – verified by well correlations
- Low reflectivity uneconomic zone – too deep or no potash well correlations
- Reflectivity void zone – chaotic or no reflections suggesting clean diapiric salt core
- Deep salt layer – Pliocene-aged Sedom Formation

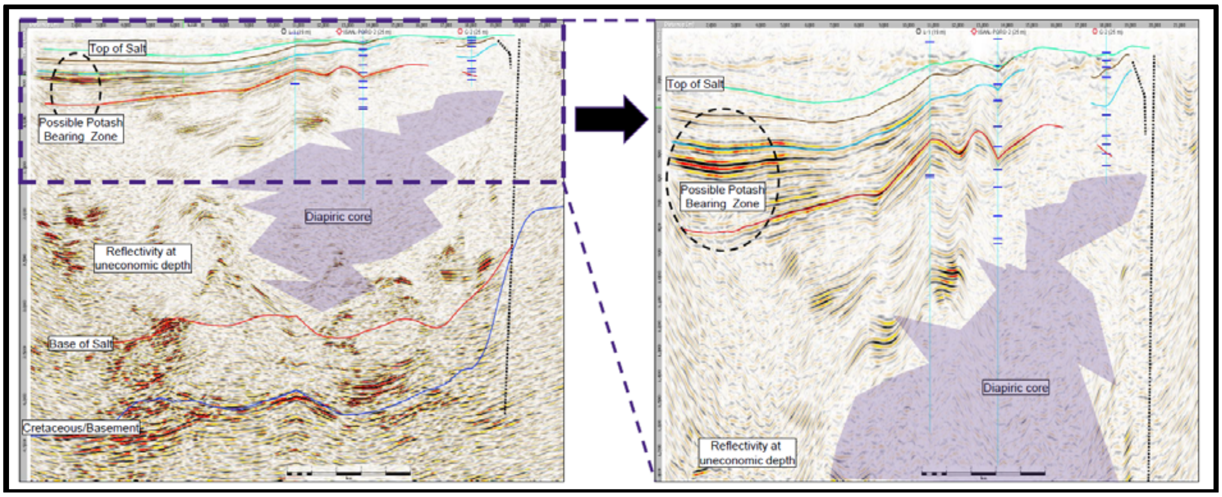

Figure 7-6. 3D Seismic Interpretation: Full Section and Potash Zone Detail

Near the Wadi Araba boundary fault there is a lack of reflectivity. It is possible that that the fault has many associated faults disrupting any coherent imaging or that the salt bounds the fault. In this study, the fault is assumed to be the eastern bound of the extent of the salt.

7.2.3 2D and 3D Seismic Horizons

With the four reflectivity packages defined in Section 7.2.2 in mind, the 2D and data were interpreted. In some areas of the 3D data, reflections were well-imaged, and mapping was straightforward. However, there were significant portions that were poorly imaged. In this regard, some 2D profiles had good imaging overlapping the poor 3D coverage. In these instances, the reflections from the 2D lines were used as guides to expand the 3D interpretation in these areas. These regions have a lower confidence and are separated from the high confidence picks with a polygon on depth structure maps.

The Top of Potential Potash Horizon (Figure 7-6, brown horizon) was picked based on the first coherent and continuous reflector within the shallow section that correlated best with the first potash well markers at ISAAL-PORO-02 and C-2. However, the well synthetic ties are poor, and this is a relative correlation at best. The Intra Potential Potash Zone Horizon (light blue horizon) was picked based on a small group of coherent, continuous reflectors that generally correlate to additional potash encounters in these two wells cited. The Base of Potential Potash Horizon (shallow red horizon) was picked along a deeper group of reflectors, which correlate to an interval of clastic dominated rock that is between some shallower and deeper potash encounters in wells ISSAL-PORO-02 and C-2. Potash encounters below this horizon did not correlate consistently to a seismic event and therefore, could not be mapped with any confidence. Additionally, two deeper reflectors were picked in the north–northwest area of the Project which could not be correlated to any well markers but were instead used to constrain the diapiric structure (Figure 7-7)

The two key 2D lines that were used to extend the bound of the 3D interpretation were DS-07 and VWJ-13 (Figure 7-8). These lines indicated reflective areas in the shallow section which corresponded to reflections seen elsewhere in the 3D data. Line DS-07 guided extrapolation of the reflections to the southern area of the 3D and line VWJ-13 does likewise

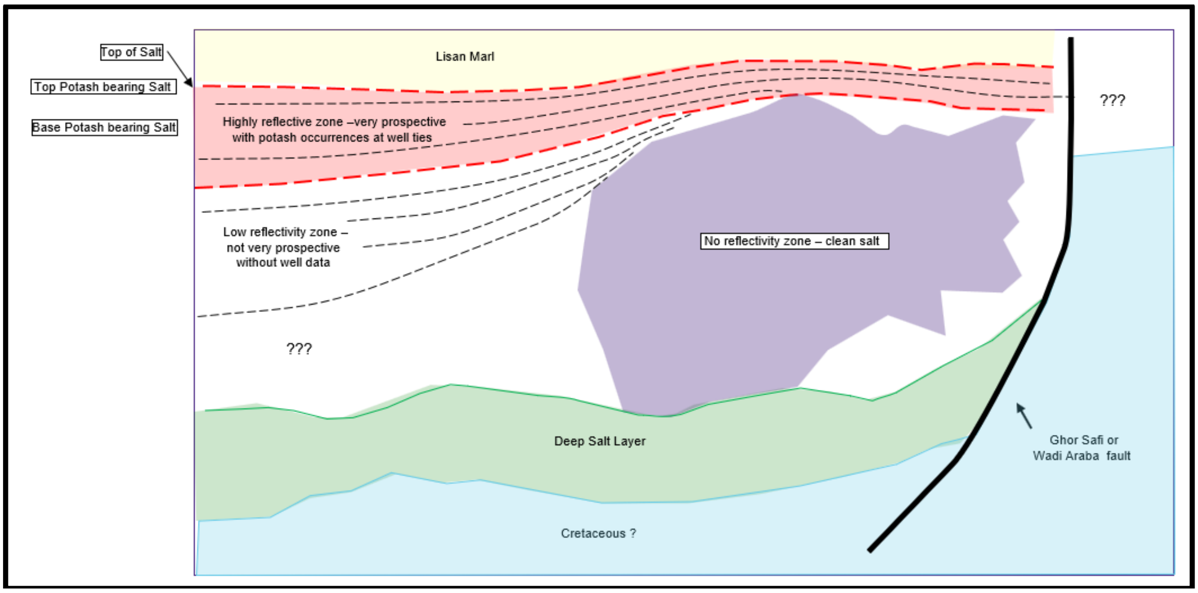

Figure 7-7. Salt Reflectivity Interpretive Model

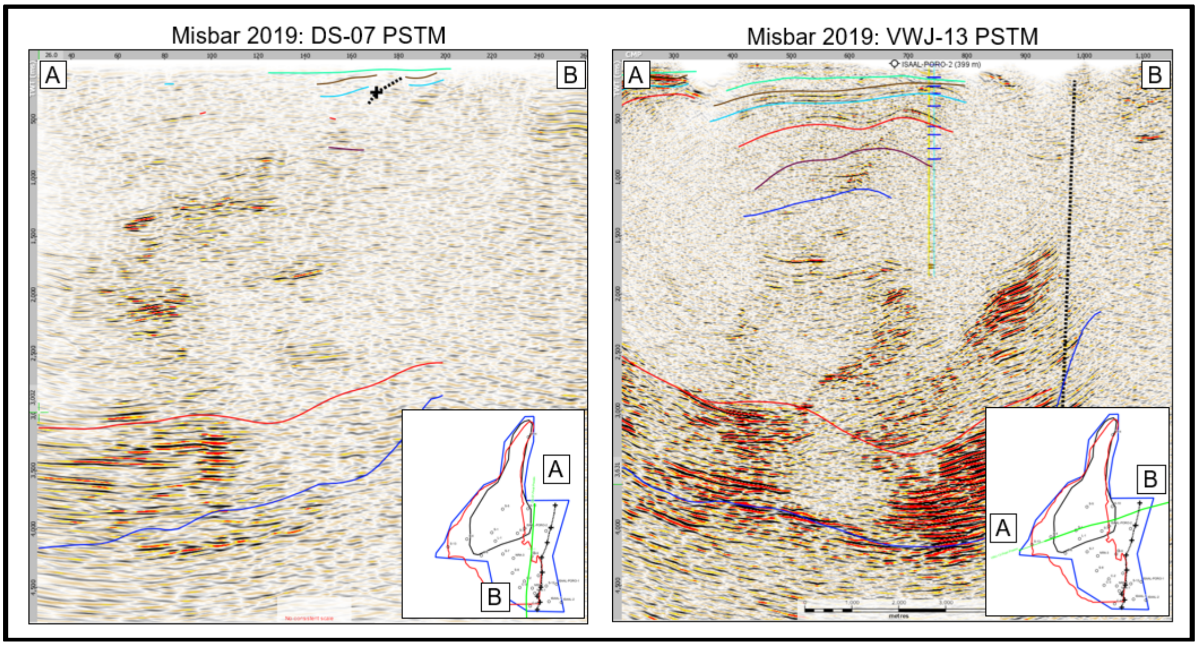

Figure 7-8. Seismic Interpretation on Two Key 2D Lines: DS-07 and VWJ-13

to the west. Unfortunately, the majority of the 2D lines reprocessed did not offer any improvement in areas overlapping the 3D seismic.

The coherency filtered, 3D PSTM provided the foundation for the interpretation over most of the Project area. Examples of the interpretation are shown using arbitrary lines in Figure 7-9 and Figure 7-10. The shallower potash interval was picked on a tightly spaced grid on reliable reflectors, interpolated and gridded to produce time-structure maps and then converted to depth. The deep reflectors of the Base of Salt and Cretaceous markers are more speculative, and a coarser picking interval was applied to follow the only events that were considered reliable. A similar interpolation and gridding scheme were then applied to the deep events.

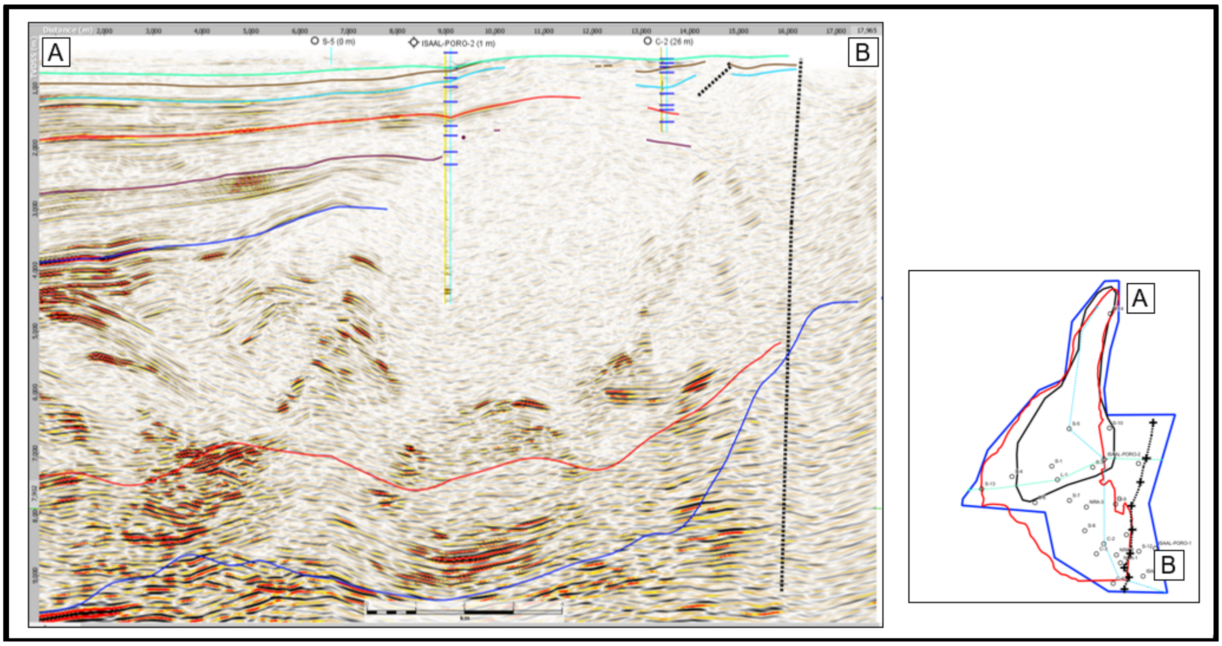

Figure 7-9. Northwest–Southeast Arbitrary Line Interpretation through the 3D Volume

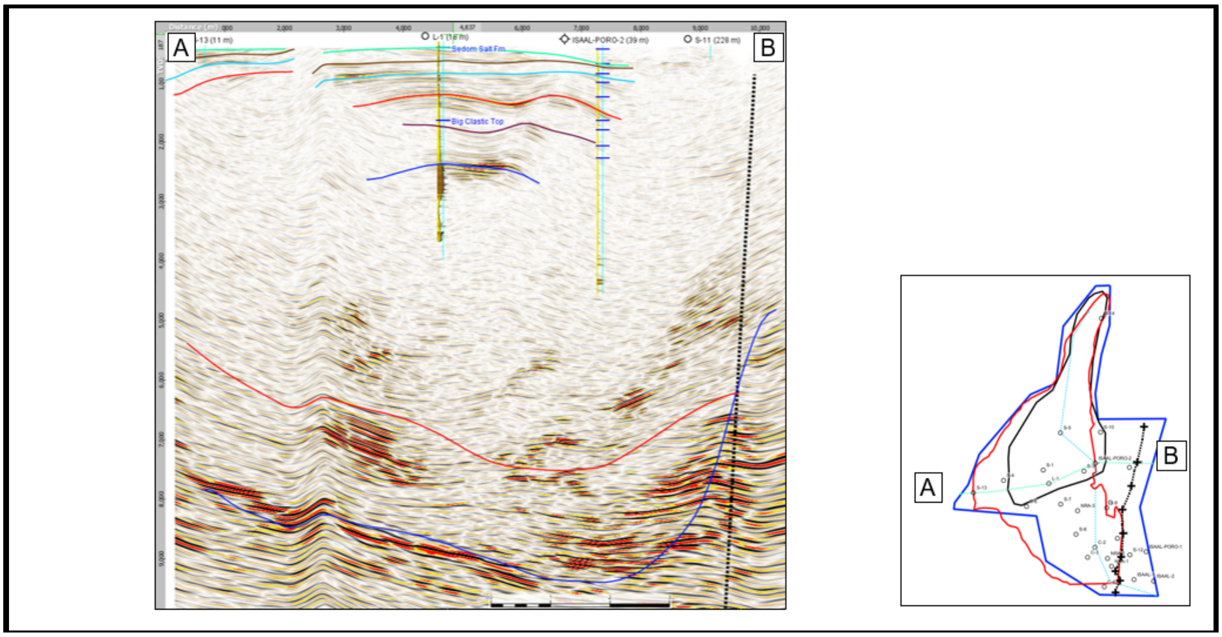

Figure 7-10. Northeast–Southwest Arbitrary Line Interpretation through the 3D Volume

7.2.4 Depth Structure Maps

The time structure grids from the interpretation were then depth-converted using the salt-velocity model discussed in Section 4.4 of Appendix A. Figure 7-11 shows the depth structure maps that bound the Dead Sea Basin for the Project area. The Top of Salt Depth Structure Map clearly shows the apex of the overall salt interval and the northwest–southeast

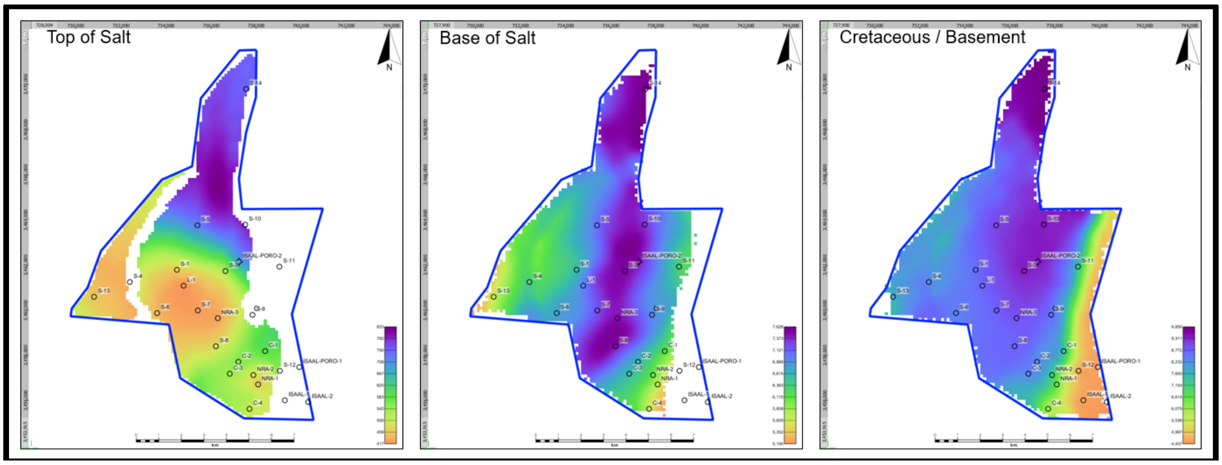

Figure 7-11. Depth Structure Maps: Top of Salt, Base of Salt, and Cretaceous/ Basement

axis along the high (Figure 7-11). There is a break to the west, though its nature is indeterminate due to poor data quality and lack of coverage (Figure 7-11). Most likely a fault or diapiric intrusion is the cause of the break in continuity. The Base of Salt (Sedom Formation) has a northeast–southwest axis indicating the deepest depth of the salt to be approximately 7,600 m. This depth compares well to previous work by Al-Zoubi and ten Brink (2001). The Cretaceous Depth Structure Map is poorly constrained east of the boundary fault as seismic data quality was very poor, making well correlation challenging. It is possible that the lack of seismic reflections is indicative of the complexity of the faulting in this area.

The prospective potash zones are shown in Figure 7-12. All three depth structures for Top of Potential Potash, Intra Potential Potash, and base of Potential Potash are high over the apex of the diapir (Figure 7-12). Discontinuity of the depth surfaces may be due to faulting. To the south, all structures are high, whereas to the north of the apex, the structures all dip rapidly to the north. It should be noted that the area contained within the black polygon represents a high confidence region where the seismic reflections were of good quality and therefore, the derived depth structure map is considered more reliable. The depth structure within the polygon dips rapidly to the north and may make mining operations less economic. In contrast, the portions of the depth structure that are in the southern high are based on poor quality reflection data. Picking through this area was discussed in Section 7.2.3 earlier. Consequently, these high areas of the depth maps outside the black polygon are of lower confidence.

Figures 7-13 and 7-14 show the depth maps in 3D view from the four corners of the Project area and illustrate the spatial relationships already discussed.

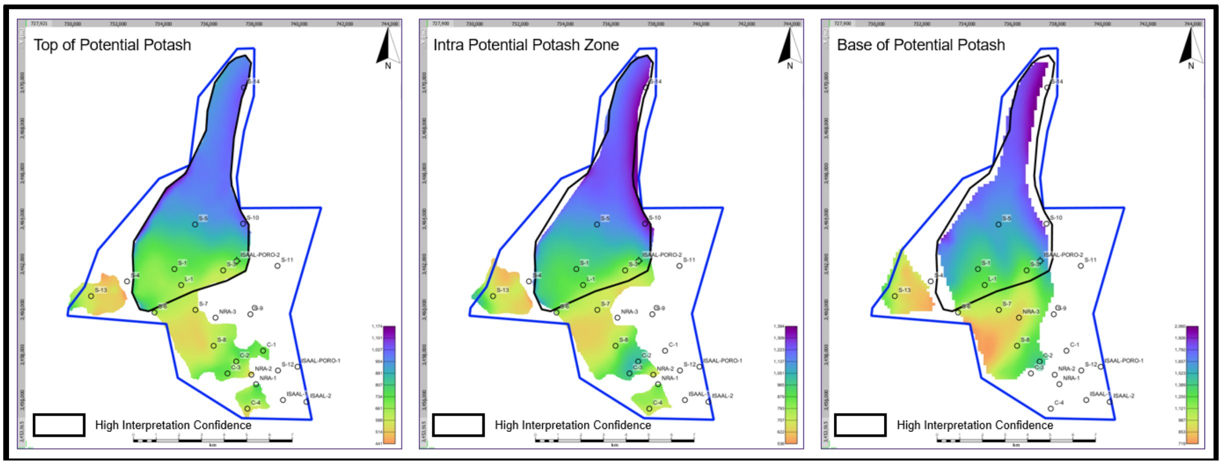

Figure 7-12. Depth Structure Maps: Top of Potential Potash, Intra Potential Potash Zone, and Base of Potash Potential

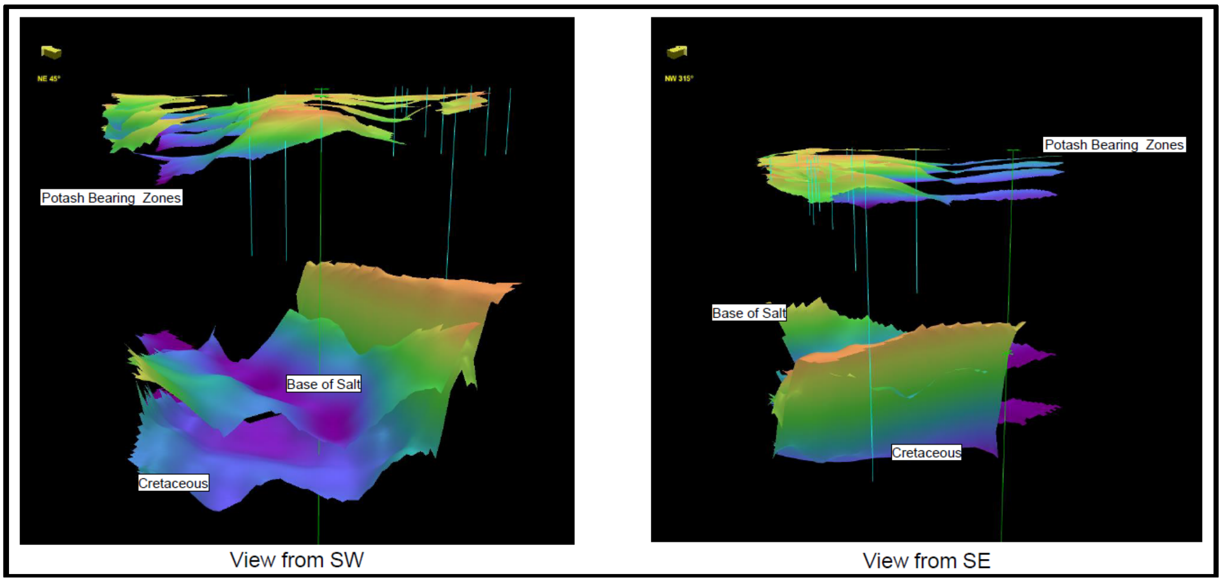

Figure 7-13. Seismic Depth Structure 3D Views, from the Southwest and the Southeast

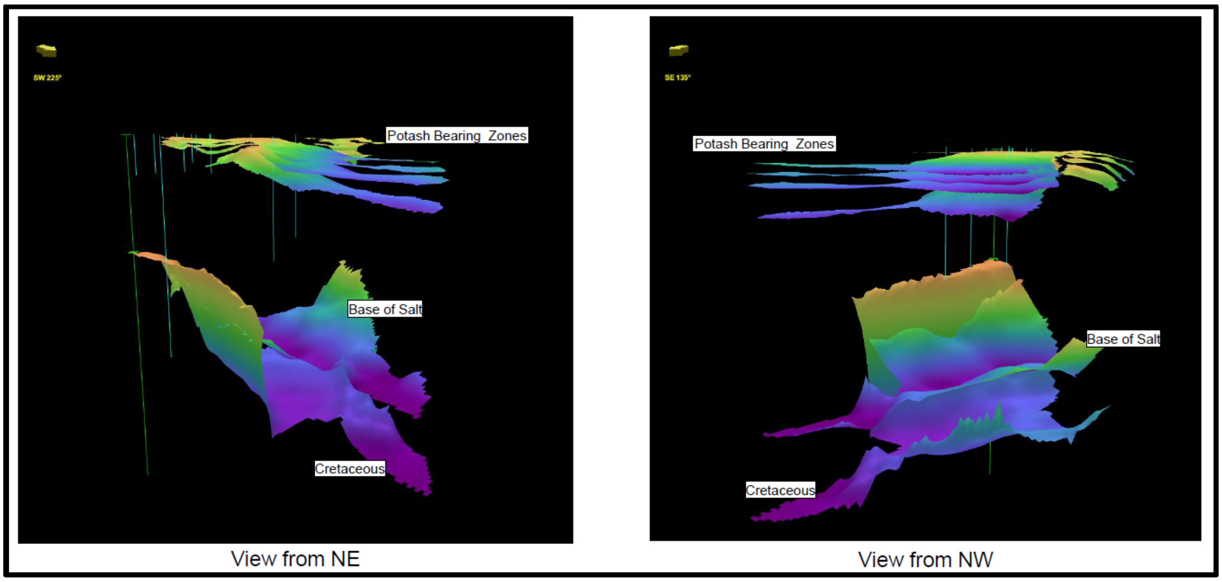

Figure 7-14. Seismic Depth Structure 3D Views, from the Northeast and the Northwest

8 GEOLOGY

Evaluation of the Project area includes the review of drilling data with stratigraphic and structural interpretation. Preliminary "picks" of potash occurrences and possible clastic maker beds within the Lisan Diapir were guided by a combination of the historical assays, downhole geophysical logs, and drilling reports. The Lisan Diapir reflects the post-potash deformation of the salt beds that host the target mineralization; the 2D and 3D reprocessing helps to define that structure. Review of drillholes outside of the Project area can assist in the interpretation where the salt beds are believed to be relatively undisturbed. The drillhole density does not allow for full interpretation of faulting nor for the determination of potash over the entire Lisan Peninsula. Exploration work by drilling and additional seismic surveying will be necessary to refine the current interpretation of potash occurrence, continuity, and grade over the Peninsula to access economic potential.

8.1 Fault Block Structure

The Lisan Formation covers most of the Lisan Peninsula. Sediments away from the edges of the Lisan Diapir have subsided to form salt-withdrawal basins or rim synclines (RS). At the edge of the anticline is a fault, defined to the east and west.

The top of the anticline shows structural complexity (Figure 8-1) at the diapir edge where drillhole NRA-1 is projected and the Lisan Formation fills the RS zone. Faults in Figure 8-1 are shown in black. The location of the historical seismic line is shown in Figure 4-4. The axis of the Lisan Diapir (Figure 4-7) has been interpreted in previous MEMR work. Surface lineaments and faults have been interpreted from aerial photographs, field mapping, and seismic surveys (Sunna 1986). The new seismic interpretation confirms the general structure off the apex of the Lisan diapir with a northerly dip. The shallower data in the southern Project area does not suggest any steep dips until below the prospective potash zone. This area is potentially more prospective than the northern area but is also considered to have low confidence in the seismic interpretation.

The new seismic interpretation may show onlapping zones as Sedom salt, which suggests continued salt deposition as the diapir developed (Section 7). This is significant as the salt beds appear relatively flattened on the flanks and crest of the anticline. While confidence in the potash picks within the salts is not certain and will need to be field checked with drilling, it is noteworthy that persistent reflectors are seen at relatively shallow intervals. Discontinuity of the depth surfaces may be due to faulting.

The drillhole density does not allow full interpretation of faulting, but the historical well reports note a large well offset between ISAAL-01 and ISAAL-02, with the latter being 525 m higher than the former. Furthermore, in ISAAL-01, the equivalent interval between 1790 and 2068 m (pre-rift Eocene WSC and URC formations) was faulted out (TransGlobal Petroleum Jordan 2005).

8.2 Stratigraphic Picks

The tops of formations were determined largely from the historical drillhole data. The upper part of the drillholes typically contain minimal information as it was not the focus of interest, except in those holes specifically drilled for potash exploration, that is, the carnallite,

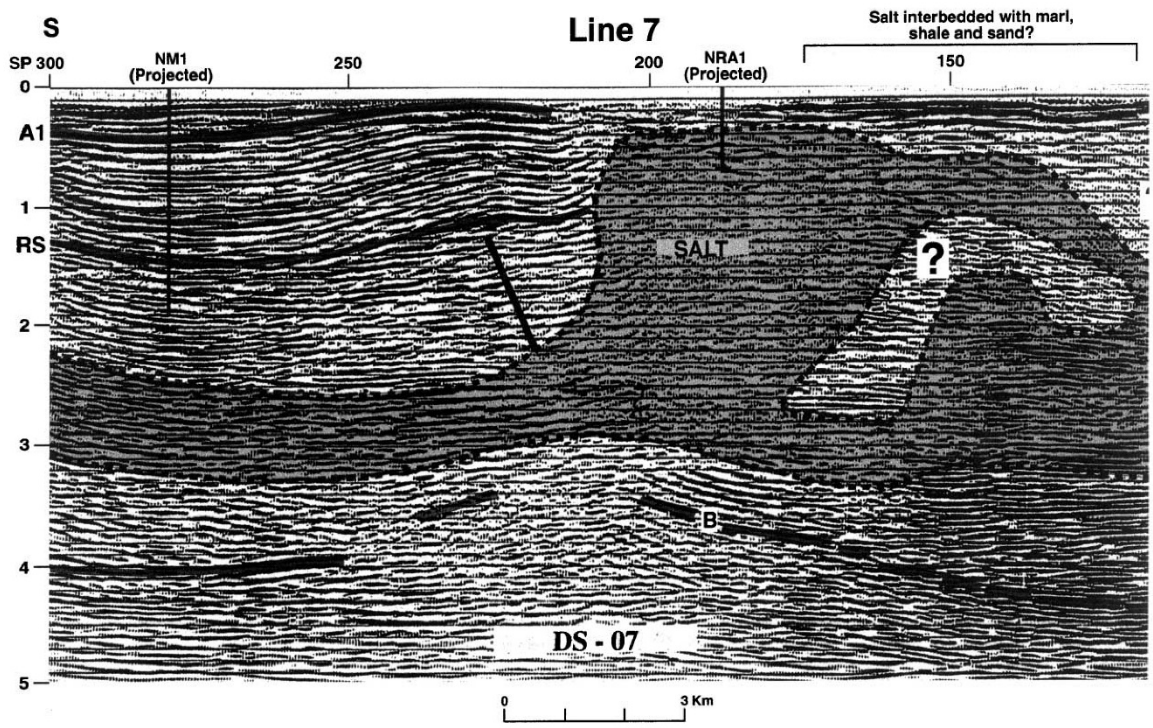

Figure 8-1. Historical Interpretation of Salt Diapirs in the Dead Sea Basin – Line 7 (Al-Zoubi and ten Brink 2001)

"C" drillholes. The "S" holes were only drilled to the top of salt. In reviewing the data, it is not always clear that consistent horizons have been picked, or if enough data exists to do so. There is incomplete up-hole information to redefine those picks.

Pre-Tertiary picks were made to determine the basement structure of the Lisan area. It is important to determine the structure upon which the salt was deposited to predict possible potash deposition. Thick salt generally accumulates in structural lows, but that signature is masked by the post-depositional salt movement. Within the Lisan Peninsula, all potash-bearing salt lithologies are assumed to be the Sedom Formation. It is clear from looking at the historical seismic interpretation that the salt has "evacuated" the surrounding area and is concentrated to great thickness within the diapir (Figure 4-5).

Salt may exist in the Dana Formation, but the formation is largely conglomeratic from material sourced for the Dead Sea Rift edge. The formation exists on the flank of the diapir. Deposition of salt is reported in the literature as early as the Miocene Epoch (Bandel and Shinaq 2003), but the presence of potash within those salts cannot be determined. It is worth noting that potash in the Red Sea and Gulf of Suez of Egypt are Miocene in age.

Within the salts, potash beds were picked along with formation tops (Table 8-1). Using a combination of the assayed potash (Table 8-2), geophysical picks (Table 8-3), and notes from the lithologic logs, AAI has initially picked up to six potash beds. The beds are informally numbered from top to bottom, which of course is incorrect geologically. These picks are preliminary and the supporting data to confirm them are not consistent. An attempt has been made to tie these picks to a persistent clastic unit, in this case, informally a bed called the "Big Clastic," consisting of anhydrite, shale, and sand. The package can be over

Table 8-1. Stratigraphic Formation Tops

	Formation Top Depth (m)									
	Quaternary	Tertiary						Mesozoic	Permo-Triassic	Pre-Cambrian
Drillhole Identifier		Lisan Marl	Sedom	Dana	WSC	URC	MCM	Cretaceous		
AH-02									0	409
ASH-01		0							180	
C-1‡	0	4	253							
C-2‡		0	200							
C-3‡		0	180							
C-4		0	126							
HD-01									0	
ISAAL-01		0	60	2100	2405	2710	2810	2910		
ISAAL-02	0	50		120	1740	2068	2223	2353		
ISAAL-PORO-1		0		200	1550	1814	1979	2100	2670	
ISAAL-PORO-2		0	75	560						
LISAN-01‡		0	310							
NM-01		0	50	1520						
S-1‡		0	94							
S-3‡		0	63							
S-4‡		0	162							
S-5‡		0	100							
S-6‡		0	79							
S-7‡		0	97							
S-8‡		0	97							
S-9		0	90							
S-9A		0	150							
S-10		0	52							
S-11		0	248							
S-12		0	193							
S-13‡		0	204							
S-14‡		0	133							
TS-1D								0		
WM-01									0	
NRA-1‡		0	128							
NRA-2‡		0	127							
NRA-3‡		0	91							

‡ Drillhole within project boundary   If field is blank, formation not present or not drilled through
WSC = Wadi Shallala Chalk; URC = Umm Rijam Chert; MCM = Muwaqqar Chalk

Table 8-2. Potash Picks from Assays

Drillhole Identifier	Potash 1 (m) From	Potash 1 (m) Thick	Potash 2 (m) From	Potash 2 (m) Thick	Potash 3 (m) From	Potash 3 (m) Thick	Potash 4 (m) From	Potash 4 (m) Thick	Potash 5 (m) From	Potash 5 (m) Thick	Potash 6 (m) From	Potash 6 (m) Thick
C-1ǂ	378.0	5.0	537.0	1.5								
C-2ǂ	332.0	2.0	423.0	4.0								
C-3ǂ												
C-4	166.0	3.2	354.0	15.0	431.7	3.5	468.0	32.0				
NRA-1ǂ	541.0	2.0	496.0	2.0								
NRA-2ǂ	149.0	16.0	347.0	4.0								

ǂ Drillhole within project boundary

Table 8-3. Potash Picks from Elogs and Lithological Logs

Drillhole Identifier	Potash 1 (m) From	Potash 1 (m) Thick	Potash 2 (m) From	Potash 2 (m) Thick	Potash 3 (m) From	Potash 3 (m) Thick	Potash 4 (m) From	Potash 4 (m) Thick	Potash 5 (m) From	Potash 5 (m) Thick	Potash 6 (m) From	Potash 6 (m) Thick
C-1ǂ												
C-2ǂ	270.4	0.6	Elog data not available over interval				767.8	1.2	958.6	2.3	1232.7	1.3
C-3ǂ												
C-4												
ISAAL-01	NP	NP	*617.0*	*13.0*	*735.0*	*40.0*	*1103.0*	*32.0*	*1346.0*	*118.0*	NP	NP
ISAAL-PO	321.7	2.6	489.7	7.3	635.2	9.8	NP	NP	1274.4	2.1	1432.0	1.0
NM-01	68.0	5.0	518.0	7.0	1076.0	4.5	1290.0	7.0	1390.0	42.0	NP	NP
NRA-3ǂ	*482.0*	*4.0*	*500.0*	*2.0*	*527.0*	*5.0*	*687.0*	*4.0*	*758.0*	*7.0*	NP	NP

ǂ Drillhole within project boundary NP = Not Present
Italicized text indicates pick made from lithologic log where Elogs were not available

100 m thick, tentatively defined between Potash 4 and Potash 5. Where spectral gamma ray logs were performed, the clastic unit shows a distinctively high uranium content. In some cases, it appears that these may not be the same clastic unit, but may provide a meaningful reflector within the salt as seen in the reprocessed seismic data.

8.2.1 Clastic Units

Potash beds cannot usually be detected in seismic surveys. The density of carnallite and sylvinite, especially in low grades, do not show discernable reflectors. It may be argued that some reflectors are seen in the re-processed seismic data, identifying beds of interest that may be carnallite with a higher water content (RPS 2019) or associated clastic units usually found at the base of the salt cycle (see Subsection 4.3.1). Potash beds may not be continuous, especially where the evaporites have undergone post-depositional movement. Salts are very mobile, and are typically identified by thick clastic units as "marker" beds within the salts. Depositionally, clastic units tend to be more persistent, so detection as a marker is possible within the stratigraphic column. Especially in the case of shales and anhydrites where large density differences occur, a reflector may be present.

8.2.2 Potash Beds from Assay

Only five historical holes were assayed for potash: C-1, C-2, and C-4 and NRA-1 and NRA-2 (Table 8-2). C-3 was reported to be absent of significant mineralization and has no assay. All the occurrences are relatively shallow, show generally poor correlation to each other, and for now, are assumed to be the uppermost potash beds. As was noted in the MEMR (2015) report, potash exploration holes NRA-1 and NRA-2 are less than 20 m apart and show poor correlation. Some assay data may be suspect if core recovery was poor due to core dissolution from undersaturated mud or incomplete mechanical recovery. The historical core is not available for review (MEMR 2019) so this cannot be resolved. The mineralogy is largely carnallite, with some potassium content high enough to indicate sylvinite at the top of a bed.

8.2.3 Potash Beds from Geophysical Logs

Potash picks were made from the geophysical logs (Table 8-3) according to the procedure outlined in Subsection 6.3.1.4.

Outside and south of the immediate Lisan Peninsula, drillhole NM-1 (Numeira-1) exists on the western edge of the APC evaporation ponds (Figure 1-1). It appears the salt in the area of NM-1 is relatively undeformed (Figure 8-1) (Al-Zoubi and ten Brink 2001), which provides guidance for picks within the diapir. Using the downhole geophysical and lithology records from this hole, general potash picks were carried over to other areas. In determining stratigraphy and continuity of potash and clastic units, relatively flat-lying units can guide selection within the diapir. This NM drillhole has detailed lithology and some geophysics, with potash detected at less than 70 m depth.

8.3 Potash Bed Composites

Composite K_2O, magnesium oxide (MgO), and calcium oxide (CaO) grades are calculated for potash beds in three holes (C-1, C-2, and C-4) based on a total of 44 assays (Section 6.1.6). The composites are summarized by drillhole and potash bed in Table 8-4. Composites are also presented for drillholes NRA-1 and NRA-2, as reported in the "Interpretation and Evaluation of the Old Exploration (1959-1989) of the Potash Rock Deposits in Lisan Peninsula-Dead Sea" report (Jordanian Geologists Association 2014). Assay data are not available for the NRA holes and, therefore, the accuracy of the composite computations could not be checked or confirmed.

The grade parameters are expressed in terms of mass (or weight) percent. Composite grades are calculated as the length-weighted average of the individual assays over the selected potash bed interval. Bed true thickness is the thickness of the potash bed calculated normal to the dip of the bed.

Composite grades are reported only for K_2O, MgO, and CaO, although other minerals were occasionally assayed, including K, Na, Cl, Ca, Mg, water (H_2O), NaCl, sulfur trioxide (SO_3), iron (III) oxide (Fe_2O_3), calcium chloride ($CaCl_2$), and insolubles. The record for these secondary minerals is incomplete and does not allow meaningful composites to be calculated for those minerals.

The mineralogy of the potash is generally indeterminate from the assay record alone. For this reason, potash grade is expressed universally in terms of K_2O. An "equivalent" KCl

Table 8-4. Potash Bed Composites

Drillhole	Potash Bed	Depth (m)		Bed Downhole Thickness (m)	Bed True Thickness (m)	Assayed Downhole Thickness (m)	Percent of Composite Thickness Assayed	Average Grade (wt%)				
		From	To					K_2O	MgO	CaO	Sylvite	Carnallite
C-1	P1	378.00	388.00	10.00	9.89	10.00	100%	2.27	ND	ND	ND	ND
	P2	535.00	540.00	5.00	4.94	5.00	100%	2.33	4.46	16.43	Negligible	13.75
C-2	P1	332.00	334.00	2.00	1.94	2.00	100%	2.37	2.06	4.08	Negligible	13.98
	P2	423.00	427.00	4.00	3.89	4.00	100%	2.51	7.77	5.97	Negligible	14.80
C-4	P1	160.00	163.20	3.20	3.14	2.00	63%	33.45	0.08	1.16	52.80	0.55
	P2	353.00	359.00	6.00	5.87	6.00	100%	4.22	3.83	3.37	Negligible	24.88
	P3	368.00	372.50	4.50	4.40	4.50	100%	5.19	4.66	1.02	Negligible	30.64
	P4	375.50	415.70	40.20	39.34	16.10	40%	2.89	4.12	0.78	Negligible	17.07
	P5	421.70	435.30	13.60	13.31	7.15	53%	6.93	5.91	0.49	Negligible	40.76
	P6	442.70	455.10	12.40	12.13	7.45	60%	3.80	9.40	0.70	Negligible	22.39
	P7	468.70	476.00	7.30	7.14	3.40	47%	8.17	8.02	0.66	Negligible	48.20
	P8	481.90	489.10	7.20	7.05	6.20	86%	12.84	11.27	0.15	Negligible	75.76
	P9	494.10	500.50	6.40	6.26	1.55	24%	9.00	8.53	0.39	Negligible	53.10
NRA-1	P1	541.00	543.00	2.00	1.64	2.00	ND	13.02	ND	ND	ND	ND
	P2	596.00	598.00	2.00	1.79	2.00	ND	14.02	ND	ND	ND	ND
NRA-2	P1	149.00	165.00	16.00	14.87	16.00	ND	13.92	ND	ND	ND	ND
	P2	347.00	351.00	4.00	3.74	4.00	ND	20.16	ND	ND	ND	ND

ND = No data or insufficient data.

weight-percent grade (KCl_{eq}) can be computed by dividing K_2O by 0.6317; however, this convention is not used to avoid suggesting that the potash is comprised of sylvite (KCl) when other potash minerals may be present, particularly carnallite ($KMgCl_3 \cdot 6(H_2O)$).

A crude estimate of mineralogy can be attempted by applying a simplifying assumption where the potash is assumed to be comprised of a binary mixture of only carnallite and sylvite, and no other forms of potash are assumed to be present. Table 8-4 estimates the proportion of carnallite and sylvite by first computing the carnallite fraction up to the limit allowed by the MgO or K_2O content, whichever is smaller. Any remnant K_2O is attributed to sylvite. By this approach, the potash beds in the C-holes are revealed to be predominantly carnallitic, except for bed P1 in drillhole C-4 which is both relatively high in K_2O grade and sylvite.

The historical assay record is continuous over the composited potash bed intervals without gaps, except in drillhole C-4 where gaps exist. NI 43-101 practice requires treating the missing assays (gaps) as zero grade, unless other information justifies otherwise. Contrary to NI 43-101 practice, composite grades in the 2015 report (Jordanian Geologists Association 2014) were calculated ignoring the missing assays and not assigning a zero value to the gaps. Instead, an average grade was calculated based on the available assays which represent only a fraction of the total composite interval. That average was then assigned, or “stretched,” over the total interval, including the gaps.

Table 8-4 compares the assayed length with the potash bed length. The table shows that assay coverage over the composite length ranges from 24% to 100% for the potash beds in drillhole C-4.

The C-4 composite grades reported in Table 8-4 were calculated by the same methodology as the 2015 report with assay gaps ignored. This method potentially over-predicts the composite grade and/or thickness of the potash beds where gaps exist in the assays, particularly where those gaps represent low-grade or barren intervals. There is reasonable expectation that the gaps in the assay record represent intervals that were never assayed because the core did not exhibit potash characteristics obvious enough to merit selection for assay.

The composites in Table 8-4 are not reliable for use with Mineral Resource estimation under NI 43-101 standards. However, the composites, as calculated, are applied to the Preliminary 3D Geological computer model because they provide a useful confirmation of potash targets that can be used for guiding future exploration drilling.

9 PRELIMINARY EARTH MODEL

A Preliminary 3D Geological Model of Potash in the Lisan Peninsula was constructed from the historical geological data compiled in Phase I utilizing Hexagon Mining © MinePlan™ 3D Version 15.40 software (MinePlan) (Hexagon Mining 2019). The purpose of the model is to provide a preliminary geometric framework and geospatial database for characterizing the Lisan potash deposit that can be used to plan exploration activities in Phase II. Any modern exploration data acquired in Phase III would be applied to advancing the model toward a Final 3D Geological Model of Potash in the Lisan Peninsula during Phase IV. The ultimate purpose of the final Phase IV model would be to support estimation of the Lisan Peninsula Potash Resource Estimate in Phase V.

MinePlan is a state-of-the-art, leading commercial-grade geology and mine planning computer platform developed for the mineral resources industry (Figure 9-1). The software allows the integration of the downhole data from the historical exploration drillholes (Section 6) with the reprocessed and reinterpreted seismic results (Section 7). The model provides a 3D representation of the ground surface, Project boundaries, and geological interpretation of the subsurface geometry of the deposit (Section 8), including top and bottom surfaces of the Lisan salt diapir, major faults, and dominant stratigraphy hosted within the diapir.

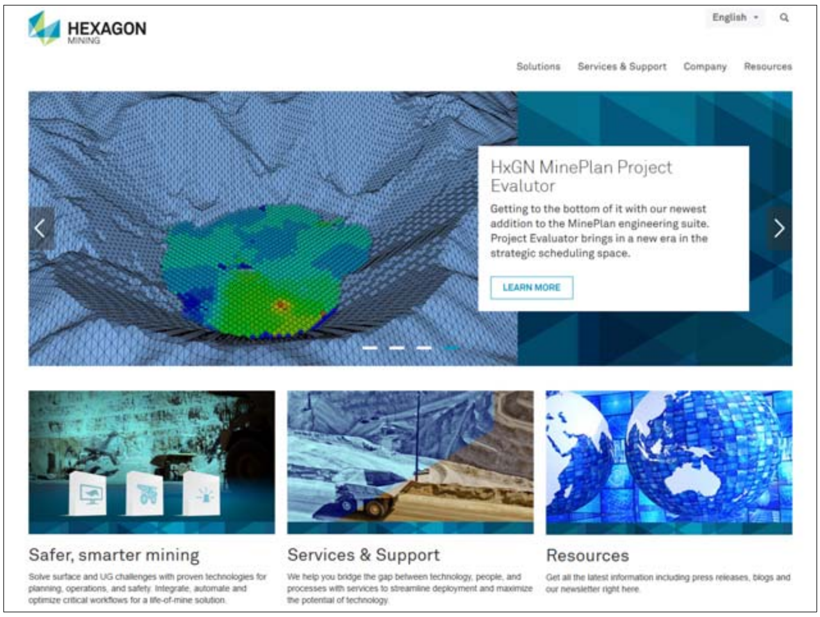

Figure 9-1. Hexagon Mining © MinePlan™ 3D Modeling Software

9.1 Methodology

The model is constructed in the UTM Zone 36N WGS 1984 coordinate system with meters (m) as the base unit for distance and depth. Historical data utilizing latitude/longitude coordinates, or the Palestine 1923 grid or other grid system, were converted to the UTM system.

Geological data applied to the model were geo-rectified where errors were identified in the historical record. Corrections were primarily applied to erroneous or conflicting coordinates and elevations of drillholes.

The MinePlan model is a gridded-seam model comprised of 2,240,000 3D blocks measuring 50 m by 50 m in plan view, covering an area of 350 km^2 (Figure 9-2). The height of blocks varies from block to block based on an interpolated thickness of the corresponding bed (stratum) at the block centroid. The elevations of the individual blocks follow the 3D structure of the geologic units, as defined by the drillholes and seismic interpretation.

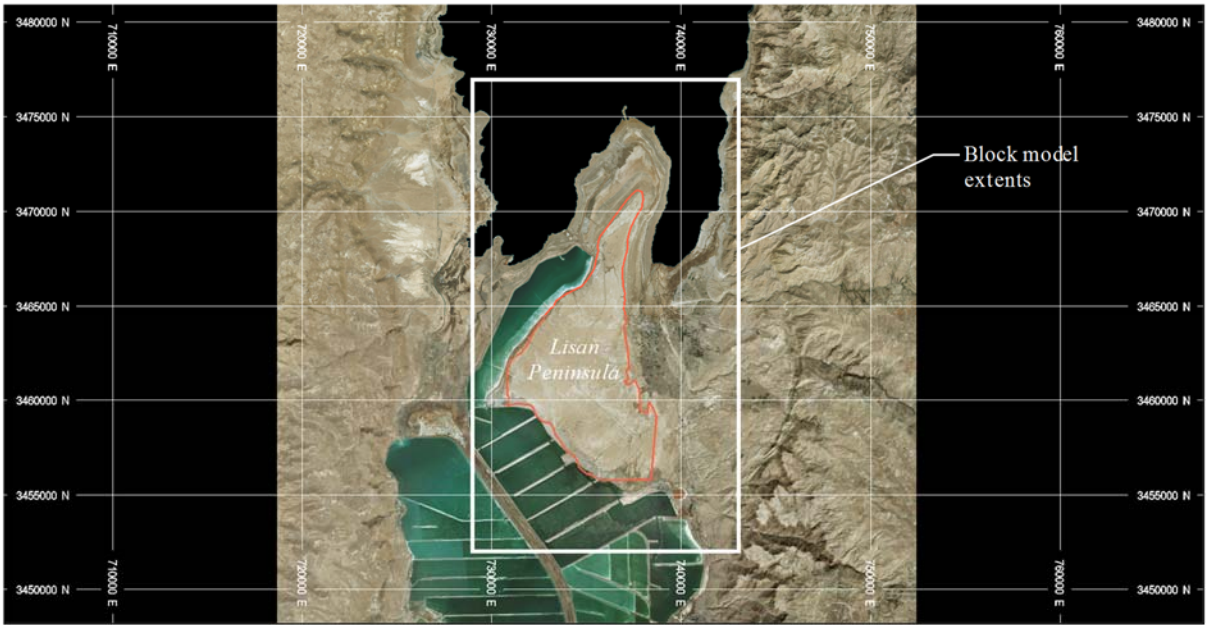

Figure 9-2. Block Model Extents (*plan view showing UTM grid*)

Each block in the model is identified by a specific stratigraphic unit, including individual potash beds. Blocks are further defined by volume, in-situ density, mineral grade, resource classification, and mining cutoff parameters. Grade parameters are estimated by interpolation between measurement points (drillholes), utilizing conventional or geostatistical methods.

9.2 Model Elements

Five principal elements of the model are presented in the following subsections that describe the functionality of the model: (1) surface terrain, (2) exploration drillholes, (3) stratigraphy, (4) geological structure, and (5) potash mineralization.

9.2.1 Surface Terrain

The surface of the Lisan Peninsula and surrounding area is represented in the model by a 3D digital elevation model (DEM) acquired through the GIS Laboratory, Department of Civil Engineering at the Jordan University of Science & Technology. The source DEM has a horizontal grid resolution of 88.7 m by 88.7 m, stated in decimal latitude/longitude coordinates with better than 1-centimeter vertical accuracy. Coordinates were transformed from latitude/ longitude to UTM using ESRI ArcView software (ESRI 2019). The DEM is shown in Figure 9-3 with three-times vertical exaggeration for effect.

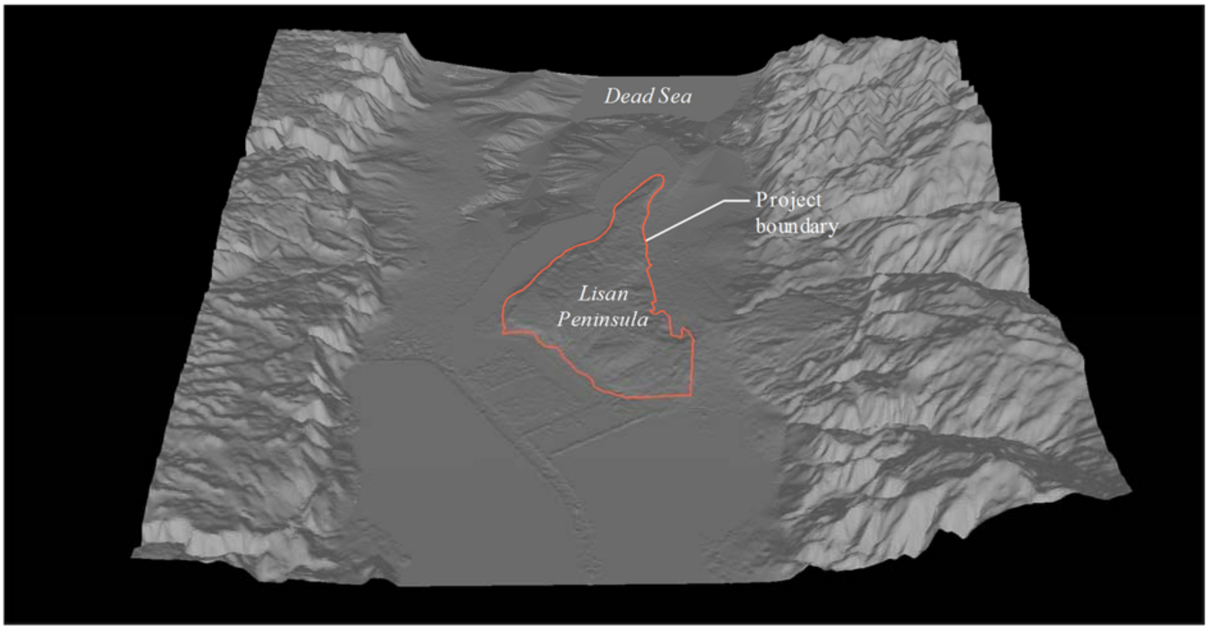

Figure 9-3. Digital Elevation Model (90-m grid resolution) (*perspective view to north*)

Elevation contours generated from the source DEM (88.7-m grid resolution) were compared against contours generated from two other sources: (1) a DEM created by Misbar using 1993 3D seismic elevation data (45.7-m grid resolution) and (2) a DEM (90-m grid resolution) from the Shuttle Radar Topography Mission Global GeoTiff (Int16) commercial database. The favorable match between the independent DEMs validates the accuracy of the Jordan University DEM used in the model.

The DEM used in the model also corresponded closely with the ground elevation reported for the majority of historical drillholes. The DEM was used to confirm the correct location of some drillholes reporting multiple locations.

In addition to the ground surface, the surface of the Dead Sea floor was generated from bathymetric contours digitized from a 2007 survey (Sade et al. 2014). The bathymetric surface was merged with the above-water surface to form a continuous ground surface over the Lisan diapir.

A high-resolution 2011 satellite image was overlain on the ground surface for reference and visual navigation in the model, as shown in Figures 9-4 and 9-5.

9.2.2 Exploration Drillholes

A total of 38 historical exploration drillholes are included in the model, of which 17 are located inside the Project boundary and 9 more within 2 km of the boundary (Figure 9-6). The drillhole geometric database includes drillhole name, collar coordinates, collar elevation, total depth, and downhole survey data (depth, azimuth, and dip).

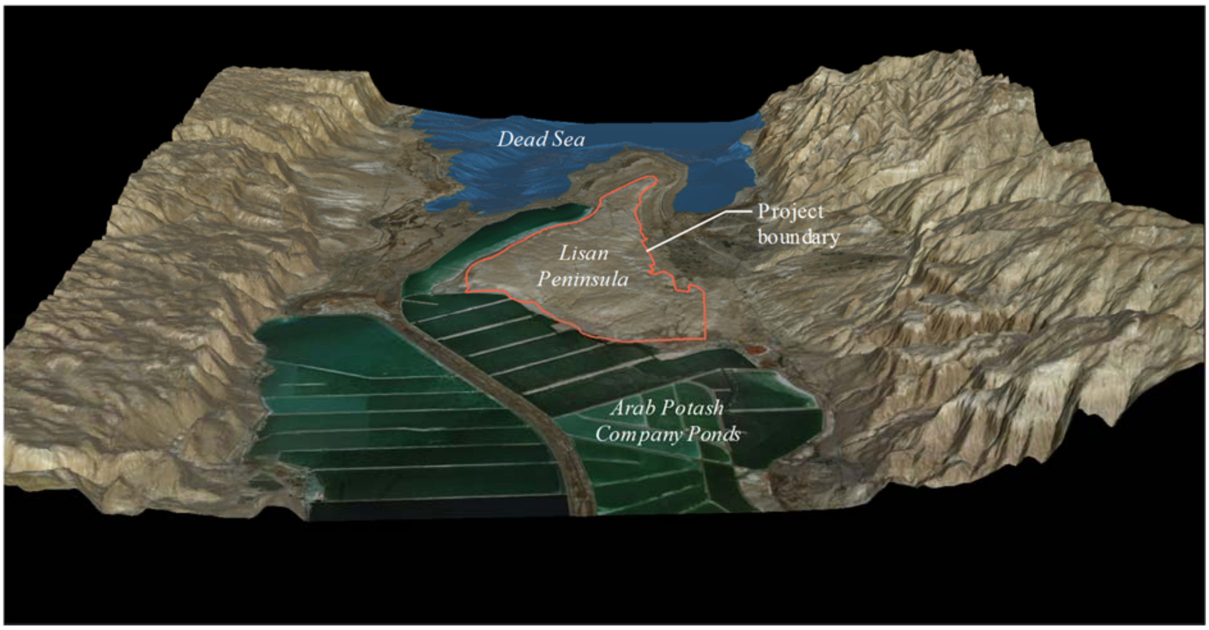

Figure 9-4. Model Satellite Image along Jordan Valley (*perspective view to north*)

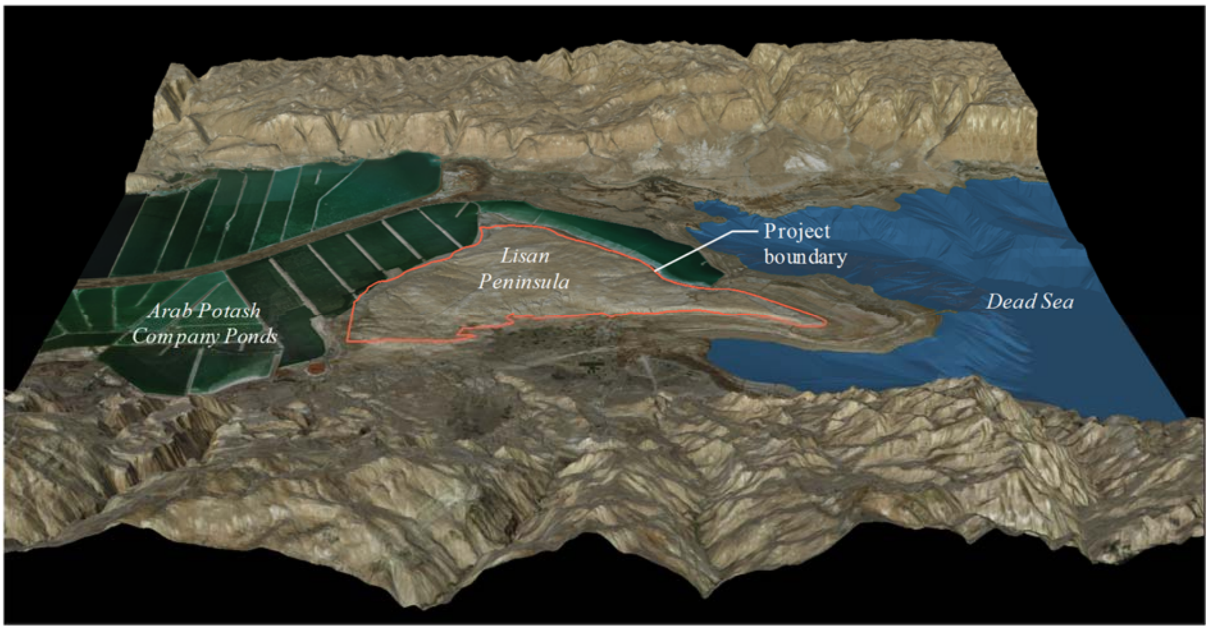

Figure 9-5. Model Satellite Image across Jordan Valley (*perspective view to west*)

Useable downhole directional survey data were acquired for four holes. Remaining holes were assumed to be vertical. The 3D geometry of the drillholes is illustrated in Figures 9-7 and 9-8. Drillholes ISAAL-PORO-1 and ISAAL-2 showed the largest deviations, each drifting approximately 440 m to the northeast from their collars, or approximately 0.16 m of horizontal deviation off vertical per meter of depth. The deviation of these holes was likely influenced by the major faults in the area.

Figure 9-6. Historical Exploration Drillholes in Model (*plan view*)

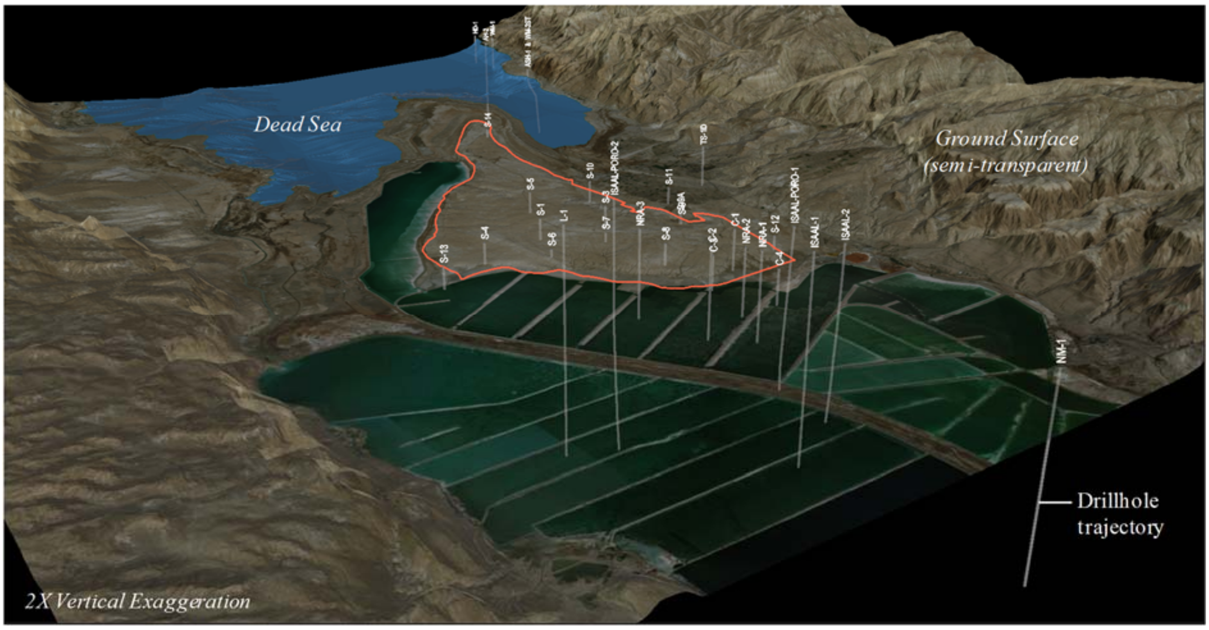

Figure 9-7. Above-Ground View of Historical Drillholes (*view to northeast*)

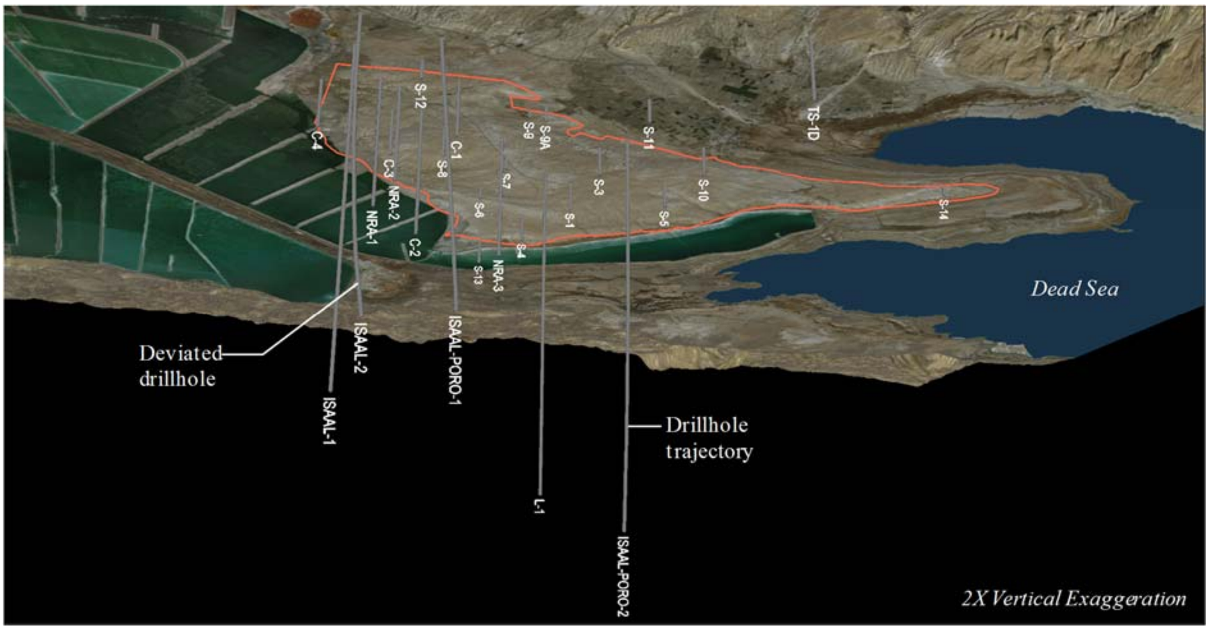

Figure 9-8. Underground View of Historical Drillholes (*view to northwest*)

Drillhole ISAAL-PORO-2 deviated approximately 220 m southeast, equivalent to approximately 0.05 m of horizontal deviation per meter of depth. There is reasonable potential that other deep holes for which deviation data were not available experienced similar magnitudes of deviation, depending upon their depth.

9.2.3 Stratigraphy

Ten principal stratigraphic units (Table 9-1) are specified for each drillhole in the model, in accordance with the stratigraphic picks developed in Section 8.2. The stratigraphic database includes drillhole name, stratigraphic unit name, downhole top and bottom depth, and a numerical stratigraphic code. For drillholes with deviation survey data, the top and bottom depths are resolved to TVD by the model. Stratigraphy in the model is illustrated in Figure 9-9.

Table 9-1. Model Stratigraphic Units

Abbreviation	Units
Qtry	Quaternary
Lisan	Lisan Marl
Sedom	Sedom Formation
Dana	Dana Formation
WSC	Wadi Shallala Chalk
URC	Umm Rijam Chert-Limestone
MCM	Muwaqqar Chalk
Mesoz	Mesozoic
PzTri	Paleozoic-Triassic
Pcm	PreCambrian

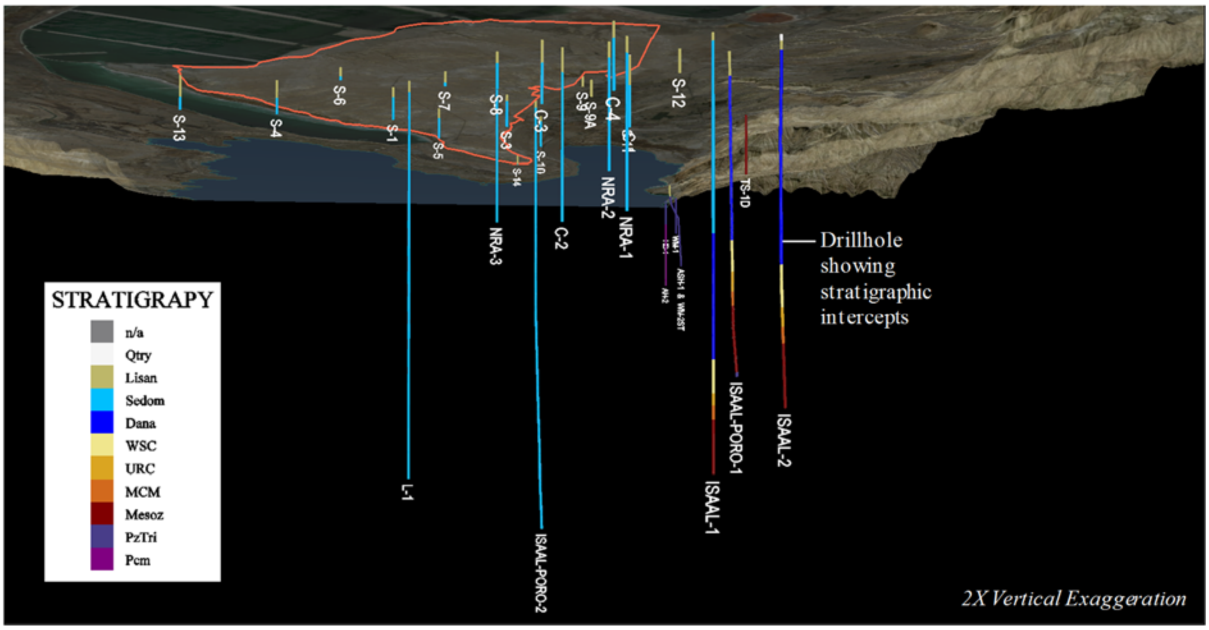

Figure 9-9. Drillhole Stratigraphy in Model (*underground view to north*)

The continuity and structure of the stratigraphy between drillholes is based substantially upon the seismic interpretation, as discussed in Section 9.2.4.

Multiple potash beds of interest are hosted within the Sedom Formation. These are discussed in Section 9.2.5.

9.2.4 Geologic Structure

The model incorporates geologic structure derived from the seismic reprocessing and re-interpretation study discussed in Section 7. The seismic study produced time surfaces for the top and bottom of the Lisan salt, the underlying Cretaceous basement, and five reflectors internal to the diapiric salt, as illustrated in Figures 9-10 and 9-11. The surfaces were converted from time to elevation (in meters) using a conversion based on the average velocity in salt.

The five reflectors within the diapiric salt provide structural definition of the primary potash host interval. An expanded view of this interval is shown in Figure 9-12. The uppermost reflector in this package approximately coincides with the uppermost potash bed (P1) identified from historical drillholes. The next reflector below the P1 reflector approximately coincides with the second potash bed (P2). These reflectors, highlighted in Figure 9-13, are interpreted to be salt-clastic contacts in close stratigraphic proximity to the potash beds and, therefore, are considered good indicators of structure and continuity within the potash beds themselves. The next three lower "clastic" reflectors characterize structure and continuity in the vicinity of the deeper potash intercepts (P3 and deeper).

Four primary faults with significant to major vertical displacement were characterized in the seismic study: the well-known Wadi-Araba (Dead Sea) fault on the eastern margin of the Jordan Valley graben, the Gohr-Safi fault, and two faults near the southern and western boundaries of the Project. The Gohr-Safi fault represents hundreds of meters of vertical displacement and is believed to define the eastern limit of the potash deposit. The southern

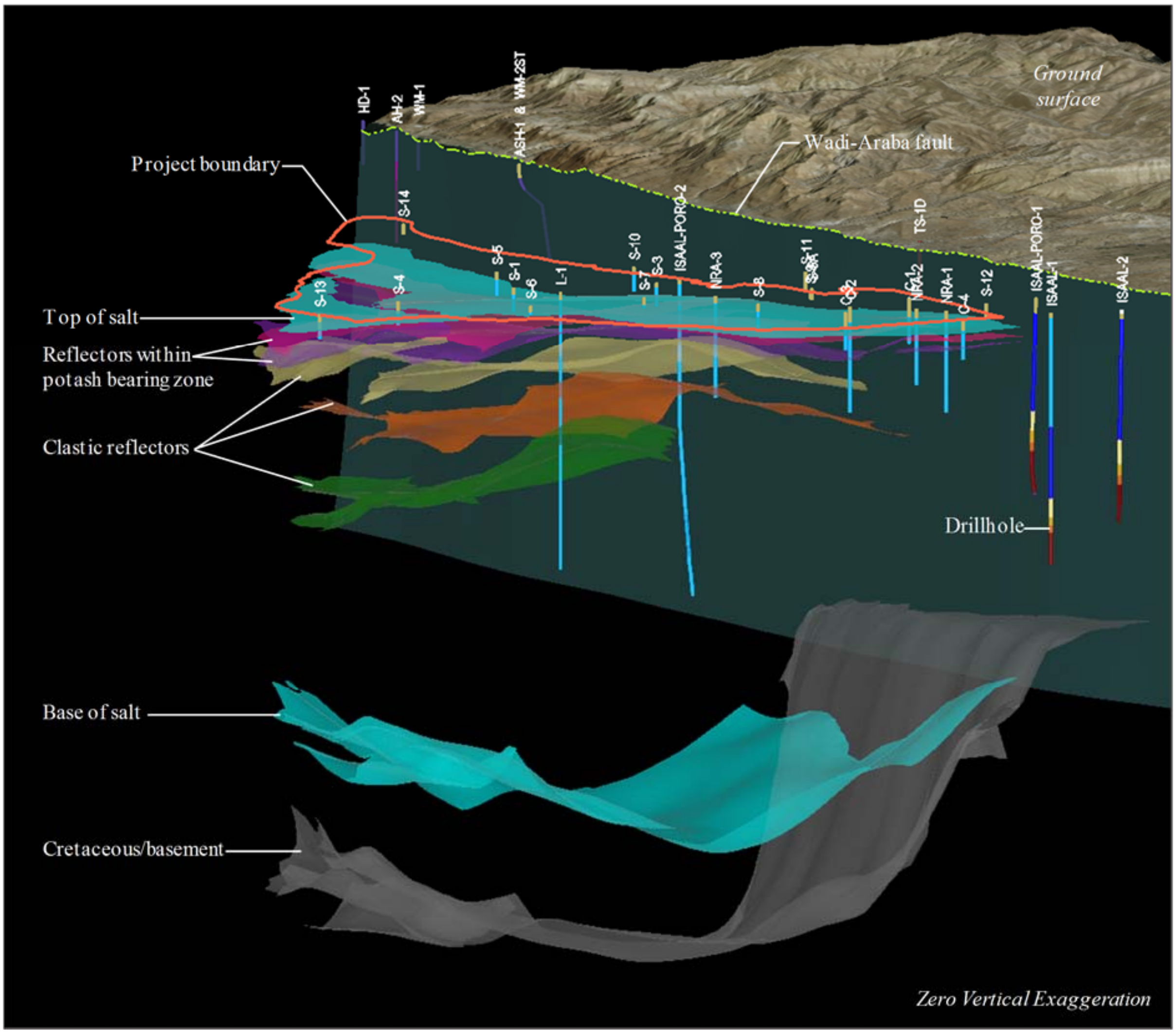

Figure 9-10. Seismic Surfaces in Model *(perspective view to northeast)*

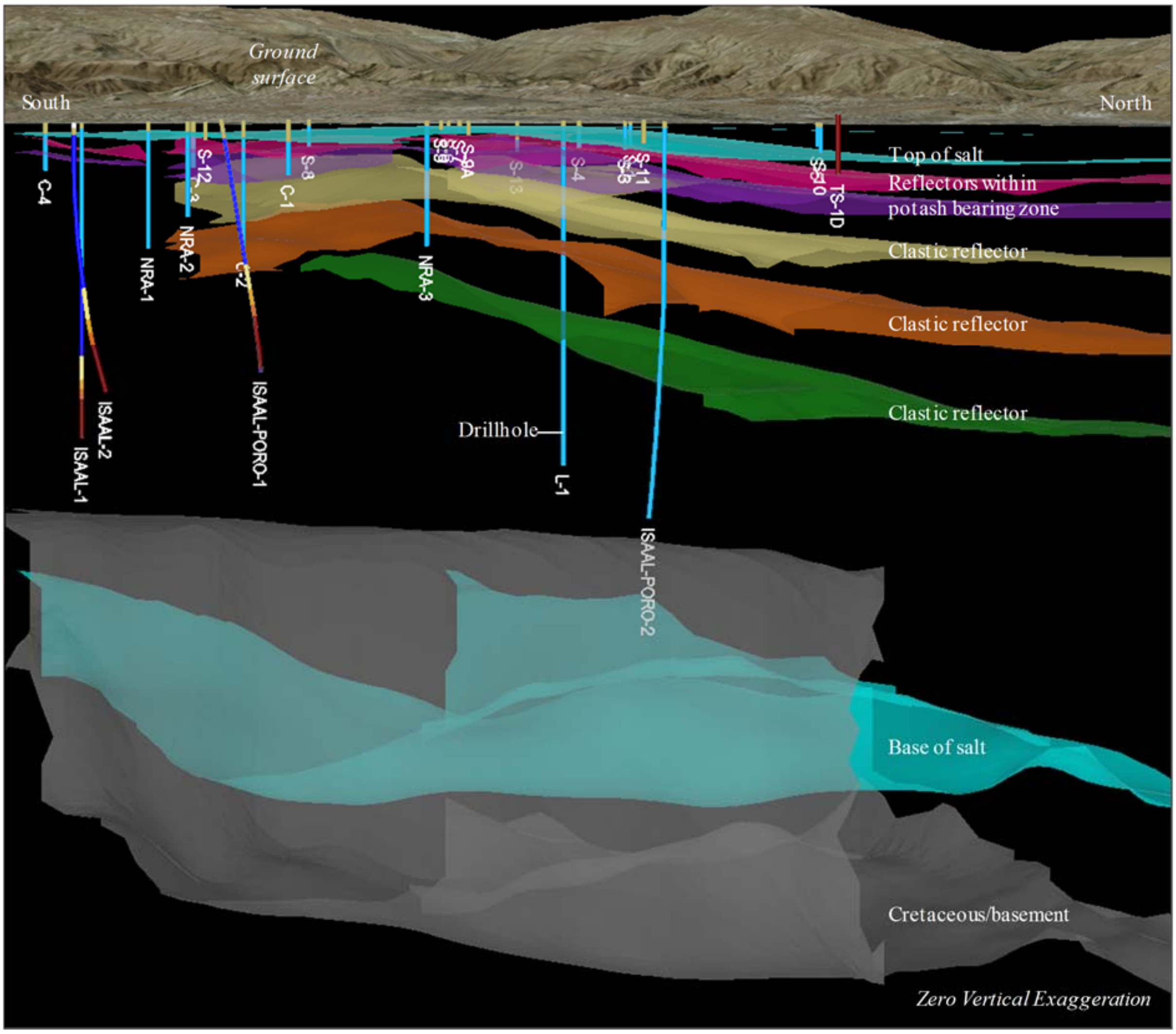

Figure 9-11. South–North Profile of Seismic Surfaces in Model (*orthographic view to west*)

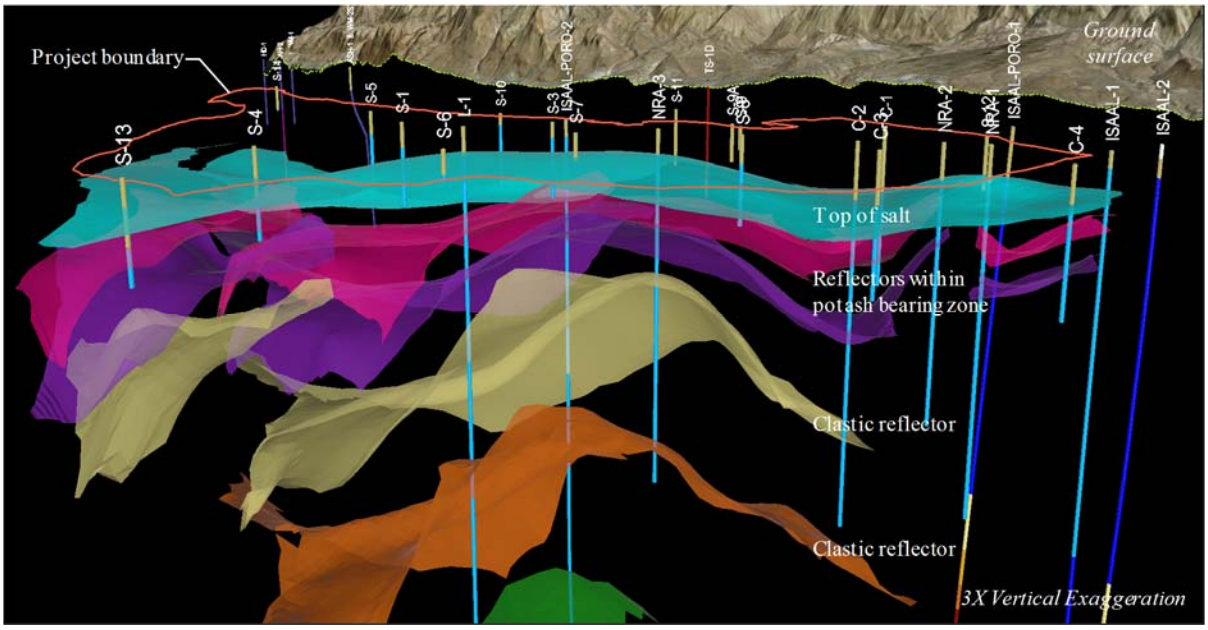

Figure 9-12. Reflectors through Potash Host Interval (*perspective view to northeast*)

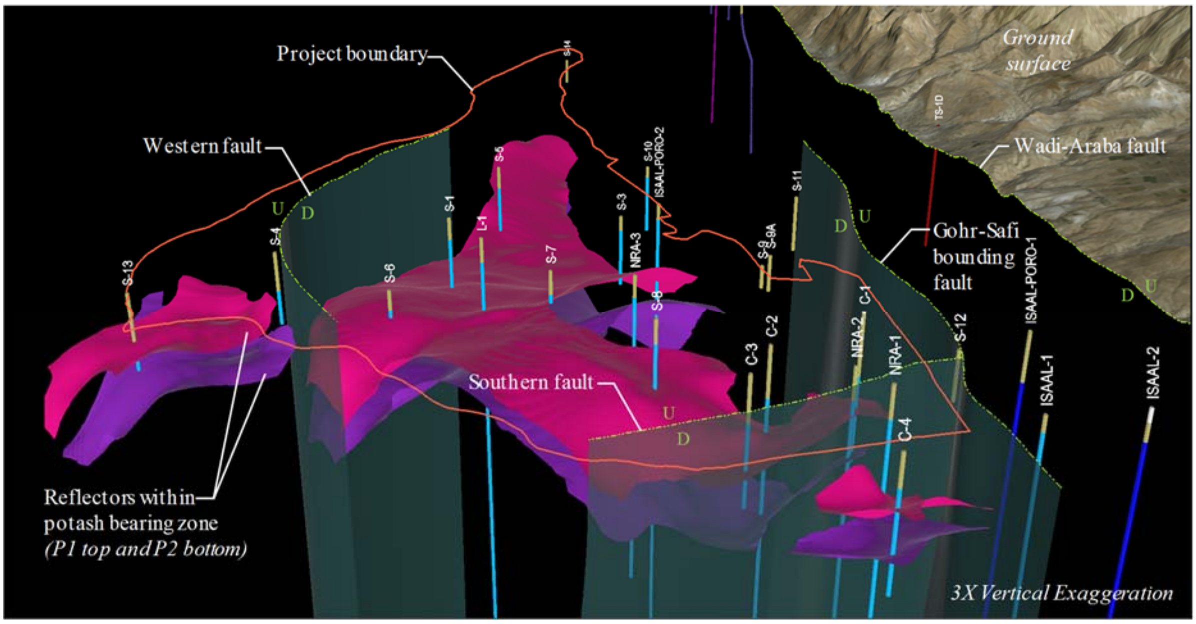

Figure 9-13. Reflectors near P1 and P2 Potash Beds (*perspective view to north*)

fault shows the potash beds to be downthrown on the order of 50 m on the south side of the fault, while the western fault reveals up to 250 m of vertical offset, downthrown to the east, along a major portion of the western project boundary. The seismic data suggest that these "faults" are likely fault zones comprised of multiple faults over a disturbed area.

Potential exits for additional minor to moderate faulting to exist in and around the diapir, particularly where seismic data are lacking or where the resolution of the historical data is limited.

The top of the salt (Sedom Formation) is shown in Figure 9-14 to be less than 100 m deep (below the surface) over a wide area at the apex of the diapir, located south of drillhole L-1. The top of salt plunges more than 450 m deep to the north. The base of the salt is interpreted to be more than 7,000 m below the surface at its deepest point within the Project area, as shown in Figure 9-15.

The reflector representing the uppermost major potash bed evident in the historical data, P1, is shown to range from less than 200 m deep at the highest point in the diapir to more than 700 m deep to the north. The reflector was interpreted to be relatively continuous and traceable across most of the Project area, as indicated by the shape of the pink footprint in Figure 9-16. While the continuity of the reflector and surrounding reflectors does not assure continuity of the P1 potash bed or other potash beds, it does indicate continuity of the stratigraphy hosting the potash. This implies potential for the occurrence of potash in bedded form across a large portion of the Project area.

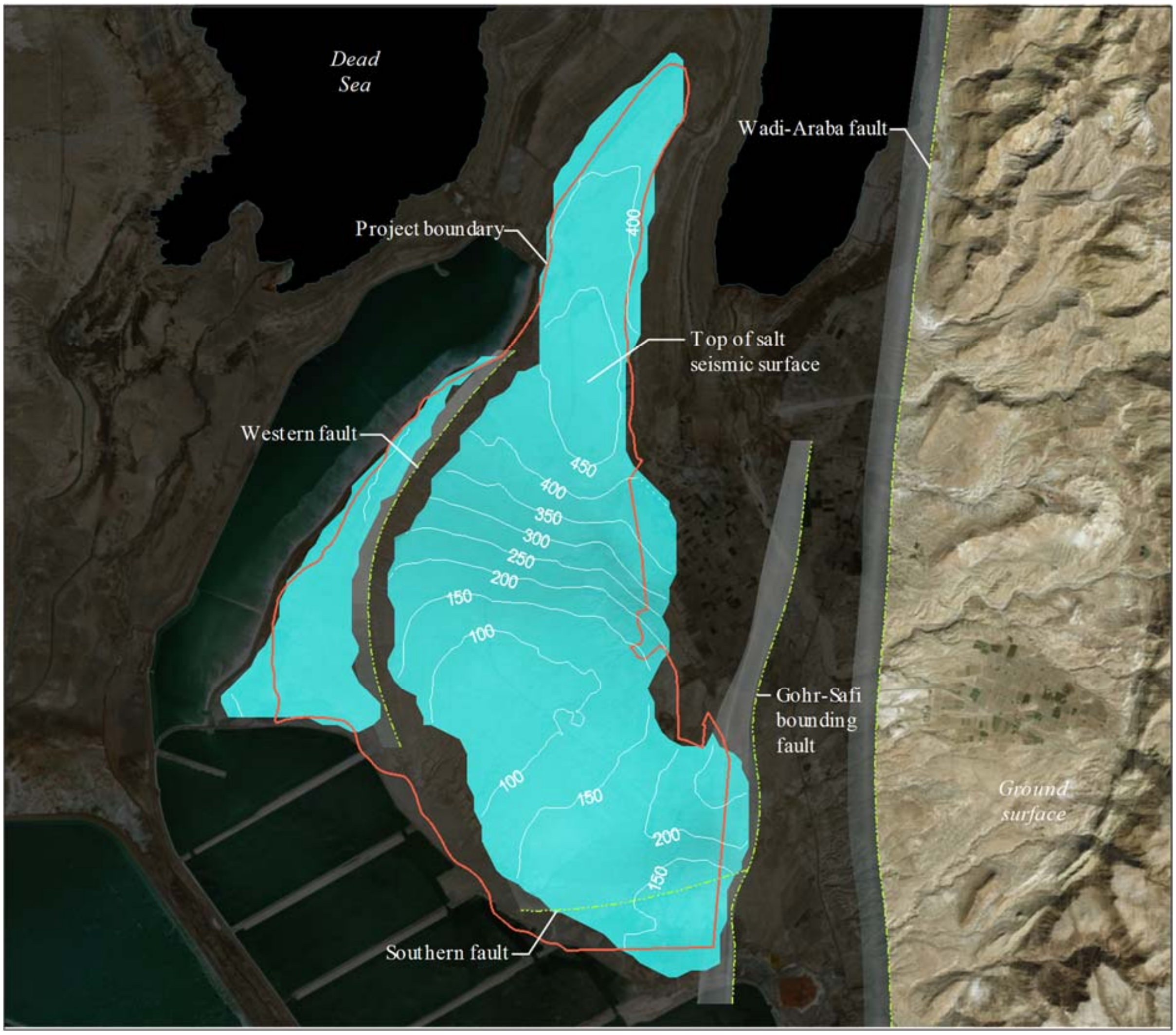

Figure 9-14. Top of Salt Surface—Depth Contours (meters) (*plan view*)

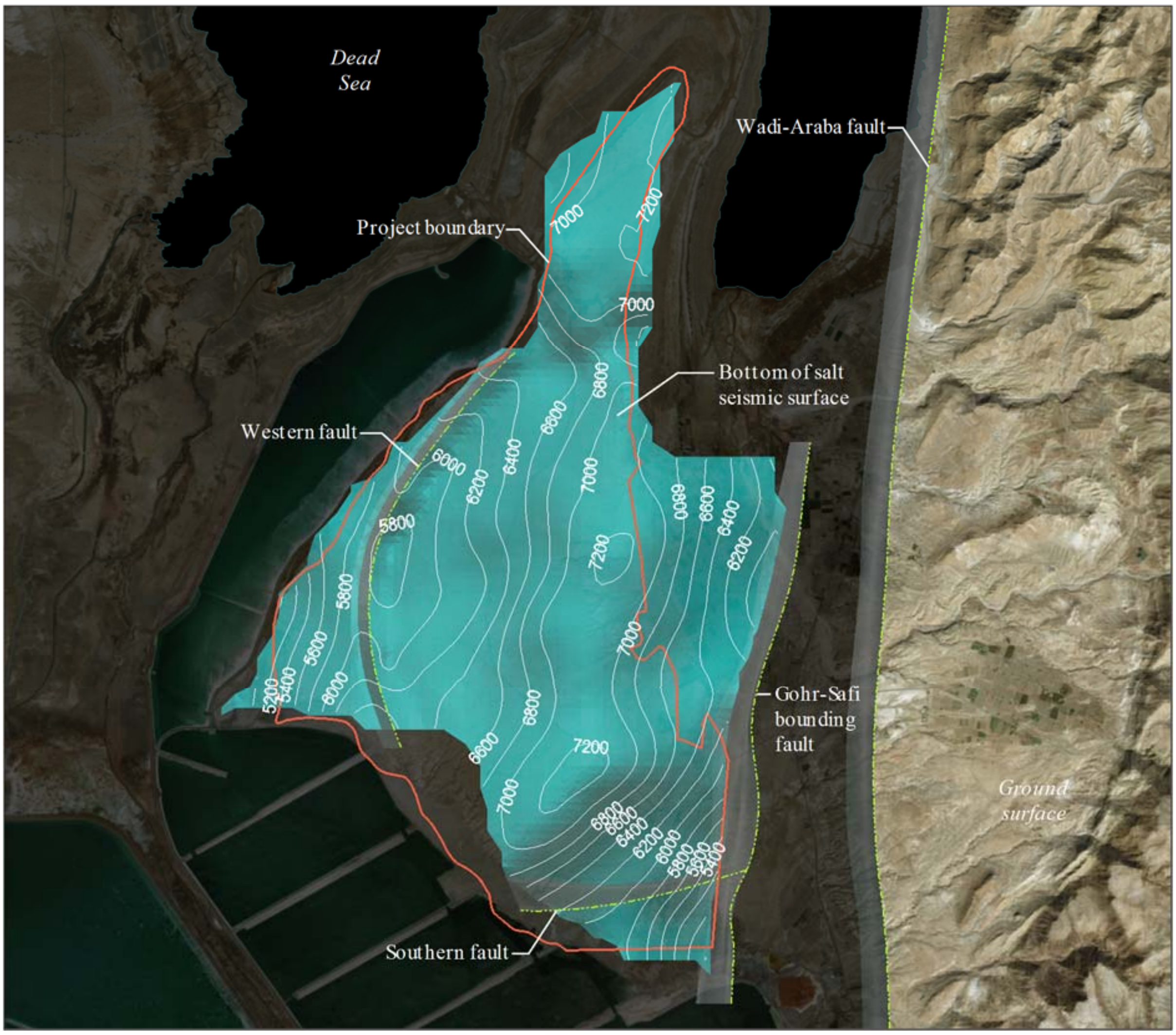

Figure 9-15. Base of Salt Surface—Depth Contours (meters) (*plan view*)

9.2.5 Potash Mineralization

Potash is evident from the geophysical and geology logs in nine drillholes located in and around the Project area. The potash mineralization was confirmed by core and assay in five of the nine holes, as described in Section 8.4. Assays included in the model for drillhole C-4 are shown by example in Figure 9-17.

Figure 9-18 illustrates the potash intercepts for the nine drillholes with log-interpreted potash intercepts. Figure 9-19 shows the intercepts confirmed by assay. Figure 9-20 shows all potash intercepts relative to the seismic reflector surfaces. The deepest intercept occurs at 1,460 m below ground surface.

Potash was geophysically interpreted from the gamma, spectral gamma, sonic, neutron porosity, and density logs. The remainder of holes lack adequate logs for determining the occurrence of potash and are, therefore, inconclusive whether potash is present or not present.

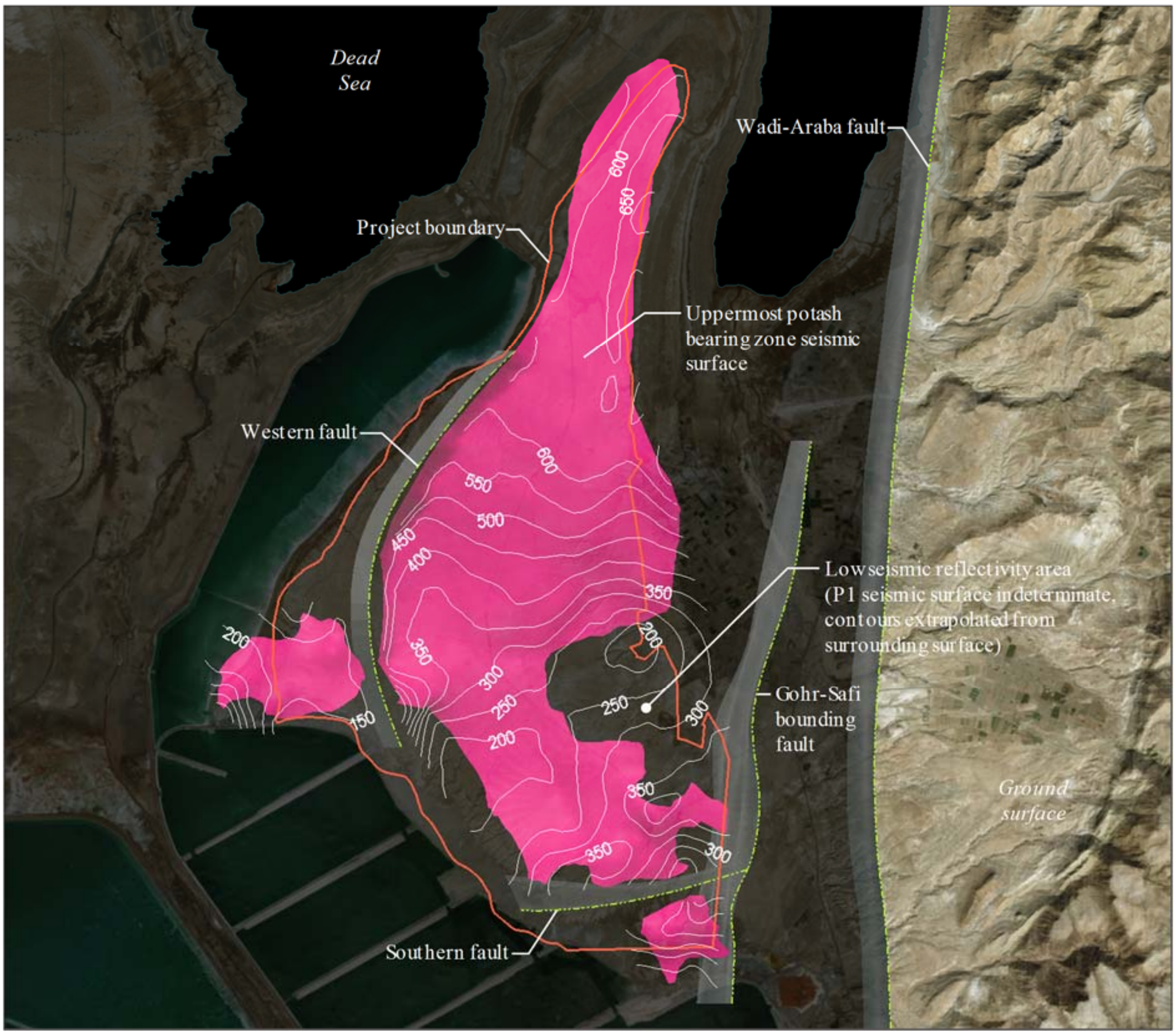

Figure 9-16. P1 Reflector Surface—Depth Contours (meters) (*plan view*)

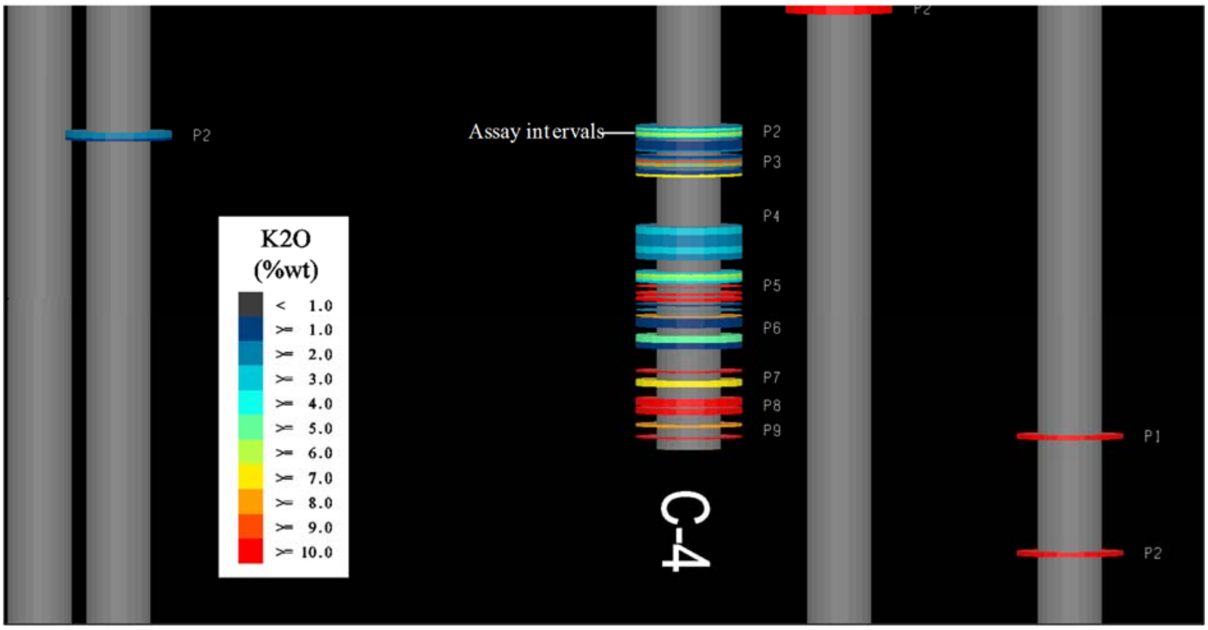

Figure 9-17. Assay Intervals for Drillhole C-4

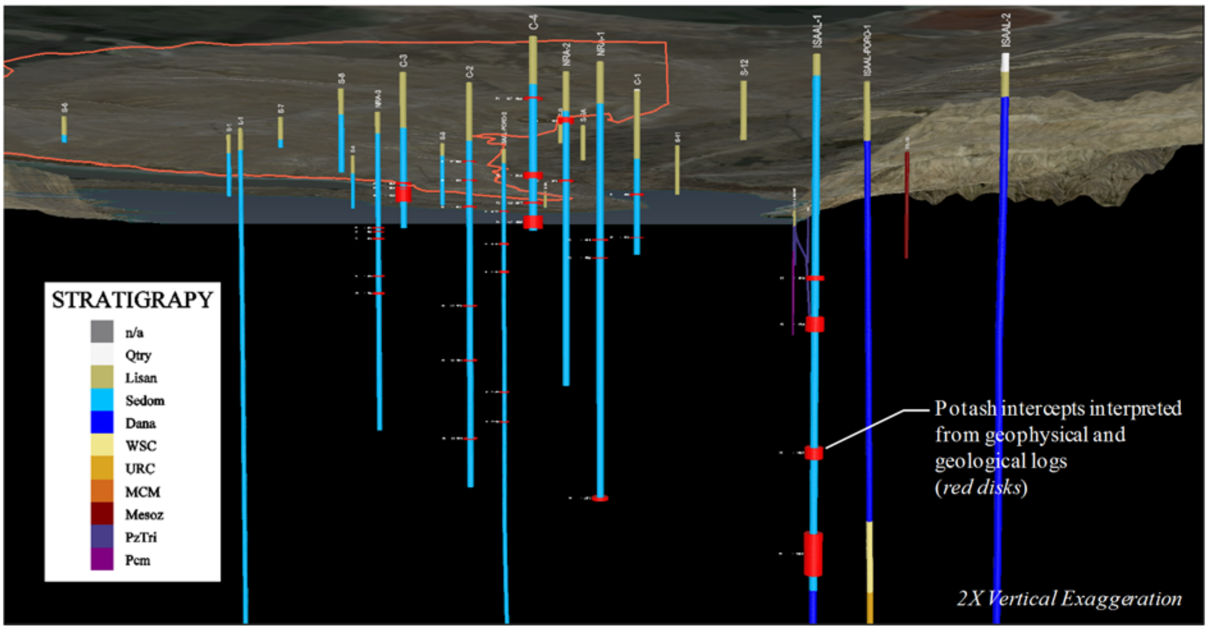

Figure 9-18. Drillhole Potash Intercepts Interpreted from Geophysical and Geologic Logs (*subsurface view to north*)

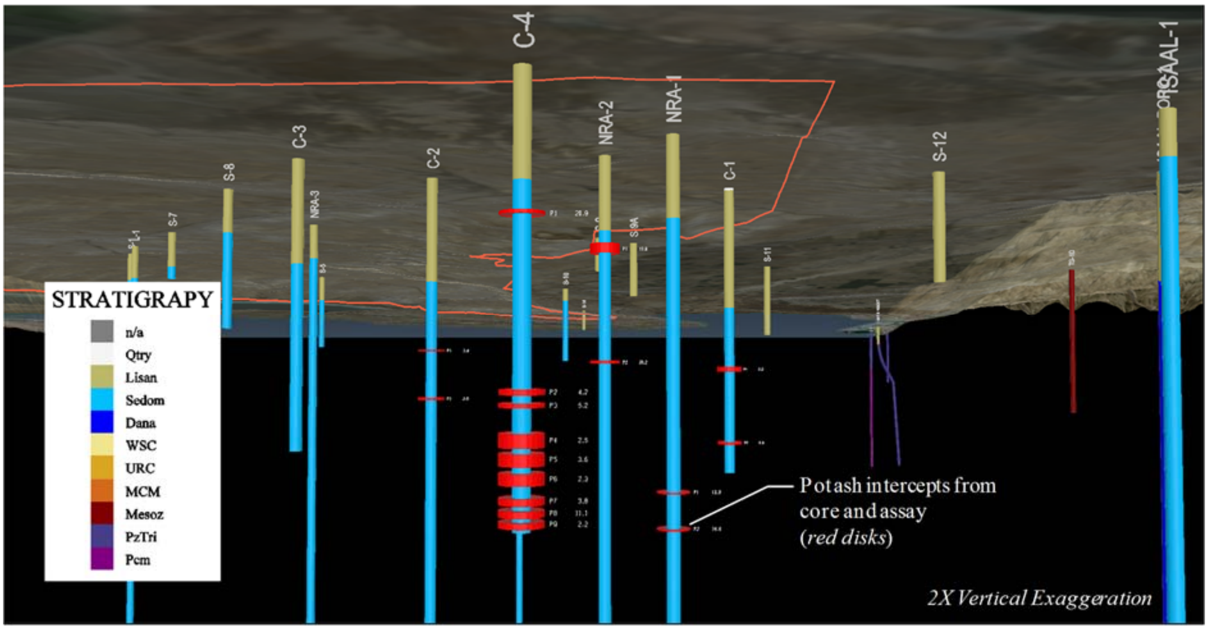

Figure 9-19. Drillhole Potash Intercepts Confirmed by Coring and Assay (*subsurface view to north*)

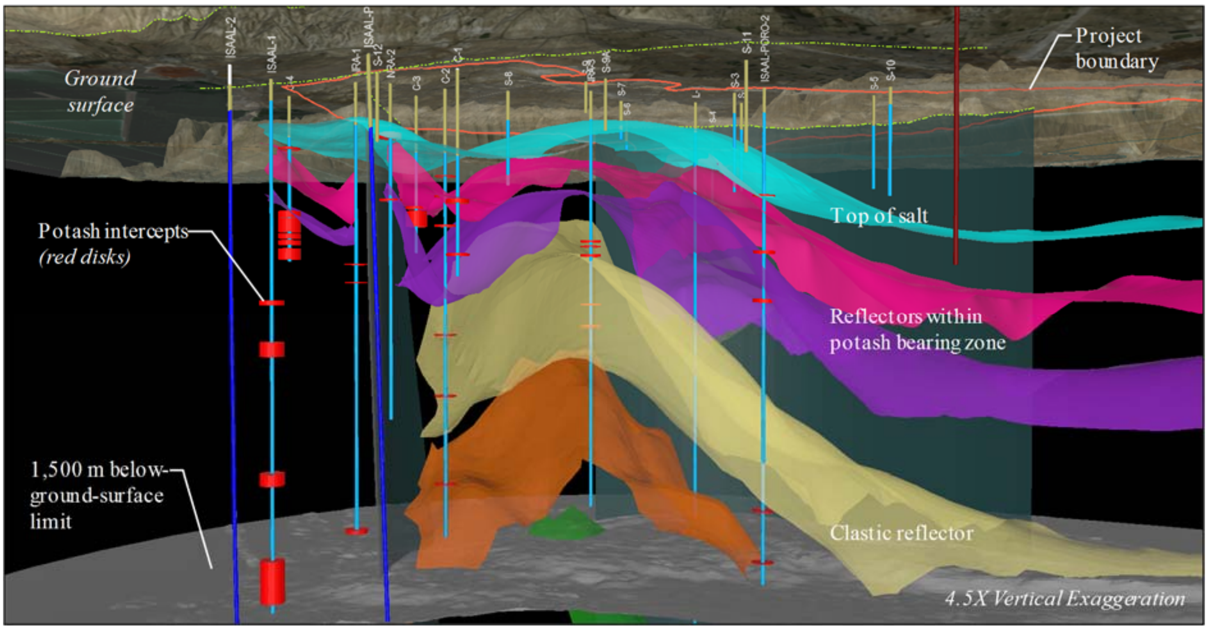

Figure 9-20. Drillhole Potash Intercepts with Seismic Reflector Surfaces (*underground view to west*)

In the nine holes with adequate logs, it is possible to estimate the approximate thickness of each potash bed and, in some cases, the mineralogy and K_2O composite grade of the bed. However, these quantitative estimates are not accurate enough and lack sufficient precision to be considered reliable for resource estimation. In some instances, it is possible that the identified potash may not be potash, particularly where conflicting geophysical information exists. While not reliable enough for resource estimation, the geophysically identified potash beds are considered reasonable indicators for planning future exploration drilling.

Potash is indicated in all holes drilled deep enough to penetrate the Sedom Formation, except for drillholes L-1, ISAAL-02, and ISAAL-PORO-01. The nine deep holes with potash mineralization are clustered in the southeast quadrant of the Project area where the most complete exploration drillhole information is available, particularly in and around the NRA-, ISAAL-, and C-series holes, as illustrated in Figure 9-21.

The logs for drillhole L-1 lack sufficient detail to determine the presence of potash. Potash may or may not exist in L-1. The preponderance of geological evidence suggests that there is reasonable potential that potash does occur in and around L-1.

Potash, as well as significant salt units, are believed to be missing in drillholes ISAAL-02 and ISAAL-PORO-01 due to faulting along the Wadi-Araba fault zone. Both holes are thought to delineate the approximate eastern margin of the Lisan potash deposit.

The historical drillhole and seismic results, when considered together, suggest that there is reasonable potential for potash to occur in one or more beds to a depth of at least 1,460 m over an area as large as 12 km^2 in the southeast corner the Project area. This approximate area is illustrated in Figure 9-22. The figure highlights the area where the historical database supports greater geologic confidence in potash continuity. Elsewhere to the west and north, minimal exploration data exist inside or outside the Project boundary.

Figure 9-21. Drillholes with Potash Mineralization (*underground view to north*)

The potash resource is considered "open," i.e., an exploration target with mineral potential, in these data-poor regions. The open resource footprint represents more than 80%, or 47 km^2, of the Project area.

Figure 9-23 shows the variation within the 3D block model of confidence in continuity for bed P1.

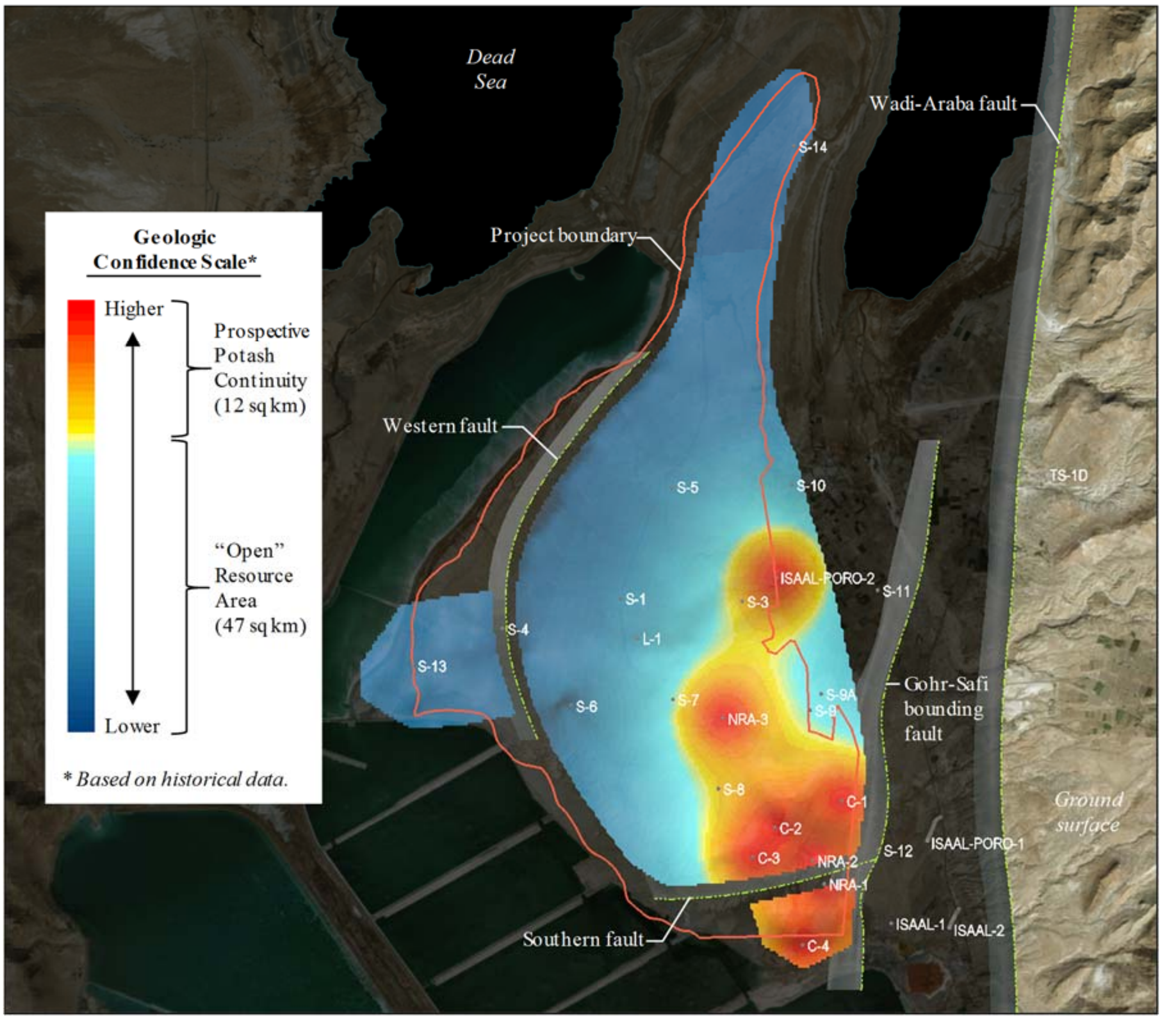

Figure 9-22. Geologic Confidence in Potash Continuity (*plan view*)

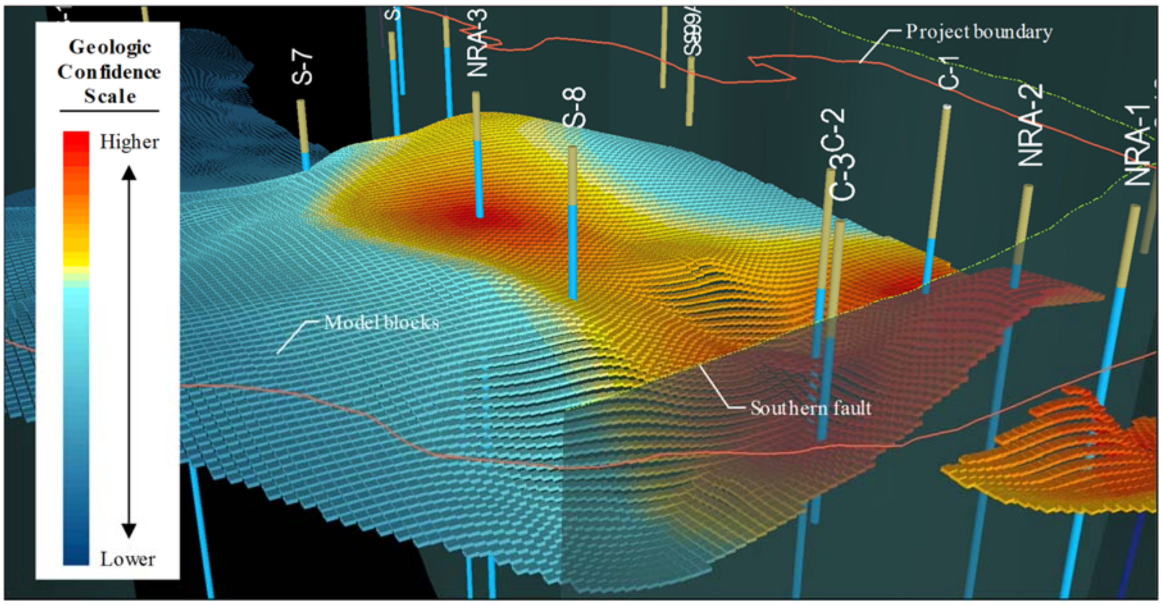

Figure 9-23. Geologic Confidence in Potash Continuity for Potash Bed P1 (*perspective view to northeast*)

10 INTERPRETATION AND CONCLUSIONS

Substantial historical exploration data were acquired and evaluated for Phase I. Based on the Phase I evaluation, the authors of this study conclude that potentially economic potash mineralization exists in a structurally complex environment in the southeastern quadrant of the Lisan Peninsula. Nine of the historical exploration drillholes, including five holes with core and assays, show potash occurring in multiple beds to a depth of at least 1,460 m with potential continuity over an area as large as 12 km^2 to the southeast inside the Project boundary.

Elsewhere to the west and north, minimal exploration data exist inside or outside the Project boundary. The potash resource is considered “open,” i.e., an exploration target with mineral potential, in these data-poor regions. The open resource footprint represents more than 80%, or 47 km^2, of the Project area.

Significant faults with major vertical offsets are evident on the western and southeastern margins of the Project boundary based on the reinterpretation of the historical seismic data. Modest faulting is implied elsewhere. The faulting is post-depositional as evidenced by the continuity of key seismic reflectors across fault zones. In some cases, seismic reflectors can be traced over the apex of the Lisan diapir and across much of the Project area, thereby supporting the likelihood that the potash, in bedded form, continues to the west and northeast over some or all of the Project area.

The authors of this study concur with MEMR’s opinion that future exploration work has reasonable potential to identify a moderate to substantial potash resource.

11 RECOMMENDATIONS

The Phase I investigators recommend that the project progress to Phase II—Data Gap Analysis and Exploration Program Development based on the Phase I conclusions, principally that the historical data locally confirm the occurrence of potash and reasonable potential exists for discovering a larger resource elsewhere with additional exploration.

The database compiled and corrected in Phase I provides sufficient information for conducting Phase II.

12 REFERENCES

Al-Zoubi, Abdallah and Uri S. ten Brink (2001), "Salt diapirs in the Dead Sea basin and their relationship to Quaternary extensional tectonics," *Marine and Petroleum Geology*, 18:779–797, Elsevier.

Arab Potash Company (2019a), "Potash Production Process," Arab Potash, http://www.arabpotash.com/Pages/viewpage.aspx?pageID=29 (accessed 2 October 2019).

Arab Potash Company (2019b), "2018 Annual Report," 168 pp.

Bandel, K. and R. Shinaq (2003), "The sea in the Jordan Rift (Northern Jordan) during Oligocene/Miocene transition with implications to the reconstruction of the geological history of the region," *Paläontologie, Stratigraphie*, Fazies, 11 (Freiberger Forschungshefte, C 499):97–115.

Bandel, Klaus and Elias Salameh (2013), "Geological Development of Jordan: Evolution and its Rocks and Life," 278 pp.

Bandel, Klaus, Ikhlas Alhejoj, and Elias Mechael Salameh (2016), "Geologic evolution of the Tertiary-Quarternary Jordan Valley with introduction of the Bakura Formation," *Paläontologie, Stratigraphie, Fazies* (23), Freibeg: Freiberg Forchungshefte, C 550:103–135.

Burchette, T. P. and V. P. Wright (1992), "Carbonate ramp depositional systems," *Sedimentary Geology*, 79:3–57.

Canadian Institute of Mining, Metallurgy and Petroleum (CIM) (2003), "Estimation of Mineral Resources and Mineral Reserves, Best Practice Guidelines: Canadian Institute of Mining, Metallurgy and Petroleum," November 23.

Canadian Securities Administrators (CSA) (2016), "National Instrument 43-101, Standards of Disclosure for Mineral Projects, Canadian Securities Administrators," May 9.

Closson, Damien, Najib Abou Karaki, Nada Milisavljević, Frédéric Hallot, and Marc Acheroy (2011), "Salt Tectonics of the Lisan Diapir Revealed by Synthetic Aperture Radar Images," *Tectonics*, Chapter 12, IntechOpen, doi:10.5772/13133.

Closson, Damien (2005), *Cooccurrence between the Geo-Hazards Induced by the Dead Sea Level Lowering and the Geological Setting, Lisan Peninsula, Lynch Strait, Ghor Al Haditah – Jordan*, PhD thesis, Universite de Liege, Faculte Des Sciences, Liége Wallonia, Belgium.

COTECNO ABT ALCHEMIA CDG MGA (a joint venture) (2005), "Third Tourism Development Project, Secondary Cities Revitalization Study, Karak, Economic Profile, Annex 3," report to The Hashemite Kingdom of Jordan, Ministry of Tourism and Antiquities and World Bank, 25 May, 34 pp., https://www.mota.gov.jo/Documents/KarakEconomic_profile.pdf (accessed 2 October 2019).

DMT GmbH & Co. KG (2018), "The New Main Brine Intake Pumping Station, Phase 1 and Phase 2, Offshore Subsurface Geophysical Investigation & Offshore and Onshore Surveys for Marine Works," report to APC, 5 February, 77 pp.

ESRI (2019), "ArcView, ArcEditor or ArcInfo," 25 June 2010, https://www.esri.com/arcgis-blog/products/arcgis-desktop/administration/arcview-arceditor-or-arcinfo/ (accessed 14 October 2019).

Garrett, Donald (1996), *Brine Processing Operations*, 10.1007/978-94-009-1545-9_6.

Halliburton Geophysical Services Inc. (1994), "Final Report of Seismic Data Processing," for the Natural Resources Authority, Area: EL LISAN 3D, Jordan.

Hashemite Kingdom of Jordan (2019), "Petroleum and Oil Shale Projects, Petroleum Exploration Blocks in Jordan," https://www.memr.gov.jo/Pages/viewpage.aspx?pageID=330 (accessed 4 November 2019).

Hexagon Mining (2019), "HxGN Mine Plan," https://hexagonmining.com/solutions/planning-portfolio (accessed 21 October 2019)

Hijazeen, K. (2019), personal communication, 20 August.

ICL (2018), "Annual Report for the Period Ended December 31, 2018," 424 pp.

International Plant Nutrition Institute (2017), "Potassium – Nutrient Source Specifics," 10 August, http://potassium.ipni.net/article/KPG-3044 (accessed 14 October 2019).

Jordanian Geologists Association (2014), "Interpretation and evaluation of the old exploration of the potash rock deposits (1959-1989), Lisan Peninsula-Dead Sea," Amman, 41 pp.

Kovach, Robert L. (1987), "Seismic Risk in Jordan," Open File Report 87-358, 9 July, 18 pp., Stanford Univesity: USGS.

MarketScreener (2018), "ARAB POTASH: Tamar partners sign additional $200 mln Jordanian gas deal," 19 November, https://www.marketscreener.com/ARAB-POTASH-CO-6493922/news/ARAB-POTASH-Tamar-partners-sign-additional-200-mln-Jordanian-gas-deal-27632656/ (accessed 4 November 2019).

MEIL (2019), "MEIL Proved its Superiority in Hydrocarbons Sector Too," Cision PR Newswire, 20 May, https://www.prnewswire.com/in/news-releases/meil-proved-its-superiority-in-hydrocarbons-sector-too-809749634.html (accessed 2 October 2019).

Ministry of Energy and Mineral Resources (2019), personal communication with the Committee, July.

Ministry of Energy and Mineral Resources, Natural Resources Authority (1987), "Al Karak 3153 III."

Ministry of Energy and Mineral Resources, Natural Resources Authority (1988), "Geological Map of Ar Rabba (3152 IV)."

Ministry of Energy and Mineral Resources, Geology Directorate (2015), "Interpretation and Evaluation of the Old Exploration (1959-1989) of Potash Rock Deposits in the Lisan Peninsula-Dead Sea," 47 pp.

Ministry of Energy and Mineral Resources, Geology Directorate (2018), “Geological Map of AYN JIDI and AS SAFI 3052-I & 3052-II.”

National Electric Power Company (2019), “Development of Electricity,” http://www.nepco.com.jo/en/electricity_improve_en.aspx (accessed 4 November 2019).

Natural Resources Authority (1987), “An Exploration Program for Solid Potash Minerals in the Lisan Peninsula, Dead Sea Area,” 51 pp.

Natural Resources Authority (1968), “Summary Report of the Geological, Geophysical, and Geomechanical Exploration Works Carried out in El-Lisan Area between 1959 and 1968,” Geology and Petroleum Division.

Porosity Ltd. (2009), “Isaal-Poro-1 Final Well Report,” February, 91 pp.

Powell, John H. and Basem K. Moh'd (2011), “Evolution of Cretaceous to Eocene alluvial and carbonate platform sequences in central and south Jordan,” *GeoArabia - Middle East Petroleum Geosciences*, 16(4):29–82.

Powell, John, Abdulkader Abed and Yves-Michel Nindre (2014), “Cambrian Stratigraphy of Jordan,” *GeoArabia*, 19.

Powell J. H., M. H. Stephenson, A. Nicora, R. Rettori, L. M. Borlenghi and M. C. Cristina Perri (2016), “The Permian -Triassic boundary, Dead Sea, Jordan: transitional alluvial to marine depositional sequences and biostratigraphy,” *Riv. It. Paleontol. Strat.* 122(3):23–40.

RAILMED (2019), “Jordanian Railway,” RAILMED, A Project for MEDA 2020, https://www.railmed.org/reports/jordan/ (accessed 2 October 2019).

Read (1985), “Carbonate platform facies models,” *American Association of Petroleum Geologists Bulletin*, 69:121.

RPS Group (2019), personal communication, Lisan reprocessing discussion with Luc Gravel and Atul Nautiyal, Lisan, October.

Sade, A. R., J. K. Hall, H. Y. Sade, G. Amit, G. Tibor, B. Schulze, L. Gur-Arieh, U. ten Brink, Z. Ben-Avraham, C. Keller, I. Gertman, J. Beaudoin, A. S. Al-Zoubi, E. Akawwi, O. Rimawi, A. Abuledas, L. A. Mayer, B. R. Calder and A. Maratos (2014), “Multibeam Bathymetric Map of the Dead Sea,” IOLR Report H-1-2014, GSI Report GSI/01/2014.

Seismograph Service Limited (1993), “3D Vibroseis reflection seismic survey conducted in the Hashemite Kingdome of Jordan for Natural Resources Authority, Party 199,” 15 January to 29 May 1993, pp. 1–49.

Schlumberger (1968), “Fundamentals of Quantitative Log Interpretation-Schlumberger Log Interpretation Principles,” Oberto Serra.

Schlumberger (1991), “Log Interpretations Principles/Applications,” in O. Serra (1994) “Evaporites and Well Logs,” in *Evaporite Sequences in Petroleum Exploration; 1.*

Geological Methods, Editions Technip, French Oil and Gas Industry Association, Technical Committee, GRECO 52 (CNRS), PA8.

Sunna, B. F. (1986), "The Geology of Salt Deposits in the Lisan Peninsula – Dead Sea," *Seminar on Salt in the Arab World*, Amman, Jordan: Ministry of Energy and Mineral Resources, Natural Resources Authority, 4–6 May.

TransGlobal Petroleum Company Jordan (2001), "Dead Sea Lisan Peninsula 3D Processing Report," Prepared by: Geophysical Service Center Company LTD (GSC), Amman, Jordan, August.

TransGlobal Petroleum Jordan (2005), "Final Geological Report (Well: Isaal – 2)," December, 41 pp.

USGS (2019), "The Modified Mercalli Intensity Scale," https://earthquake.usgs.gov/learn/topics/mercalli.php (accessed 4 November 2019).

Western Atlas (1994), "Seismic interpretation and seismic modelling of the El-Lisan Peninsula, Dead Sea," report prepared for Natural Resources Authority, Hashemite Kingdom of Jordan, pp. 1–133.

Western Geophysical (1994), "Seismic Interpretation and Seismic Modelling of the El-Lisan Peninsula, Dead Sea," report to Natural Resources Authority of Jordan, October, 133 pp.

Williams-Stroud Sherilyn (1994), "The Evolution of an Inland Sea of Marine Origin to a Non-Marine Saline Lake: The Pennsylvanian Paradox Salt," *Sedimentology and Geochemistry of Modern and Ancient Saline Lakes Models*, Robin W. Renaut and William M. Last, editors, 1 January, doi: https://doi.org/10.2110/pec.94.50.0293.

Wikipedia (2019), "Dead Sea," 28 October (accessed 4 November 2019).

Wyllie, B. K. N. (1931), "The Geology of Jebel Usdum, Dead Sea," *Geol. Mag*., 68:366–372.

Zak, I. (1967), "The Geology of Mount Sedom," Ph.D. thesis, Jerusalem: Hebrew Univ., 208 pp. cited acc.

Other Reviewed References

Abbott, B. M., P. R. Johnson and G. P. Long (1987), "Jordan Surface Geochemistry Pilot Study," Amoco, August, 88 pp.

ALZyod, Hisham and Reem Qashtawi (2019), "Mineral Resources in Jordan," Ministry of Energy and Mineral Resources, January, 21 pp.

Amoco Company (n.d.), "Seismic Program, Blocks 1 and 4," 15 pp.

Amoco Company (1987), "Structural Geology Seminar, Amman, Jordan," February, 41 pp.

Barton, Yuval, Amotz Agnon, Yehouda Enzel, and Mordechai Stein (2006), "Late Quaternary faulting and subsidence in the central Dead Sea basin," *Israel Journal of Earth Sciences*, April, 16 pp., doi:10.1560/E3RK-0RDY-3CUP-LN5A.

Bender, Friedrich (1975), "Geology of the Arabian Peninsula, Jordan," Geological Survey Professional Paper 560-I, 43 pp., Washington, DC: US Government Printing Office.

Buiskool Toxopeus, J. M. A. and G. W. van Graas (1988), "Geochemical Investigation of Two Impregnated Outcrop Samples North of Wadi Issal, Jordan," Confidential report, RKER.88.268, November, 22 pp.

Claypool, G. E. and J. R. Gormly (1990), "Geochemical Charasterics of Outcrop's Samples and Hamzeh Field Crude Oil, Jordan-Dead Sea Area; Evaluation of Oil/Source Correlation," Mobil Research and Development Corporation, Dallas Research Laboratory, December, 47 pp.

Closson, Damien, Philip E. LaMoreaux, Najob Abou Karaki, and Hassan al-Fugha (2007), "Karst system developed in salt layers of the Lisan Peninsula, Dead Sea, Jordan," *Environ Geol*, 52:155–172, Springer-Verlag, doi:10.1007/s00254-006-0469-9.

"Hydrocarbon Potential of the Dead Sea Basins of Jordan," (n.d.), 45 pp.

DEMINEX – Deutsche Erdölversorgungsgesellschaft mbH (n.d.), "Jordan Dead Sea – Jordan Rift System, Review of Hydrocarbon Prospectivity," 36 pp.

Larson, Daniel M. (1992), "Wadi-Araba, Jordan Seismic Processing," Houston, TX: Marathon Oil Company, Seismic Services Group, October, 5 pp.

Mika, James E. (1987), "Gravity and Magnetic Interpretation of Block 4, Jordan," Report No. 87022, August, 28 pp.

Ministry of Energy and Mineral Resources (n.d.), "Mineral Resources in Jordan," 32 pp.

Murtada, Hani (1968), "Summary Report of the Geological, Geophysical and Geochemical Exploration Works carried out in El-Lisan Area between 1959 and 1968," Amman: Natural Resources Authority, Research and Investigation Department, Geology and Petroleum Division, September, 27 pp.

TAHAL Consulting Engineers Ltd. in association with The Geological Survey of Israel and associates (2011), *Red Sea – Dead Sea Water Conveyance Study Program, Dead Sea Study*, GSI Report Number: GSI/10/2011, TAHAL Report Number: IL-201280-R11-218.

Trollinger Geological Associates, Inc. (1975), "Photographic and Geomorphic Evaluation Memorandum Report of the Dead Sea, Jordan Valley and Northern Highlands Area, Jordan," report to Filon Exploration Corporation, October, 44 pp.

Weinberger, R., Z. B. Begin, N. Walkmann, M. Gardosh, G. Baer, A. Frumkin, and S. Wdowinski (2006), "Quaternary rise of the Sedom diapir, Dead Sea Basin," Geological Society of America, Special Paper 401, 20 pp.

Wilburn, David R., Carl Di Francesco, and Donald I. Bleiwas (1996), "Estimated Use of Explosives in the Mining Industries of Egypt, Jordan, Syria, Tunisia, and Turkey," Golden, CO: USGS, UCRL-CR-125620, P.O. B291867, 244 pp.

Yilmaz, Öz (2001), “Seismic data analysis,” Society of Exploration Geophysicists, ISBN 1-56080-094-1.

Zak, I. and Freund, R. (1966): Recent strike-slip movements along the Dead Sea Rift. – Israel J.Earth Sci., 15: 33–37.

APPENDIX A

RPS SEISMIC REINTERPRETATION REPORT

LISAN PENINSULA POTASH EXPLORATION
Final Interpretation Project

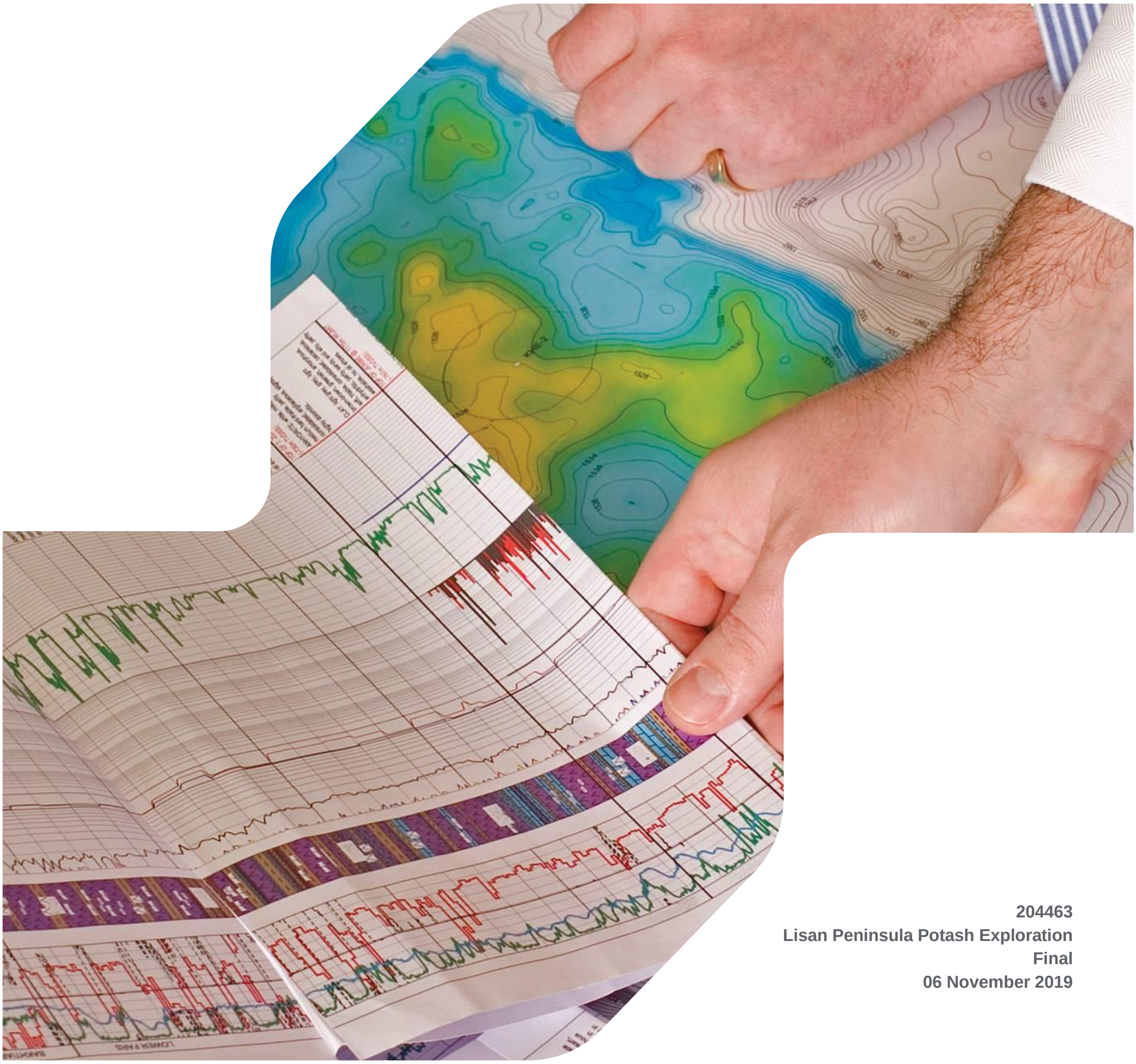

204463
Lisan Peninsula Potash Exploration
Final
06 November 2019

Approval for issue

Roger Edgecombe	Roger.edgecombe@rpsgroup.com	6 November 2019

This report was prepared by RPS Energy Canada Ltd ('RPS') within the terms of its engagement and in direct response to a scope of services. In preparing the report, RPS may have relied upon information provided to it at the time by other parties. RPS accepts no responsibility as to the accuracy or completeness of information provided by those parties at the time of preparing the report. The report does not take into account any changes in information that may have occurred since the publication of the report. If the information relied upon is subsequently determined to be false, inaccurate or incomplete then it is possible that the observations and conclusions expressed in the report may have changed. The opinions and interpretations presented in this report represent our best technical interpretation of the data made available to us. However, due to the uncertainty inherent in the estimation of all sub-surface parameters, we cannot and do not guarantee the accuracy or correctness of any interpretation and we shall not, except in the case of gross or wilful negligence on our part, be liable or responsible for any loss, cost damages or expenses incurred or sustained by anyone resulting from any interpretation made by any of our officers, agents or employees.

Except for the provision of professional services on a fee basis, RPS Energy Canada Ltd., does not have a commercial arrangement with any other person or company involved in the interests that are the subject of this report.

Prepared by:

RPS Energy Canada Ltd.

Roger Edgecombe, M.Sc., P.Geoph., P.Geo.
Senior VP - Geoscience

Suite 600
555 4th Avenue SW
Calgary AB
T2P 3E7

T +1 403 265 7226
E roger.edgecombe@rpsgroup.com

Prepared for:

Agapito Associates Inc.

Leo Gilbride, P.E., P.Eng.
Senior Consultant

Suite 340
715 Horizon Drive
Grand Junction CO
81506

T +1 970 242 4220
E gilbride@agapito.com

Our ref: 204463

Suite 600
555 4th Avenue SW
Calgary AB
T2P 3E7
T +1 403 265 7226

Date: 06 November, 2019

Agapito Associates Inc.
Suite 340
715 Horizon Drive
Grand Junction CO
81506

Re: Lisan Peninsula Potash Explortation – Seismic Interpretation Report

Leo,

Please find attached our report documenting the Initial Interpretation of the 2019 Lisan Peninsula Exploration Project completed by RPS Energy Canada Ltd., on behalf of Agapito Associates Inc. for the benefit of the Jordanian Ministry of Minerals and Energy Resources.

We have thoroughly enjoyed working on this project with you and your team and look forward to working on the next phase(s) of the project with the Team.

Yours sincerely,
for RPS Energy Canada Ltd.

Roger Edgecombe, M.Sc., P.Geoph., P.Geo.
Senior VP - Geoscience
roger.edgecombe@rpsgroup.com
+1 403 543 5365

EXECUTIVE SUMMARY

As part of a subsurface investigation by the Ministry of Energy and Mineral Resources, Natural Resources Authority of the Hashemite Kingdom of Jordan, RPS Energy Canada Ltd. (RPS) was contracted by Agapito Associates Inc.(AAI) to interpret reprocessed 2D and 3D seismic data as part of a four-phase exploration project on the Lisan Peninsula to assess the potential for an economic potash deposit.

The primary objective of the seismic interpretation project was to properly image and map the top of the salt and the distribution of any prospective potash interval within the salt. The interpretation work used legacy seismic data from earlier petroleum exploration in the area as well as newly reprocessed seismic data. Overall, data quality was poor-to-fair but with potential for improvement, both spatially and temporally.

RPS completed the correlation of geological markers to seismic events from recently reprocessed 2D and 3D seismic data provided by Misbar Geophysical Services. Reprocessing was critical in improving the geophysical data and the subsequent subsurface images. Geological guidance from well data was provided by Agapito Associates and enabled the identification and mapping potential potash bearing zones. At the onset of the project, it was determined that interpreting the depth structure would be necessary to meet the objectives of the 2019 Lisan Peninsula seismic. Therefore, all seismic mapping was depth converted. Additionally, the 3D volume has been depth converted with a simple velocity model.

The mapped potash bearing zones were constrained laterally and in depth. The prospective area in the northern portion of the project area is well defined by high confidence seismic interpretation and shows the general structure to rapidly fall off the apex of the Lisan diapir with a northerly dip. The shallower data in the southern project area does not suggest any steep dips until below the prospective potash zone. This area is potentially more prospective than the northern area but is also considered to have low confidence in the seismic interpretation. These finding are encouraging for the potash potential of the area and further investigation is warranted.

Contents

EXECUTIVE SUMMARY I
1 INTRODUCTION 3
1.1 Geological Setting 4
2 COMPANY PROFILE 5
2.1 Corporate Qualifications 5
3 DATA ACQUISITION & PROCESSING 7
3.1 General Comments 7
3.2 Seismic Data Acquisition 7
3.3 Seismic Data Time Processing 7
3.3.1 Seismic Data Reprocessing 8
4 INTERPRETATION PROCEDURES 11
4.1 General Comments 11
4.2 Synthetic Seismograms and Geological Correlation 11
4.3 Seismic Events 12
4.4 Depth Conversion 12
4.5 Interpretation Risk Assessment 13
5 INTERPRETATION ANALYSIS 14
5.1 General Comments 14
5.2 Salt Reflectivity Interpretive Model 14
5.3 2D & 3D Seismic Horizons 15
5.4 Depth Structure Maps 17
6 CONCLUSIONS 20
7 RECOMMENDATIONS 21
8 REFERENCES 22
9 DIGITAL INFORMATION 23
9.1 Final Products 23
10 AUTHORIZATION 24

Figures

Figure 1: Location and Seismic Database Map. 3
Figure 2: Simplified Anticline Geological Section taken from Rabba *et. al.* (2015). 4
Figure 3: 2D Seismic Reprocessing: CGG Legacy and Misbar 2019. 8
Figure 4: 2D and 3D Reprocessing: Leveraging Areal Coverage to Mitigate Noise. 9
Figure 5: 3D Reprocessing: GSC 1993 Legacy and Misbar 2019 Pre-Stack Time Migration. 9
Figure 6: 3D Reprocessing: Misbar 2019 Pre-stack Time Migration Coherency Filter. 10
Figure 7: ISAAL-PORO-2 Synthetic and Geological Correlation. 11
Figure 8: Two Depth Conversion Velocity Models. 12
Figure 9: 3D Seismic Interpretation: Full Section and Potash Zone Detail. 14
Figure 10: Salt Reflectivity Interpretive Model. 15
Figure 11: Seismic interpretation on two key 2D lines; DS-07 & VWJ-13. 16
Figure 12: NW-SE Arbitrary Line Interpretation through the 3D volume. 16
Figure 13: NE-SW Arbitrary Line Interpretation through the 3D volume. 17
Figure 14: Depth Structure Maps: Top of Salt, Base of Salt and Cretaceous/Basement. 17
Figure 15: Depth Structure Maps: Top of Potential Potash, Intra Potential Potash Zone and Base of Potash Potential. 18

Figure 16: Seismic Depth Structure 3D Views: From the Southwest and the Southeast. 18
Figure 17: Seismic Depth Structure 3D Views: From the Northeast and the Northwest. 19

1 INTRODUCTION

Over the last decade, the surface seismic method has gained widespread recognition in the potash industry, both as a valuable mine planning tool and as an analytical tool for anomalous underground encounters at the mining level. Today, problems such as analysis of site-specific solution collapse anomalies, void space mapping, and brine inflow site identification are being solved using surface seismic investigations.

Historically, the seismic method was first applied to the potash industry in Canada during the 1960’s and 1970’s. Despite its initial technological limitations and resultant slow acceptance, the seismic method has today been embraced by the global potash industry as a useful tool. By incorporating regional two dimensional (2D) studies over large areas, mine planning progressed from geological extrapolation between test holes to more detailed evaluation of the subsurface based on three dimensional (3D) seismic.

As the acceptance of the 2D seismic ability to answer questions about the subsurface grew and, in turn, the ability of the seismic method to resolve smaller and smaller features evolved, the demand for seismic increased. In the mid 1980’s, the three-dimensional seismic method was introduced, and the ability to create detailed spatially correct images of the subsurface gained popularity.

The recognition by earth scientists and mining engineers of the on-going potential of seismic to contribute to the success of a mining operation has driven the continual evolution of the method. Today, the seismic method is used in a variety of applications in the potash industry, some proven by successes and some in the research and development stage.

As part of a subsurface investigation by the Ministry of Energy and Mineral Resources (MEMR), Natural Resources Authority of the Hashemite Kingdom of Jordan, RPS Energy Canada Ltd. (RPS) was contracted by Agapito Associates Inc. (AAI) to interpret 2D and 3D seismic data as part of a four-phase project for potash on the Lisan Peninsula. Phase I, of the five-phase project, was to interpret approximately 100 linear kilometres of 2D and 100 km^2 of 3D seismic coverage.

As illustrated in Figure 1, the Lisan Peninsula is located on the east bank of the Dead Sea, in the Hashemite Kingdom of Jordan. The Lisan Peninsula now effectively divides the Dead Sea into a north and south portion, where the southern portion is used for an open-pan salt and potash production (Fig. 1).

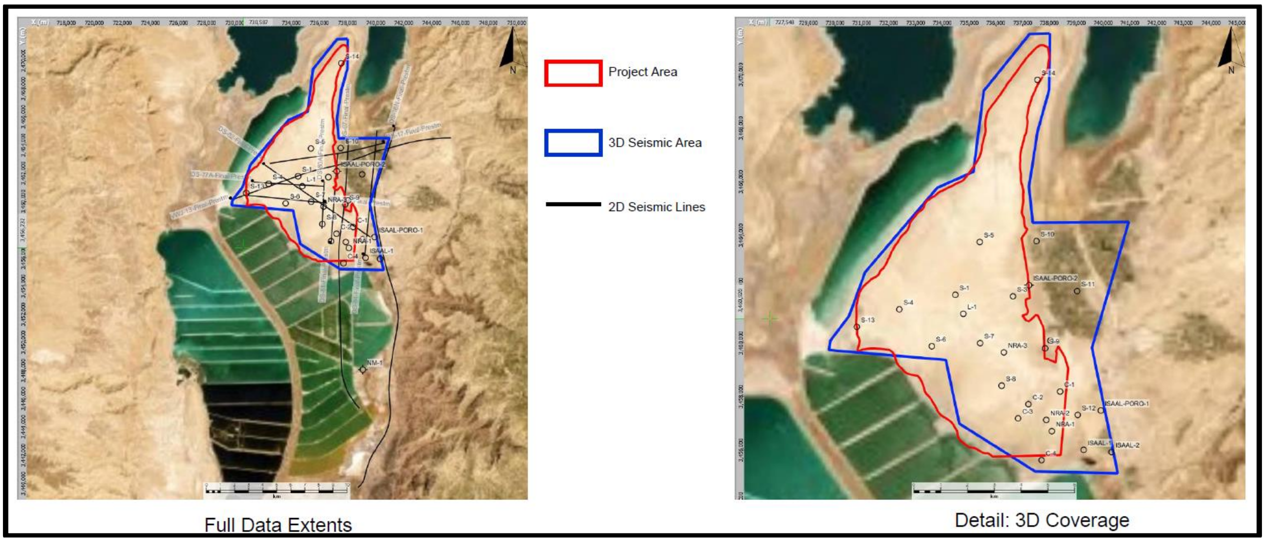

Figure 1: Location and Seismic Database Map.

Although a number of tasks and objectives comprise Phase I, one of the primary goals of the first phase of the 2019 Lisan Peninsula Potash Exploration Project was to use historical geological and geophysical data to contribute to the subsurface knowledge in an area where geological information was sparse and assist in the resource evaluation of potash potential.

The main objectives of the program include, but are not limited to the following:

- Evaluate legacy and newly reprocessed seismic data;
- Identify seismic events and correlate to geological horizons wherever possible;
- Prepare time structure maps and fault planes;
- Compute seismic velocities and convert key seismic events to geologically reasonable depth maps;
- Provide any risk and quality constraints that may affect resource estimates.

The combined interpretation results are presented in this report as a series of cross-sectional views of individual lines and plan view maps of geological surface structure. The 2D and 3D seismic data set provides subsurface information that facilitates the assessment of the geologic conditions that future mining operations may encounter. Maps created from the seismic data can be used to assess the potash potential of the area, assist mine planners in assessing hazard potential in this area, and to assist in delineating future seismic and drilling programs.

1.1 Geological Setting

Although Agapito Associates Inc. are responsible for the detailed geological and mining evaluation portion of the Lisan Potash Exploration Project, at a regional scale the tectonics and geology of the Dead Sea pull-apart basin are well discussed in Al-Zoubi and ten Brink (2001). These authors suggest that the differential overburden loading giving rise to the Lisan diapir is caused by deformation due to the extensionally formed graben. The current report used this broad framework for a more regional interpretation of the 2D seismic data.

As noted above, in contrast to a detailed geological model, geophysically, a simple model was used as the starting point (Fig. 2). Rabba *et. al.* (2015) extended the work of Ajamieh (1987) and suggested a thin marl section of the Lisan Formation (yellow in Fig. 2) overlying a massive diapiric salt of the Sedom Formation (pink Fig. 2).

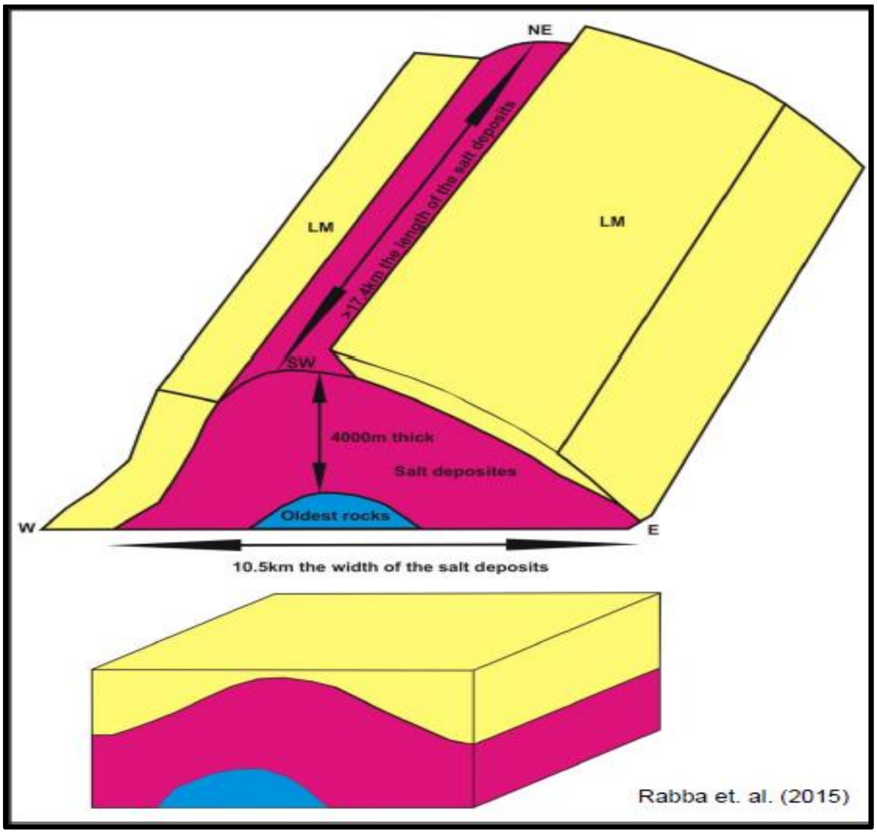

Figure 2: Simplified Anticline Geological Section taken from Rabba *et. al.* (2015).

2 COMPANY PROFILE

RPS Energy is a multi-disciplinary consultancy, providing technical, commercial and project management support services in the fields of operations, geoscience, engineering, and health, safety and environment to the energy sector worldwide.

Our clients include governments, national oil companies, integrated majors, independents, start-ups, legal and financial institutions.

RPS Energy is part of the larger UK based RPS Group Plc. that employs over 5000 staff based in offices in the UK, across Europe, Middle East, North America and South-East Asia and Australia.

RPS Energy is an international multi-disciplinary consultancy, providing technical, commercial and project management support services in the fields of operations, geoscience, engineering and health, safety and environment to the energy sector worldwide. RPS Energy focuses on upstream oil and gas, renewable energy and nuclear sectors from operating bases in the UK, USA, Canada, Australia and Malaysia.

RPS Energy has an enviable track record in providing specialist consultancy services to clients with a broad-based technical and project management service that can be accessed to provide support to client projects at all stages of an asset life cycle

As an independent and experienced consultancy with a global capability, RPS Energy is well qualified to provide independent technical and economic assessments of exploration, production and downstream oil and gas as well as mining projects.

RPS Energy’s services are delivered worldwide through the RPS network of offices. Each office has access to the company's resources and can draw on any particular expertise irrespective of where it is located.

RPS Energy Canada Ltd. (RPS) is a wholly owned subsidiary of the RPS Group Plc. It represents one of the three main businesses of RPS Group Plc.

2.1 Corporate Qualifications

RPS has been involved with seismic acquisition and interpretation since 1977. Specifically, RPS has been involved with potash mine development, salt mine development, and gas and chemical storage facilities since 1984. RPS has conducted similar potash projects for several companies, including BHP Billiton Canada, Potash Corp. of Saskatchewan, International Minerals Corporation, Potash One, Western Potash, Vale Potash Canada, and Agrium Potash.

RPS has been the primary seismic consulting firm for all operators in the Canadian potash industry since 1986. As the preferred seismic technology services provider for Potash Corp. of Saskatchewan, Vale Potash Canada, BHP Billiton Canada, Western Potash, and Agrium Potash, RPS has an unprecedented understanding of the Prairie Evaporite geological section gleaned from thousands of kilometres of 2D and tens of thousands of square kilometres of 3D seismic in the vicinity of Saskatoon, Regina, and Esterhazy, Saskatchewan.

During this time RPS has undertaken in excess of 70 projects at 13 different mine sites. Mining depths on these projects have ranged from less than 450 metres to over 1,500 metres. Geological conditions have included both horizontally layered Western Canadian sites and highly structured sites in Canada’s Maritime Provinces. Projects have included high priority, fast track seismic imaging to resolve critical, time-sensitive, and operational concerns. Re-evaluating seismic interpretations subsequent to mining operations has helped our clients ‘calibrate’ seismic signatures to actual mined geology.

Projects typically involve all facets of seismic exploration: survey design, acquisition, processing, interpretation, reporting, and final presentation. For each mine site, all available seismic data (current and historic) is maintained in a single interpretation project for reference when mine operations require immediate information. Final reports and maps are delivered in hard copy and digital formats.

RPS is proud to be the only geophysical operations management company to be awarded the Partnership in Injury Reduction Certificate from Alberta Human Resources and Employment. RPS has maintained this certificate since 1995 in recognition of our commitment to raise the standards of worker health and safety through active involvement in assisting others and in developing and implementing independent health and safety programs throughout our industry.

RPS is proud to have been selected for the "Work Safe Alberta 2009 Best Safety Performer Award" for exceptional safety performance in workplace health and safety. Of Alberta's 140,000 employers, 700 earned this award.

RPS is a registered Certificate of Recognition (COR) holder and requires all subcontractors to have a COR in good standing. RPS will continue our efforts to enhance the safety of our employees, our subcontractors and our business partners.

Based not only on our experience, but also on lessons learned from previous programs, RPS ensures an optimal project outcome based on competitive subcontractor bidding, advanced technical capabilities, experience and breadth of services provided.

3 DATA ACQUISITION & PROCESSING

3.1 General Comments

Rather than discuss, in detail, the legacy data acquisition and processing, RPS has provided general comments on how these items affect the current interpretation of the data. Details on the legacy data acquisition and processing can be found within the archives of the Ministry of Energy and Mineral Resources for those wishing to investigate further.

3.2 Seismic Data Acquisition

Lisan legacy 2D seismic data were acquired with deep petroleum exploration parameters consistent for 1980s level technology. Notwithstanding the generally poor-to fair-quality of the data, an important artefact in the presence of salt domes is i) side-swipe noise for seismic profiles off any axis of symmetry and ii) salt-flank reflections. These are critical to understand as conventional 2D processing is inadequate to mitigate their presence.

In 1993 approximately 100 km^2 of 3D seismic was acquired in two separate surveys and merged together to form a single volume for interpretation (Seismograph Service Ltd, 1993). Again, parameters are consistent for deep petroleum exploration. Ideally the data would have been acquired as a single survey but seismic technology available at the time was not adequate. The advantages of a well-designed and acquired 3D seismic survey in the Lisan area should have reduced the effect of side-swipe and salt-flank reflections with the appropriate processing. However, the acquisition on two parts limited the azimuth of the surveys and likely negated the potential benefits of the 3D data.

Typically, the 2D data will have higher resolution in both time and spatial frequency compared to 3D data. However, what 3D data loses in resolution it gains in spatial coherency and correct positioning of reflections not in-line with seismic sources. Thus, there is a trade-off between coherency and resolution, and this requires the use of both 2D and 3D data for optimal interpretation.

A shortcoming that afflicts both 2D and 3D seismic data is the near-surface solution. This correction accounts for elevation and velocity variations in the near-surface which can drastically affect the imaging of deeper data. In many cases a separate refraction survey is conducted to better constrain the near-surface solution, but this was not done at Lisan.

In summary, the legacy 2D and 3D seismic data are of consistent vintage, poor-to-fair in quality, designed for petroleum exploration, contaminated with out-of-plane noise and may have sub-optional near-surface corrections. The advancement in processing technology offers the opportunity to re-examine these data through a new lens and to modify the processing parameters for shallow potash targets.

3.3 Seismic Data Time Processing

As part of Phase I of the Lisan Potash Exploration Project, the historic 2D and 3D seismic data were reprocessed by Misbar Geophysical Services (Misbar) in Amman, Jordan with collaboration from RPS personnel in Calgary, Canada.

In Section 3.2 the near-surface solution was identified as a critical limiting factor for producing a clear subsurface image. Previous processing used a generalized linear inversion refraction statics method to solve for velocity variations in the near-surface. In contrast, Misbar have applied a modern tomographic ray-tracing approach to refraction statics. The Misbar approach can provide superior results in the case where velocity variation departs from a layer-cake model. The Lisan Peninsula has topographical variations such as wadis and karsted surfaces which are not well represented as simple horizontally stratified layers. Therefore, an uplift in imaging is expected using tomographic refraction statics.

In addition to the use of a more modern static solution, another area for leveraging the modern processing algorithms is through the use of pre-stack time migration (PSTM) which would not have been available to data processors when the historic seismic data was originally processed. Processing using PSTM of fit-for-purpose data should theoretically account for side-swipe and salt-flank reflections, as discussed in the previous section. The original post-stack migration could not account for these and resulted with images containing conflicting dips making interpretation difficult. A second round of reprocessing used dip-moveout plus post-stack migration, a predecessor to PSTM. Neither of these approaches yielded an adequate image but did provide a starting point for evaluating whether PSTM is a useful approach.

3.3.1 Seismic Data Reprocessing

For a thorough discussion of the processing, the reader is referred to the Section 7.1 in the Phase I Report. However, to follow a number of comparisons are provided to demonstrate the results of seismic imaging/reprocessing in the context of interpretation for potash exploration.

A comparison between CCG legacy processing and Misbar 2019 modern reprocessing is shown in Figure 3. Line VWJ-13 was used for comparison as it intersects the project area from northeast to southwest (Fig. 1). Unfortunately, no migrated stack for the CGG processed line was made available and a structure stack was used in its place. The benefit of the comparison in this case then illustrates the benefit of seismic migration as well as the benefit of modern processing. As illustrated by the data in the lower box in Figure 3, previously unmigrated diffraction energy has now moved to its correct position. The upper box in Figure 3 shows that previously where there were no reflections well imaged, coherent reflectors now exist and indicate shallow geological strata. Seismic migration it a natural noise attenuator and as a result, there is overall a significant reduction of ambient noise in the profile (Fig. 3). Reprocessing with modern techniques, such as migration, has resulted in an improvement of data quality.

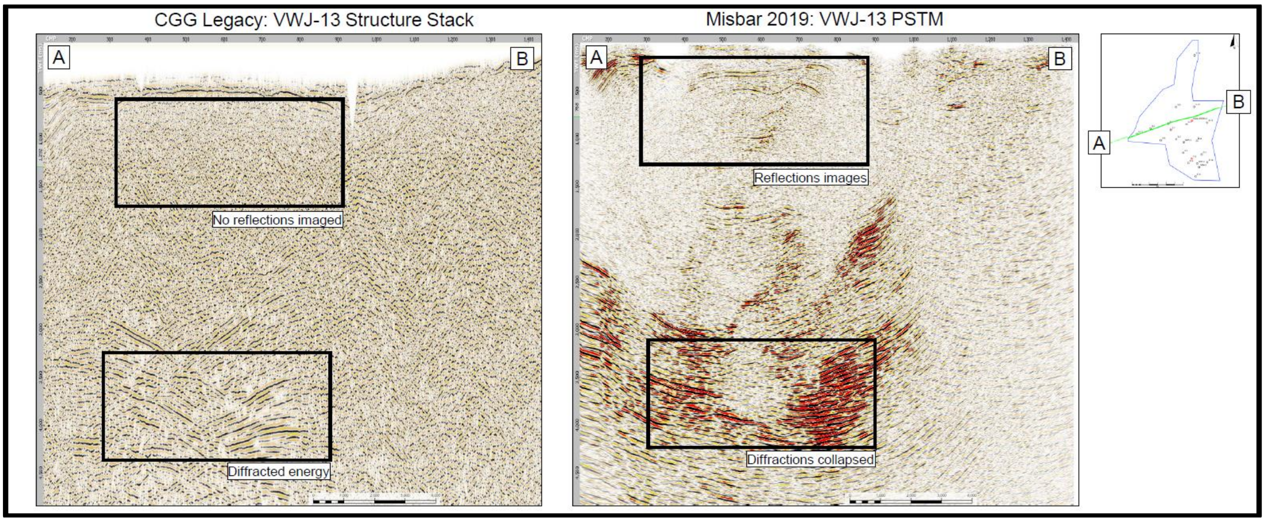

Figure 3: 2D Seismic Reprocessing: CGG Legacy and Misbar 2019.

That fact that 2D seismic Line VWJ-13 overlaps a significant portion of the 3D seismic survey allow a direct comparison between image quality based on the acquisition of 2D and 3D data. As illustrated in Figure 4, the lower box highlights the fact that that seismic events seen on the 2D have been removed in the 3D image. This is a result of out-of-plane energy recorded on 2D data being migrated properly using 3D data.

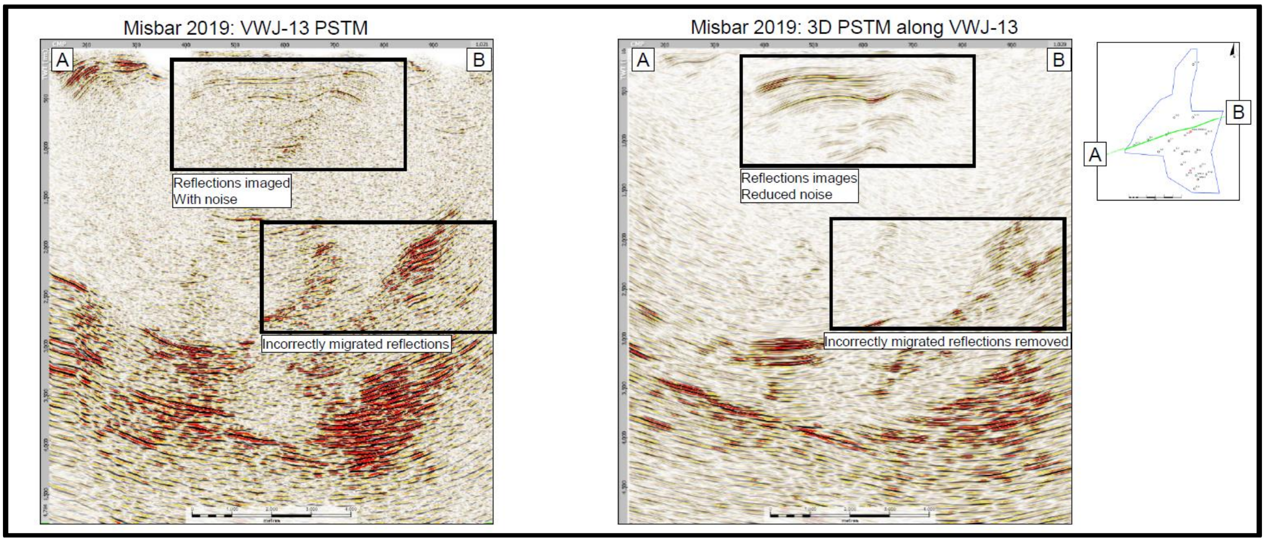

Figure 4: 2D and 3D Reprocessing: Leveraging Areal Coverage to Mitigate Noise.

In the upper box of Figure 4 there is substantial uplift in the coherency of the reflections captured by 3D data over 2D data. Again, there is out-of-plane energy that is being properly migrated to the apex of the structure. As in Figure 3 there is a reduction in ambient noise. This is expected as random noise is cancelled out in the stacking process where 3D data have more samples to contribute to the cancellation. Acquiring 3D seismic data is a natural noise attenuation technique.

In 1993 when the Lisan 3D data were acquired a recent processing break-through in addressing conflicting dips and salt-flank reflections was dip moveout or DMO. DMO processing followed by post-stack migration approximates what is now pre-stack time migration. Figure 5 illustrates the difference between the legacy GSC processing using DMO plus post-stack migration and the recently reprocessed Misbar 2019 pre-stack migration. Similar to the images provided in Figure 3 and Figure 4, improvements in the subsurface image are noted. The lower box of Figure 5 shows that reflection energy has been removed and deeper reflections are enhanced. The upper box of Figure 5 shows that shallow reflectors are better imaged. Though subtle at times, pre-stack time migration has improved image quality due to proper handling of conflicting dips and salt-flank reflections.

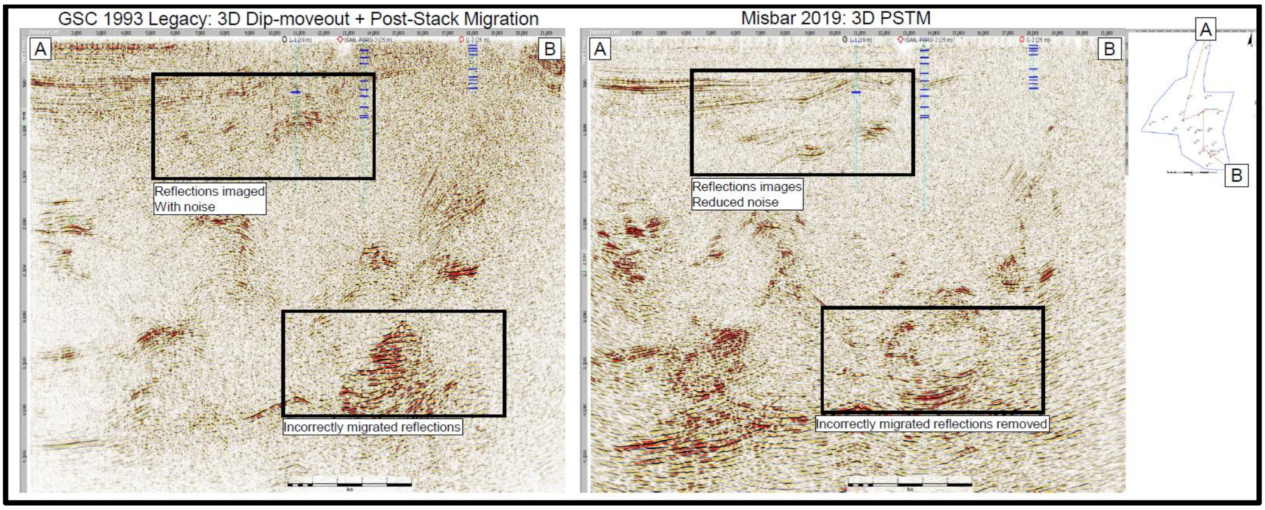

Figure 5: 3D Reprocessing: GSC 1993 Legacy and Misbar 2019 Pre-Stack Time Migration.

Finally, the application of a coherency filter to the 3D pre-stack time migrated data yields further improvements in noise attenuation and enhanced reflection character, and ultimately the subsurface image. In Figure 6 the lower boxes show marginal enhancements in the deep reflectors. However, the upper boxes highlight significant refinement in the shallow reflector package (Fig. 6).

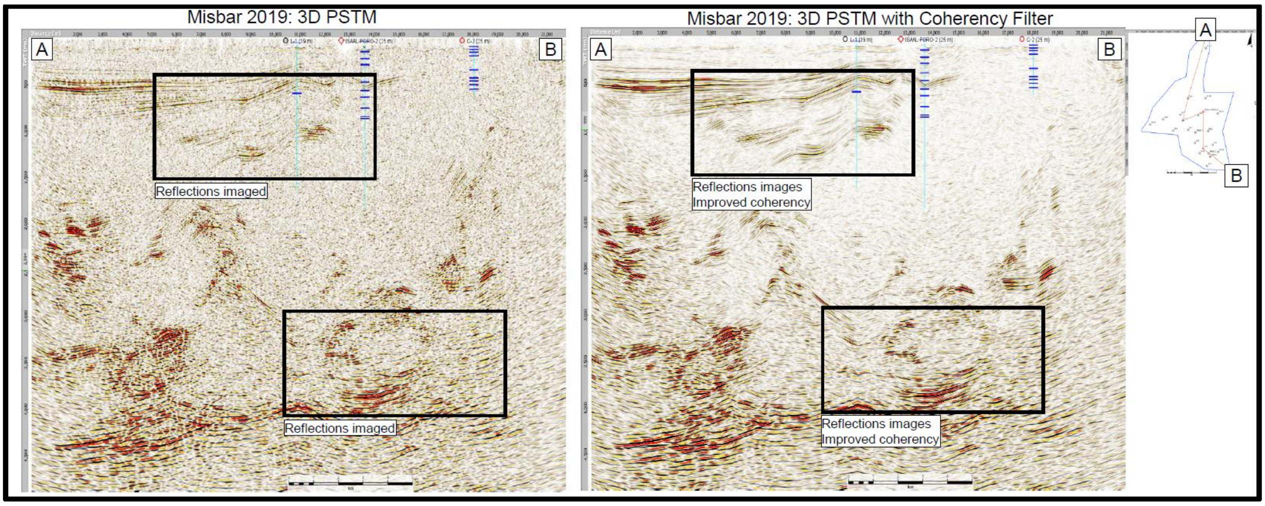

Figure 6: 3D Reprocessing: Misbar 2019 Pre-stack Time Migration Coherency Filter.

Overall, reprocessing old data with new techniques has advanced the image quality for seismic interpretation. While deep reflections have been enhanced, it is in the shallow section that the data have been accentuated. The improved image in the shallow subsurface is the most beneficial as this is the area of interest where exploring for thin potash-bearing strata is most economically feasible.

4 INTERPRETATION PROCEDURES

4.1 General Comments

RPS followed standard, industry accepted professional practice and interpretation procedures in evaluating the 2019 Lisan Peninsula seismic dataset. The analysis and interpretation of the 2D/3D dataset was completed using Down Under Geophysics Insight seismic interpretation software on a PC workstation.

4.2 Synthetic Seismograms and Geological Correlation

Tying seismic data to available well data is accomplished with the use of synthetic seismograms generated from down-hole density and sonic logs. A synthetic seismogram is a forward modelling technique that convolves a wavelet with the reflectivity sequence from well logs. If a zero-phase wavelet representative of the seismic data was used, then the output is a predicted zero phase seismic trace at that well location. Typically, a mistie analysis between the stacked seismic data and a synthetic seismogram determines a phase rotation that, when applied to the stacked data, produces a zero phase dataset.

As described above, the identification of various seismic events is accomplished with the use of synthetic seismograms generated from down-hole density and sonic logs from nearby wells. Correlating the synthetic seismograms to the time based seismic sections allows for the correlation of geological events to seismic reflections.

Figure 7 illustrates the synthetic seismogram generated at Well ISAAL-PORO-2 which allowed for the correlation of key geologic horizons from well data onto the seismic data. The synthetic seismogram is generally devoid of any strong reflections except near the top and bottom of the logs. The lack of reflectivity should not be a surprise as most of the geologic column is dominated by the presence of salt which lacks internal character. In contrast, the seismic data appear to be divided into two intervals of high and low reflectivity (Fig. 7). The high reflectivity zone may be contaminated with multiple reflections from the strong shallow reflectors correlated to potash-bearing formations (Fig. 7). The strong events in the deep portion of the synthetic seismogram are rather anomalous as they are completely missing in the seismic data tying the well (Fig. 7).

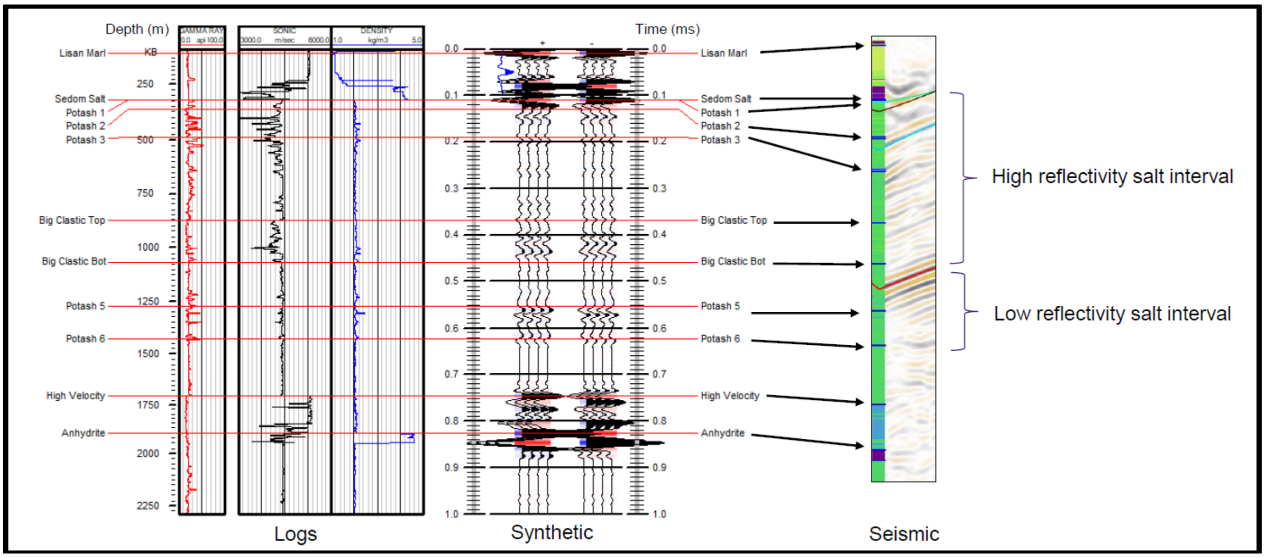

Figure 7: ISAAL-PORO-2 Synthetic and Geological Correlation.

Utilizing the ties to the available well data (Wells C-2 and ISAAL-PORO-1 also provided calibration points) and 3D data, key potash-bearing horizons were interpreted on the 2019 Lisan Peninsula seismic dataset.

4.3 Seismic Events

Following the identification of the seismic signature of individual geological layers from the synthetic seismograms, the seismic events are picked on the stacked processed data. It should also be noted that a formation "marker" is a seismic horizon with no geological equivalence.

The structure information of seismic data has very little inherent interpretive risk where the quality of the reflection is good. Picked horizons where the quality of the reflection is not as strong or consistent may have greater inherent interpretive risk.

Seismic horizon picking is itself based on decisions made by the interpreting geophysicist. Only a small portion of the horizons picked for the 2019 Lisan Peninsula seismic were made using automatic computer tracking of laterally discontinuous and poorly images seismic horizons. The automatic picking pass is then followed by meticulous, though highly interpretive, manual edits. This process of seismic event picking is robust, and the interpretive risk is low in high quality data with good well control.

Overall, the data quality in the Lisan area is uniformly fair-to-poor, resulting in high interpretive risk associated with this dataset.

4.4 Depth Conversion

Two approaches to depth conversion were investigated. First, a tops-based approach combining the tops picked with the corresponding seismic times to estimate velocity. While the results appeared to be reasonable there is significant uncertainty in the continuity of the geological tops due to well log quality. That is, a geological pick in one well may not be the same pick in another well. This creates potentially large errors in the Top of Potential Potash and Base of Potential Potash Markers. The second method takes advantage of the fact that the entire project area is dominated by salt; less the near-surface marl. Therefore, a simple model used a reasonable value for salt from the Top of Salt to the Base of Salt (Sedom Formation). Faster velocities were introduced below the Base of Salt to estimate depth to Cretaceous and Pre-Cretaceous (Bottom). The derived velocities for the two models are provided in Figure 8.

Stratigraphic Interval	Tops Based Velocity (m/s)	Constant Interval Velocity (m/s)
Seismic datum - Top Salt	Co-Krigged Map	Co-Krigged Map
Top of Salt – Top of Potential Potash	Co-Krigged Map	4300
Top of Potential Potash - Base of Potential Potash	Trend Map	4300
Base of Potential Potash - Base of Salt	4300	4300
Base of Salt - Cretaceous	4500	4500
Cretaceous - End of Data	5000	5000

Figure 8: Two Depth Conversion Velocity Models.

It should be noted that the Top of Salt could not be imaged on the seismic data because it is too shallow. The depth estimate for this surface was derived by co-kriging the densely sampled digital elevation model with the sparse Top of Salt penetrations from the S series, C series, NRA series and deep wells

The salt-velocity model was preferred due to concerns over the negative effects of mis-picked tops and horizons on interval velocities which far outweighed the lack of detail in the salt-velocity model. The salt-velocity model is simpler and better reflects what is known of the geological environment at the present time.

Typically, a few iterations of depth conversion are required to converge to a practical solution. Due to a lack of reliable geological well log data and time constraints it was not possible to investigate alternative velocity models. However, it is suggested that even an increased effort under the circumstances would not likely yield any benefit. Despite the shortcomings outlined, the simple salt model should capture the correct relative structural architecture of the geology. The error is expected to be largely in the absolute value of the depth structure. In the end, the salt-based velocity model was used to depth convert the 3D seismic volume.

4.5 Interpretation Risk Assessment

Deficiencies in the data acquisition, data processing, geological correlation and depth conversion have been discussed in previous sections. These limitations manifest themselves in interpretation as the two following errors:

- Horizon correlation error - refers to misidentifying a seismic event with a geologic top at the well correlation;
- Horizon picking error - refers lithological variations along a seismic event away from the well correlation.

This is considered the interpretation risk. The overall interpretation risk assessment at this stage of the project should be considered high.

5 INTERPRETATION ANALYSIS

5.1 General Comments

Following the acquisition and processing of the original 3D seismic survey, Western Atlas (1993) provided a thorough interpretation for petroleum prospectively on the Lisan Peninsula. However, the Western Atlas (1993) work did not consider any shallow reflections which were correlated to potash-bearing strata.

5.2 Salt Reflectivity Interpretive Model

The simple geologic model provided in Figure 2 represents the salt is one massive layer. However, the seismic data along a general North-to-South profile (Fig. 9) suggest that there are zones of varying reflectivity below the salt top encountered by the shallow wells. There appear to be four reflectivity packages below the Top of Salt:

- High reflectivity potash-bearing zone – verified by well correlations;
- Low reflectivity uneconomic zone – too deep or no potash well correlations;
- Reflectivity void zone – chaotic or no reflections suggesting clean diapiric salt core;
- Deep salt layer – Pliocene-aged Sedom Formation.

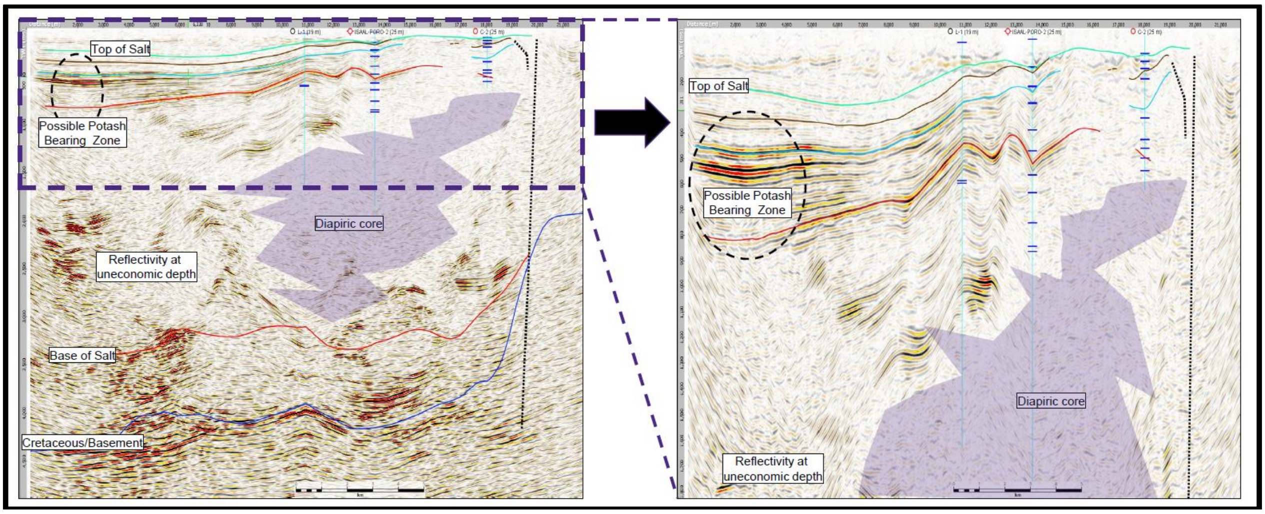

Figure 9: 3D Seismic Interpretation: Full Section and Potash Zone Detail.

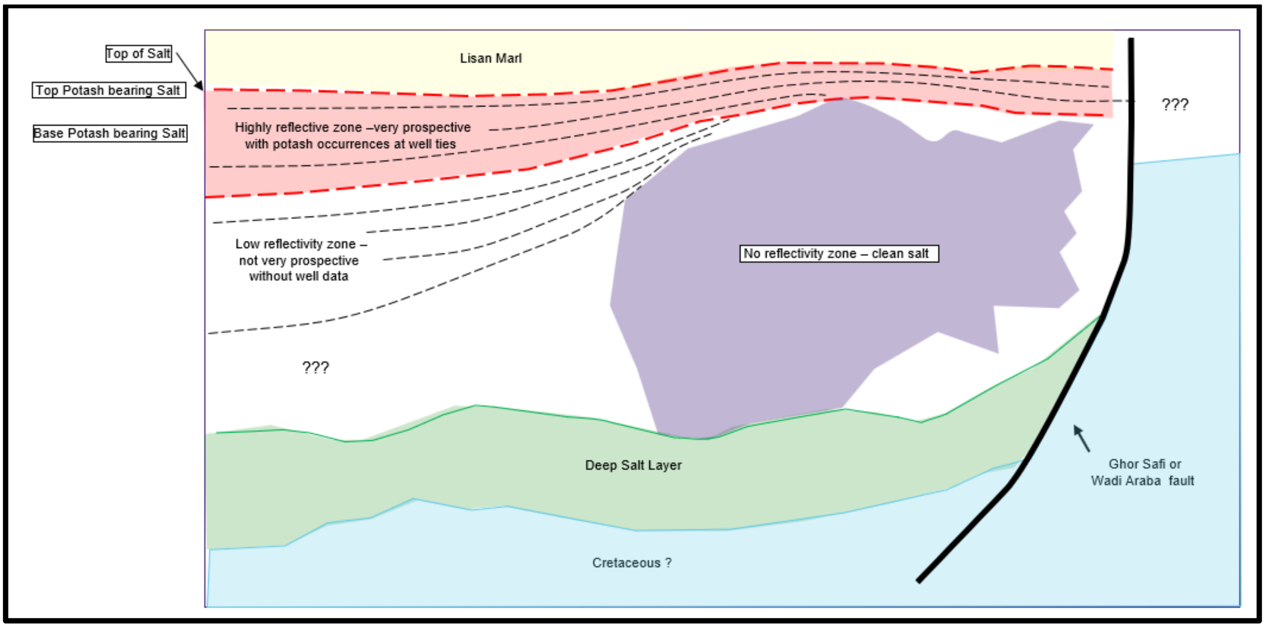

Figure 10: Salt Reflectivity Interpretive Model.

Near the Wadi Araba boundary fault there is a lack of reflectivity. It is possible that that the fault has many associated faults disrupting any coherent imaging or that the salt bounds the fault. In this study the fault is assumed to be the eastern bound of the extent of the salt.

5.3 2D & 3D Seismic Horizons

With the four reflectivity packages defined in Section 5.2 in mind, the 2D and data were interpreted. In some areas of the 3D data reflections were well imaged and mapping was straight forward. However, there were significant portions that were poorly imaged. In this regard, some 2D profiles had good imaging overlapping the poor 3D coverage. In these instances, the reflections from the 2D lines were used as guides to expand the 3D interpretation in these areas. These regions have a lower confidence and are separated from the high confidence picks with a polygon on depth structure maps.

The Top of Potential Potash Horizon (brown horizon) was picked based on the first coherent and continuous reflector within the shallow section that correlated best with the first potash well markers at ISAAL-PORO-2 and C-2. However, the well synthetic ties are poor, and this is a relative correlation at best. The Intra Potential Potash Zone Horizon (light blue horizon) was picked based on a small group of coherent, continuous reflectors that generally correlate to additional potash encounters in these two wells cited. The Base of Potential Potash Horizon (shallow red horizon) was picked along a deeper group of reflectors which correlate to an interval of clastic dominated rock that is between some shallower and deeper potash encounters in Wells ISSAL-PORO-2 and C-2. Potash encounters below this horizon did not correlate consistently to a seismic event and therefore could not be mapped with any confidence. Additionally, two deeper reflectors were picked in the north-northwest area of the project which could not be correlated to any well markers but were instead used to constrain the diapiric structure.

The two key 2D lines that were used to extend the bound of the 3D interpretation were DS-07 and VWJ-13 (Fig. 11). These lines indicated reflective areas in the shallow section which corresponded to reflections seen elsewhere in the 3D data. Line DS-07 guided extrapolation of the reflections to the southern area of the 3D and line VWJ-13 does likewise to the west. Unfortunately, the majority of 2D lines reprocessed did not offer any improvement in areas overlapping the 3D seismic.

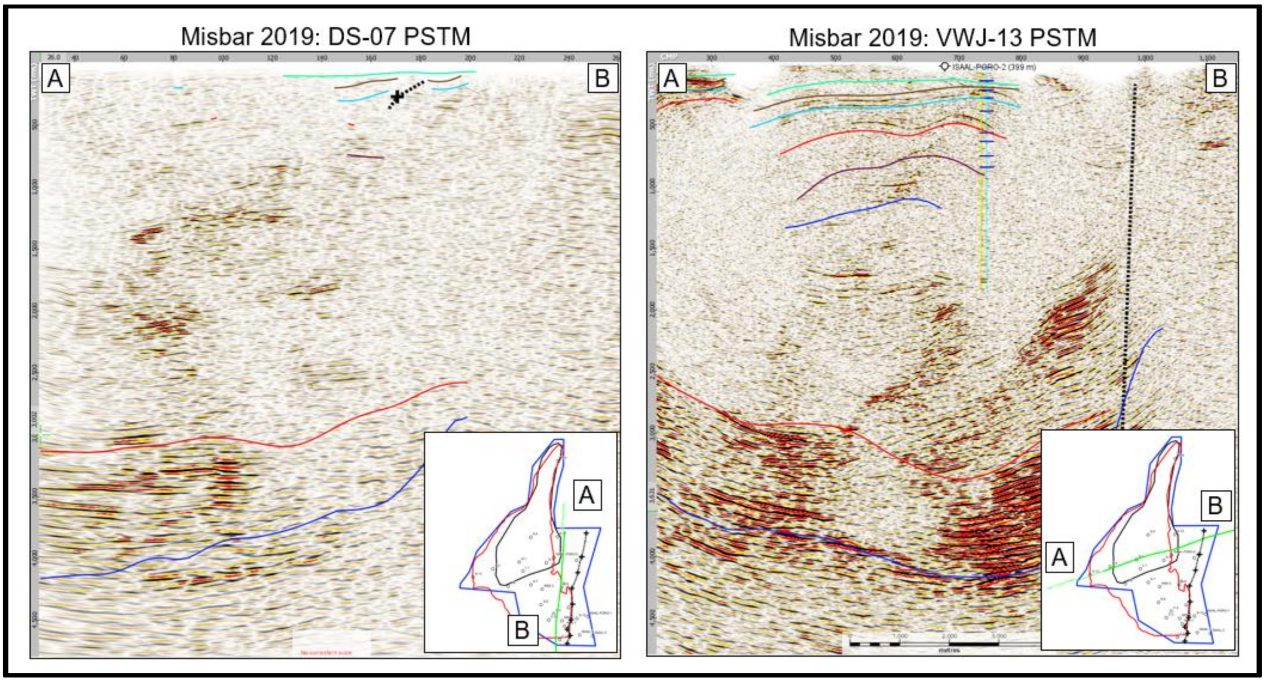

Figure 11: Seismic interpretation on two key 2D lines; DS-07 & VWJ-13.

The coherency filtered 3D PSTM provided the foundation for the interpretation over most of the project area. Examples of the interpretation are show using arbitrary lines in Figure 12 and Figure 13. The shallower potash interval was picked on a tightly spaced grid on reliable reflectors, interpolated and gridded to produce time-structure maps and then converted to depth. The deep reflectors of the Base of Salt and Cretaceous markers are more speculative, and a coarser picking interval was applied to follow only event that were considered reliable. A similar interpolation and gridding scheme was then applied to the deep events.

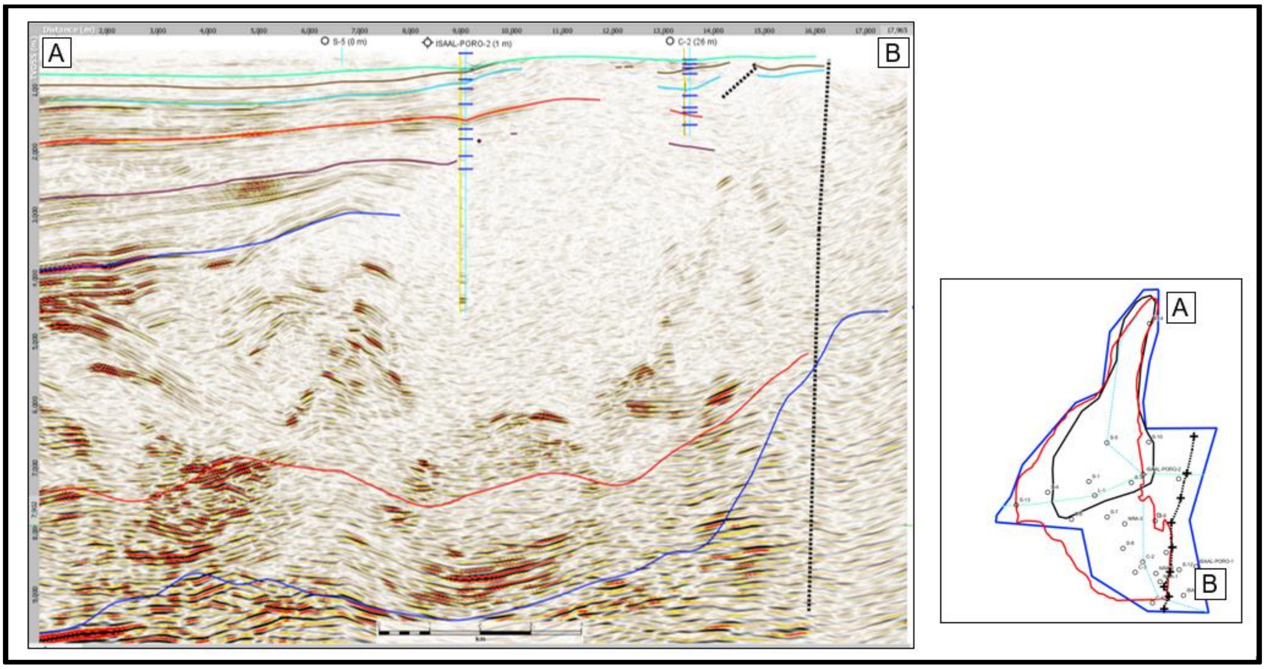

Figure 12: NW-SE Arbitrary Line Interpretation through the 3D volume.

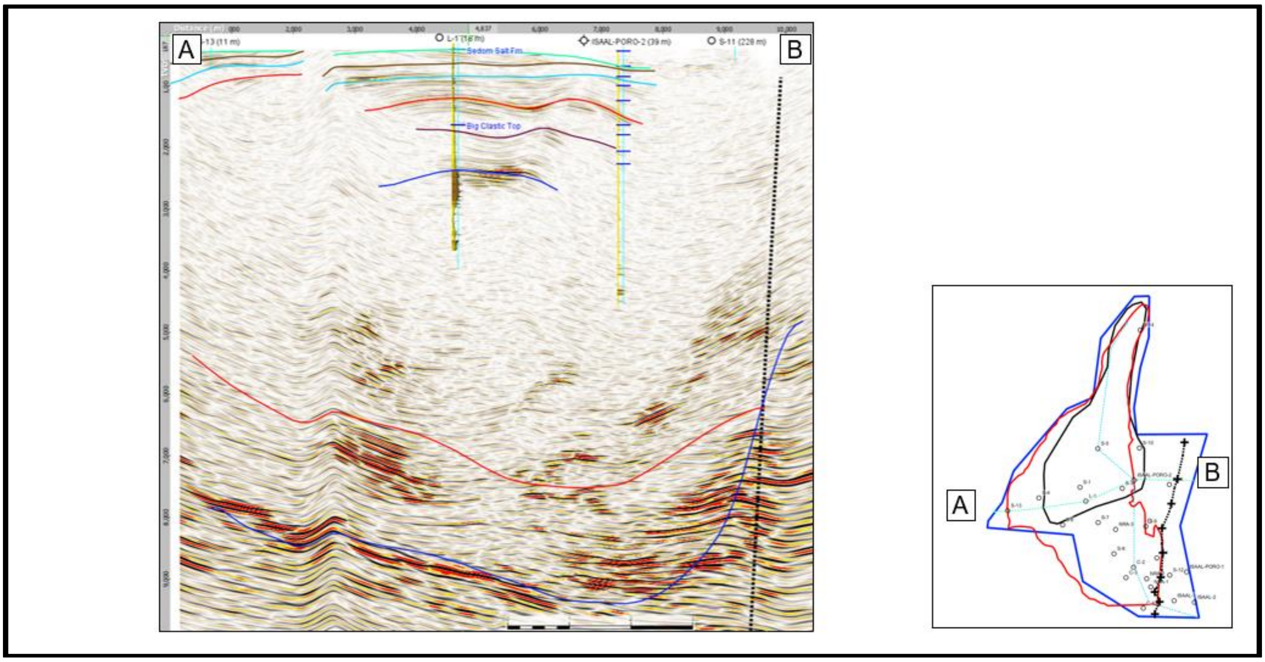

Figure 13: NE-SW Arbitrary Line Interpretation through the 3D volume.

5.4 Depth Structure Maps

The time structure grids from the interpretation were then depth converted using the salt-velocity model discussed in Section 4.4. Figure 14 shows the depth structure maps that bound the basin for the project area. The Top of Salt Depth Structure Map clearly shows the apex of the of the overall salt interval and the northwest-southeast axis along the high (Fig. 14). There is a break to the west though its nature is indeterminate due to poor data quality and lack of coverage (Fig. 14). Most likely a fault or diapiric intrusion is the cause of the break in continuity. The Base of Salt (Sedom) has a northeast-southwest axis indicating the deepest depth of the salt to be approximately 7,600m. This depth compares well to previous work by Al-Zoubi and ten Brink (2001). The Cretaceous Depth Structure Map is poorly constrained east of the boundary fault as seismic data quality was very poor making well correlation challenging. It is possible that the lack of seismic reflections is indicative of the complexity of the faulting in this area.

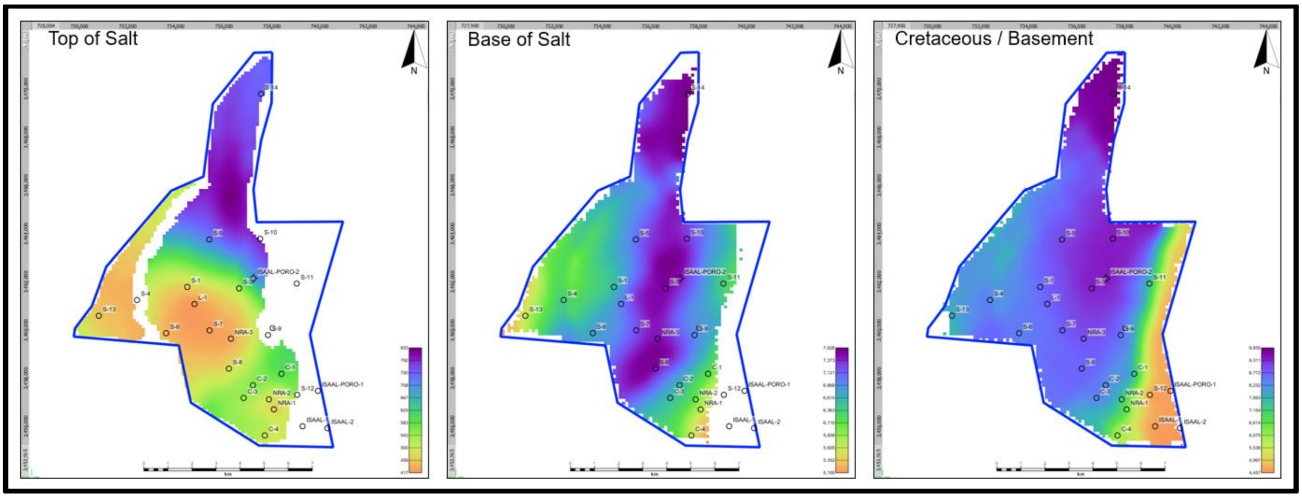

Figure 14: Depth Structure Maps: Top of Salt, Base of Salt and Cretaceous/Basement.

The prospective potash zones are shown in Figure 15. All three depth structures for Top of Potential Potash, Intra Potential Potash and base of Potential Potash are high over the apex of the diapir (Fig. 15). Discontinuity of the depth surfaces may be due to faulting. To the south, all structures are high whereas to the north of the apex the structures all dip rapidly to the north. It should be noted that the area contained within the black polygon represents a high confidence region where the seismic reflections were of good quality and therefore the derived depth structure map is considered more reliable. The depth structure within the polygon dips rapidly to the north and may make mining operations less economic. In contrast, the portions of the depth structure that are in the southern high are based on poor quality reflection data. Picking through this area was discussed in Section 5.3 earlier. Consequently, these high areas of the depth maps outside the black polygon are of lower confidence.

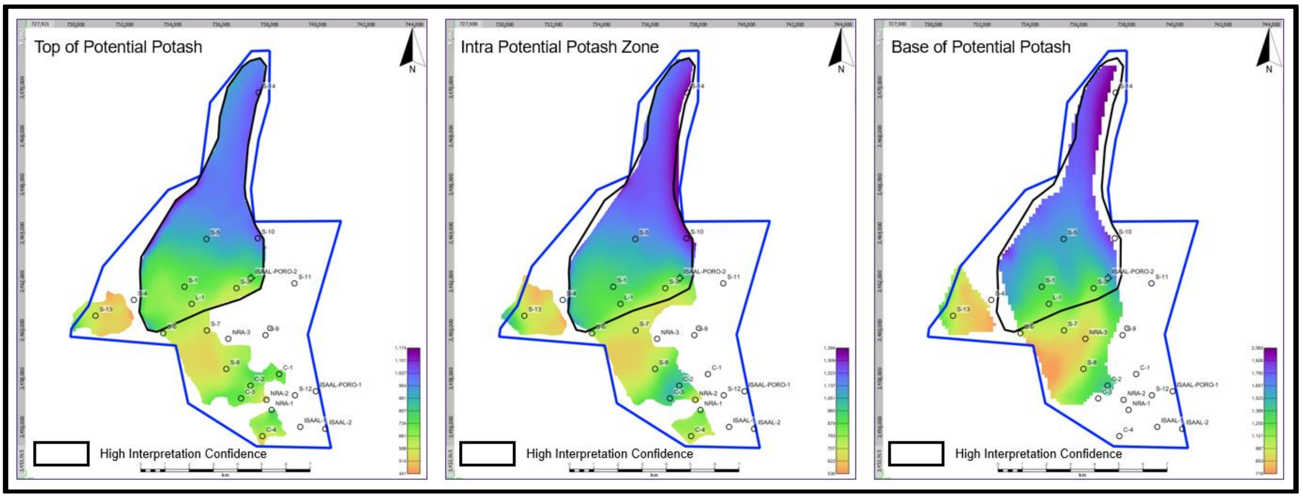

Figure 15: Depth Structure Maps: Top of Potential Potash, Intra Potential Potash Zone and Base of Potash Potential.

Figures 16 and 17 show the depth maps in 3D view from the four corners of the project area and illustrate the spatial relationships already discussed.

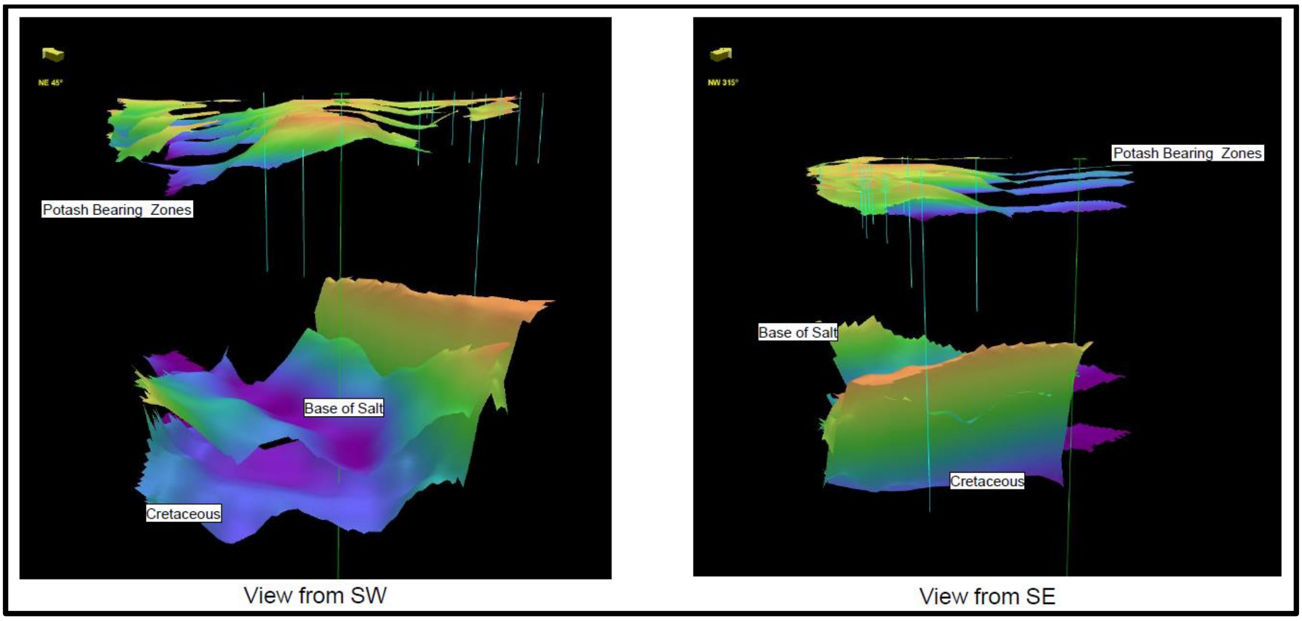

Figure 16: Seismic Depth Structure 3D Views: From the Southwest and the Southeast.

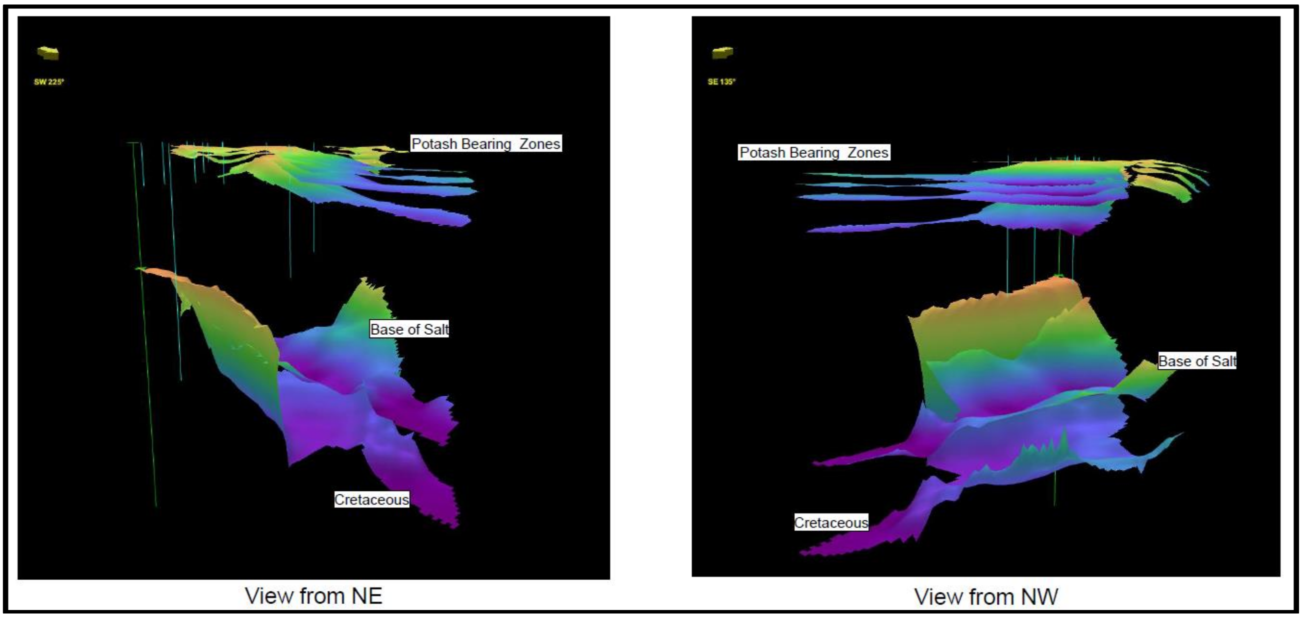

Figure 17: Seismic Depth Structure 3D Views: From the Northeast and the Northwest.

6 CONCLUSIONS

As part of a subsurface investigation by the Ministry of Energy and Mineral Resources, Natural Resources Authority of the Hashemite Kingdom of Jordan, RPS Energy Canada Ltd. was contracted by Agapito Associates Inc. to interpret 2D and 3D seismic data (approximately 100 linear kilometres of 2D and 100 km^2 of 3D seismic coverage) for the 2019 Lisan Peninsula Potash Exploration Project.

As part of Phase I of the Lisan Peninsula Potash Exploration Project, the Legacy 2D and 3D seismic data was reprocessed by Misbar Geophysical Services out of Amman, Jordan. The legacy and reprocessed seismic data forms the basis for the reinterpretation presented here.

Reprocessing of the legacy 3D data with modern techniques has resulted in an improvement of data quality. Unfortunately, the majority of 2D lines reprocessed did not offer any improvement in areas overlapping the 3D seismic. In general, the overall data quality in the Lisan area is uniformly fair-to-poor, resulting in high interpretive risk associated with this dataset.

RPS completed the correlation of geological markers to seismic events from recently reprocessed 2D and 3D seismic data. This step of reprocessing was critical in improving the geophysical data and producing seismic images. Geological guidance from well data was provided by Agapito Associates Inc. and enabled the identification and mapping potential potash bearing zones. Depth structure maps were derived from the seismic data and well-based geology.

The mapped potash bearing zones were constrained laterally and in depth. The prospective area in the northern portion of the project area is well defined by high confidence seismic interpretation and shows the general structure to rapidly fall off the apex of the Lisan diapir with a northerly dip. The shallower data in the southern project area does not suggest any steep dips until below the prospective potash zone. This area is potentially more prospective than the northern area but is also considered to have low confidence in the seismic interpretation.

7 RECOMMENDATIONS

The following recommendations are made based on the interpretation of the reprocessed seismic data:

- Although the seismic data were reprocessed and showed improvement, the legacy data acquisition was not designed for shallow potash exploration. The acquisition of a new, fit-for-purpose 3D seismic program is required to adequately image the targets identified in this study.

- Geological data were either lacking or, where present, inadequate for the correlation of geology to seismic data. A significant geological drilling program with the appropriate geophysical logging suite (gamma ray, P sonic, S sonic and bulk density) should be acquired prior to the acquisition of further seismic data.

- Results were maximized based on the quality and quantity of geological and geophysical data under a very aggressive work schedule. If new data are acquired with state-of-the-art technology, then it is highly recommended that the schedule be amended to allow for a thorough analysis and interpretation of what would be a very rich dataset.

8 REFERENCES

Ajamieh, M.A., 1987. An exploration program for solid potash minerals in the Lisan Peninsula, Dead Sea, Ministry of Energy and Mineral Resources, Natural Resources Authority, Technical Report Series, Hashemite Kingdom of Jordan, pp1-51.

Al-Zoubi, A. and ten Brink, U.S., 2001. Salt diapirs in the Dead Sea basin and their relationship to Quaternary extensional tectonics. Marine and Petroleum Geology, v18, pp779-797.

DMT, Offshore subsurface geophysical investigation and offshore and onshore surveys for marine works, 2017. Report prepared for Arab Potash Company Ltd., pp1-77.

Rabba, I.A, Al Russan, A, Al Hawamdeh, M. and Abweny, M.S., 2015. Interpretation and evaluation of the old exploration (1959-1989) of the potash rock deposits in Lisan Peninsula-Dead Sea. Ministry of Energy and Mineral Resources, Hashemite Kingdom of Jordan, Internal Report, pp1-43.

Seismograph Service Ltd., 1993. 3D Vibrioses reflection survey conducted in the Hashemite Kingdom of Jordan for Natural Resources Authority, pp1-49.

Western Atlas, 1994. Seismic interpretation and seismic modelling of the El-Lisan Peninsula, Dead Sea. Report prepared for Natural Resources Authority Hashemite Kingdom of Jordan, pp1-133.

9 DIGITAL INFORMATION

All digital data is in coordinate system WGS84 / Zone 36N unless otherwise specified.

9.1 Final Products

A hard drive is included with the original copy of this report, which contains the archived data for this project. A project archive hard drive is included with this report and is organized into seven main directories. The sevens directories are listed as follows:

- Report – contains the final report in Microsoft Word and Adobe PDF file formats and the larger 11"x17" report figures in Microsoft Power Point and Adobe PDF file formats.
- Images – contains all preliminary Power Point files.
- Horizons – contains horizon ASCII files.
- SEGP - SEGP survey files.
- Shape files – contains individual ESRI shape files for the interpreted anomalies as well as key overlay drawing files used in the creation of maps within this report.
- SEGY – contains a copy of the 2019 Lisan Peninsula seismic dataset in SEGY format.
- Down Under Geophysics – an updated Insight seismic project data archived at RPS including all seismic data interpreted by RPS.

10 AUTHORIZATION

This Final Interpretation Report of the 2019 Lisan Peninsula Seismic Project is respectfully submitted to Agapito Associates Inc. this November 6, 2019.

Atul Nautiyal, P.Geoph.
Geophysicist

Luc Gravel, P.Geoph.
Geophysicist

Roger Edgecombe, M.Sc., P.Geoph., P.Geo.
Senior VP – Geoscience